CHARACTERIZATION OF CHEMICALLY DEPOSITED COPPER SELENIDE THIN FILMS FOR SOLAR CELL APPLICATION

M.Phil. DISSERTATION

June 2003

SUBMITTED TO: DEPARTMENT OF PHYSICS
UNIVERSITY OF DHAKA
BANGLADESH

SUBMITTED BY: AL - MAMUN
REGISTRATION NO-286/1997-1998
EXAMINE BEARING ROLL NO-7

M.Phil. DISSERTATION

CHARACTERIZATION OF CHEMICALLY DEPOSITED COPPER SELENIDE THIN FILMS FOR SOLAR CELL APPLICATION

A DISSERTATION SUBMITTED FOR THE REQUIREMENT OF THE DEGREE OF MASTER OF PHILOSOPHY (M. Phil.) IN PHYSICS, 1998-1999.

SUBMITTED TO: DEPARTMENT OF PHYSICS
UNIVERSITY OF DHAKA
BANGLADESH

SUBMITTED BY: AL - MAMUN
REGISTRATION NO-286/1997-1998
EXAMINE BEARING ROLL NO-7

Dedicated

To

Late Professor Sultan Ahmed

Department of Physics

University of Dhaka

পদার্থ বিজ্ঞান বিভাগ
ঢাকা বিশ্ববিদ্যালয়
ঢাকা-১০০০, বাংলাদেশ
ফোন : ৯৬৬১৯০০-৫৯/৪৯৪২
ফ্যাক্স : ৮৮০-২-৮৬১৫৫৮৩

DEPARTMENT OF PHYSICS
UNIVERSITY OF DHAKA
DHAKA-1000, BANGLADESH
Phone : 9661900-59/4942
Fax : 880-2-8615583
E-mail: Tista.physics@du.bangla.net

নং.....পদার্থ/প

তারিখ .....

No.....Ph./

Dated, the.....

Date: June 30, 2003

Declaration Letter

I am submitting herewith four copies of my Dissertation entitled "**Characterization of Chemically Deposited Copper Selenide Thin Films for Solar Cell Application**" as a requirement for M.Phil. degree in Physics.

I hereby declare that the work of this dissertation is original, unpublished and not being considered for publication elsewhere.

Submitted by: Al-Mamun
30/6/06
Registration No.: 286 / 1997-98

Supervisor: Dr. A. B. M. Obaidul Islam
30.06.2003.
Associate Professor
Department of Physics

Acknowledgments

I am deeply indebted to my reverend teacher Dr. A. B. M. Obaidul Islam, Associate Professor, Department of Physics, University of Dhaka, for his kind and sympathetic supervision and constant guidance throughout the progress of the work.

I would like to express my gratitude to Professor Rezaul Karim Mazumder, Director, Semiconductor Technology Research Center (STRC), Dhaka University, for permitting me to work in STRC.

I would also like to express my gratitude to the Director, Bose Center for Advanced Study and Research in Natural Sciences for providing me the financial support. I am thankful to Professor Altaf Hossain and Prof. Amir Hossain Khan, Department of Chemistry for their kind help to explain the chemical reaction.

I would like to thank Chairman, Department of Physics, Dhaka University, for permitting me to work in our Science Workshop.

I would like to acknowledge Prof. W. Jaegermann, TU Darmstadt, Germany for allowing his laboratory to do the AFM and XPS measurements.

I would also like to acknowledge Dr. Sabina Hussain, Assistant Professor of Physics, D.U. and Dr. Aminul Islam Talukder, Assistant Professor of Physics, D.U. for their occasional help during my research.

My special thanks to Mr. Md. Shahidul Islam, former student, Department of Physics, University of Dhaka, for his help to take Hall measurement and Mr. Shajedul Hossain Sharkar Shaheen, Instrument Engineer, STRC, D.U. for technical help in setting up experimental systems needed for carrying out investigations.

I am thankful to the technical staff of the Mechanical Section, Science Workshop, D.U. and BRTC, BUET and Bangladesh Council for Scientific and Industrial Research (BCSIR) for providing XRD facilities.

Lastly, not the least I am grateful to A. Z. Ziauddin Ahmed, Ph.D. student, Department of Physics, University of Dhaka, S. H. Firoz, Scientific Officer, BSCIR, Md. Nurul Kabir Bhuiyan, Ph.D. student, Toyama University, Japan and to all of my friends, Alok Kumer Day, Tareq Monsor, Md. Saeem Mahmood and others for their help throughout the work.

ABSTRACT

A low cost chemical bath deposition (CBD) technique has been used for the preparation of $Cu_{2-x}Se$ (x=0.1–0.5) and Cu_3Se_2 thin films on glass substrate. Different thin films were prepared by adjusting the bath parameter like pH value, deposition time, temperature of the solution and the ratios of the mixing composition between copper and selenium in the reaction bath. Structural, electrical and optical properties of these films (0.2–0.6 μm) have been characterized. Sodium selenosulphate has been used as a source of selenide ions. Surface morphology has been studied by Atomic Force Microscopy (AFM). X-ray Diffraction (XRD) is used as a major tool for identification of $Cu_{2-x}Se$ and Cu_3Se_2 phases. When the film annealed at 250°C in air, both these phases become crystalline with structures of berzelianite (cubic) and tetragonal, respectively, whereas, dis-order surface is obtained for as-deposited film. Annealing these films above 250°C in air results in loss of selenium. Results have been made confirm using X-ray Photoelectron Spectroscopy (XPS) and absorption studies. The resistivity is estimated in the range $(2–25)\times10^{-3}$ Ω-cm from as-deposited to annealed sample. Hall effect measurements performed on as-deposited thin films and found a career density of $(5–6)\times10^{23}$ cm^{-3}. All the films (as-deposited and annealed) show *p*-type conductivity. The transmittance and reflectance is obtained to be about 3-75% and 4–20% in the wavelength range 400–1100nm from as-deposited to annealed samples. Optical absorption in the films observed free carrier absorption in the near infrared region with absorption coefficient of $\sim10^5$ cm^{-1}. The band gap for direct transitions $E_{g,dir}$ varies in the range 1.9–2.6 eV and for indirect transition $E_{g,indir}$ is in the range 1.3–2.0 eV from as-deposited to annealed samples. From our study it reveals that chemical bath deposition techniques can be used to prepare thin films of $Cu_{2-x}Se$ (specially for x=0.2) and Cu_3Se_2 and these films could be used in various purposes of thin film technology especially for solar cell applications.

CONTENTS

CHAPTER 1

INTRODUCTION

In this chapter, background, review of the previous research works, aim of the present research work and outline of each chapter are explained.

1.1 BACKGROUND

Energy, the agency of work manifests in the form of heat, light, electricity etc. The conventional resources of energy are depleting very fast due to increased demand in recent years and run short by next half a century. Aiming at to face this problem, scientist's attention has turned towards renewable energy resources.

Primitive man had only his own muscles to help him and convert energy into useful work. He had only two sources of energy: one was the radiant energy of sunlight, which warmed him; the other was the food he ate. The chemical energy in food is the radiant energy of the sun stored up in the cell of plants. In fact the sun was the source of all his energy. Quality of human life has undergone a significant change over the last few decades demanding more and more energy. Out of many options like solar energy, wind energy, tidal wave energy etc., solar energy has received special attention. Apart from the lavish supply in nature this non-conventional form of energy is also free from environmental pollution. Moreover, it can be used in a decentralized manner reducing the cost of transmission and distribution of power. The potential application of solar energy is becoming popular day by day due to public awareness. The practical use of solar energy depends on the collection of insulation and its conversion from thermal energy to electrical energy.

As the demand for more electric power increases and present power plants reach end of life, the need for an environmentally benign means of generating electricity becomes imperative. Conversion of sunlight directly to electricity using photovoltaic (PV) is a means of generating electricity without causing changes to the environment because the fuel consumed is external to the Earth. Photovoltaic technologies are still in their infancy, but have the potential to play an important role

in meeting electric power needs in the next decades, provided that PV systems can be made competitive with conventional power generation and other emerging renewable energy technologies. Present-day crystalline copper indium di-selenide (CIS) technology is approaching its lower limit in terms of production costs. Thin-film photovoltaic modules can be produced by economical, high volume manufacturing techniques, dramatically reducing cost, and are in a pre-manufacturing development stage. However, unlike crystalline CIS, equipment for these technologies is largely unique and custom designed. In addition, the processes involved for making large-area, high-volume, thin-film PV modules are very complex. As a result, the translation of the laboratory results to large-scale manufacturing has been much more difficult than expected [1].

The semiconductive metal chalcogenide represent as interesting class of materials, which are attractive for large-scale applications because of the easy availability, and low cost of the starting materials. In recent years, semiconductive chalcogenide films of different metals have found worldwide application in various fields of science and technology. The utilization of these promising semiconductive materials needs low-cost production and pollution-free techniques. The direct collection of solar energy involves artificial devices, called solar collectors that are designed to collect the energy, sometimes through prior focusing of the sun's rays. The energy, once collected, is used in a thermal or a photoelectric or photovoltaic process. In the photovoltaic process, solar energy is converted directly to electrical energy without intermediate mechanical devices (*by* Photoelectric Effect). Solar cells made from thin slices of crystalline silicon, gallium arsenide, or other semiconductor materials convert solar radiation directly into electricity. Cells with conversion efficiencies in excess of 30% are now available [2]. By connecting large numbers of these cells into modules, the cost of photovoltaic electricity has been reduced to very low. Current use of solar cells is limited to remote, unattended low-power devices such as buoys and equipment aboard spacecraft.

The origin of solar cells can be traced back to 1839 and Becquerel's discovery of a photovoltage when light was shone on an electrode in an electrolyte solution [3,4]. Adams and Day [3] reported a similar effect in solid selenium material in 1877. Subsequent work on selenium and copper oxide led to development of the selenium

solar cell and its wide use in photographic exposure meters. By 1914 selenium solar cells had reached about 1% efficiency in directly converting sunlight into DC electricity. The modern semiconducting solar cells began in 1954. Chapin et al. reported 6% conversion efficiency for a single-crystal silicon cell [5], and Reynolds et al. reported 6% efficiency from what was later understood to be a copper sulfide/copper selenide/cadmium sulfide cell [6].

The major advantage of the use of thin films over bulk materials are; reduction of material consumption, lower energy requirements for the fabrication process and the large number of possibilities for integrated module structures, which can be developed via tailoring of the deposition parameters. Thin film photovoltaic modules have the potential for large scale and economic power generation. Most of the previous work carried out was involved II-VI materials such as CdS, III-VI materials have found application in opto-electronics and photovoltaic device; and have characterized intermediate band gaps (e.g. 2.07 eV) [7].

The optical properties of usual interest are reflectance, transmittance, absorptance and index of refraction etc [8]. An ideal solar window layer thin film would be one that highly conductive but high transmittance and low reflectance. Taking this point into consideration, it was decided to develop thin films as window layer for solar cell application.

Copper selenide exists in widely differing crystallographic modifications even at room temperature. This includes various structures depending on the method of preparation. The techniques adopted for deposition of this metal chalcogenide vary from reaction of metallic copper with selenium dissolved in an aqueous medium [9] or a benzene medium [10], flash evaporation [11], vacuum evaporation [12,13], melting of Cu and Se [14,15] and electrodeposition [16], to the simplest method of chemical bath deposition (CBD) [17-26]. The perspectives of the CBD technique to obtain thin films of metal sulfides and selenides for solar energy applications developed. The composition of the chemically deposited thin films using selenosulfate as the source of selenide ions has been reported as CuSe in references [17,18], and as $Cu_{2-x}Se$ in reference [27]. The films obtained using N, N-dimethylselenourea as the source of selenide ions is reported to be of CuSe

composition [28]. There has also been a report that depending on the selenosulfate to copper-ion ratio in the bath either Cu_2Se or CuSe may be obtained [19].

1.2 REVIEW OF THE PREVIOUS RESEARCH WORKS

During the last few years several authors reported the properties of copper selenide thin films deposited by different method. Here in this section a survey on the reported works are given.

A phase transformation from orthorhombic copper (I) selenide to its cubic (super conducting) structure has been carried out at room temperature by controlling the parameters of the electroless deposition by Haram and Santhanam [9]. They found a direct band-gap semiconductor with a band gap of 1.31 eV and heaving a resistivity of 0.52×10^{-3} Ω-cm at 296K.

Ellis studied thin film of $Cu_{1.8}Se$ prepared by flash evaporation technique and found that for a 297 μm film thickness the resistivity were 1.6×10^{-4} Ω-cm and absorption coefficient were 1.18×10^{3} cm^{-1} [10].

Tell and Wiegand reported the photo detection characteristics of heterojunction formed by vacuum evaporation of *p*-type Cu_2Se on *n*-type $AgInSe_2$ substrates [11]. They found that in the dark, the structure exhibits reasonable diode characteristic and under illumination, the diode characteristic deteriorate resulting in a dramatic increase in reverse current.

Shafizade *et al.* have studied the phase transformation of cubic CuSe to $Cu_{2-x}Se$ (cubic) and then to Cu_2Se (cubic) by slow heating [12]. Cubic Cu_2Se can be transformed back to orthorhombic CuSe potentiostatically.

Herman and Fabick studied the preparation (emphasizing thin-film deposition) and characterization of semiconducting materials such as $Cu_{2-x}S$, $Cu_{2-x}Se$, CdTe and $CuInSe_2$ [13]. Photovoltaic device characteristics of these absorbers with heterojunction partners such as CdS were also studied. A 5.3% efficiency of CVD Au/n-CdTe Schottky barrier cell is described, and cell efficiencies exceeding 4% for vacuum evaporated CdS/Cu_2Se and chemically sprayed CdS/CdTe cells were found.

Yamamoto and Kashida studied the structures of the antifluorite-type copper chalcogenide Cu_2Se using single crystal XRD data both below and above the

transition point [14]. They found using the cubic indexing main reflections, the average structure of the compounds were refined by least squares method: a face centered arrangement of the chalcogen atoms was assumed and copper atoms were distributed at the tetrahedral, trigonal and octahedral interstitial sites, and their relative populations were refined The refined occupation ratios of the cations at the tetragonal and trigonal sites is 0.37 and 0.63 for Cu_2Se.

Okimura *et al.* reported the electrical properties of $Cu_{2-x}Se$ thin films and their application for solar cells [15]. They deposited $Cu_{2-x}Se$ thin films on glass substrate by vacuum evaporation method and found *p*-type conduction with low resistivity, which has a maximum solar efficiency of 8.8%.

Massaccesi *et al.* studied thin film using the reaction accompanying the electrodeposition of binary copper selenium compounds from cupric sulfate and selenious acid solutions by voltammetry [16]. The deposition composition were determined by the fluxes of the Cu (II) and Se (IV) species arriving at the electrode in a relatively narrow potential range, from –0.5 to 0.8 V for mercurous sulfate electrode (MSE). They also found that for the more negative potential, only Cu_2Se phase is obtained as a solid by nonadherent compound.

Mondal and Pramanik observed the effect of bath parameters on chemically deposited thin films of copper selenide and found that an initial induction period of about half an hour to one hour is required after which film deposition starts [17, 18]. They also found that an optimum amount of the selenosulfate solution is required to deposit the thickest film and with the increases of solution temperature the rate of deposition of CuSe increases.

Grozdanov presented a simple and low cost electroless technique to deposited thin film on small and large substrate of different material like CdSe, CdS, $Cu_{2-x}Se$ etc [19]. Depending on the deposition time and the individual system of preparation, films of upto 0.3μm were found and optical energy gaps, sheet resistance and type of conductivity for each kind of thin film were also reported. It was found that for 0.1μm thickness of $Cu_{2-x}Se$ thin films have polycrystalline phase with energy gap of 2.33 eV, sheet resistance of 300 Ω/cm and of *p*-type conductivity.

Lakshmi *et al.* observed different phases of copper selenide thin films by controlling bath parameters [20]. Thin films of cubic $Cu_{2-x}Se$ and tetragonal Cu_3Se_2,

of band gaps 2.20 and 2.83 eV, respectively, have been prepared using the CBD technique by adjusting the bath parameter like pH, temperature and the ratio between copper and selenium atoms in the reaction bath. The grain size was found about 0.3–0.4 μm. The band gap of the $Cu_{2-x}Se$ and Cu_3Se_2 phase was found to be 2.20 and 2.83 eV, respectively. They have also reported the phase conversion of $Cu_{2-x}Se$ and Cu_3Se_2 thin films prepared using the CBD technique [21]. With aging the $Cu_{2-x}Se$ phase gets converted to the Cu_3Se_2 phase along with the formation of copper oxide impurity. The Cu_3Se phase is stable in ambient condition but unstable at temperature above 140°C where it reveals to the $Cu_{2-x}Se$ phase. This inter phase conversion is found to be cyclic.

Clement *et al.* deposited $Cu_{2-x}Se$ thin film on inert Pt substrate using CBD containing bath at 75°C [22]. They found the lattice parameter of the fcc $Cu_{2-x}Se$ increases from 5.742 to 5.761 Å due to the decrease of the concentration of Cu vacancies upon electrochemical polarization. They found transformation of the cubic to an orthorhombic phase starts to occur when copper vacancies reach a critical value of $x<0.15$. They also reported the electrochemical transformation of cubic phase of copper (I) selenide back to the orthorhombic phase. Inter phase conversion of copper (I) selenide and copper (II) selenide is also possible.

Nair *et al.* presented the basic concepts underlying the CBD technique of good quality thin films of CdS, CdSe, ZnS, ZnSe, PbS, SnS, Bi_2S_3, Bi_2Se_3, Sb_2S_3, CuS, $Cu_{2-x}Se$ etc [23,24]. The effects of annealing the films in air on their structure were also reported. This involves to very small substrate separation, 0.1 mm, to eliminate the passive layer of the bath mixture is held by surface tension between pairs of substrate. The final thickness estimated for the films is about 40-50 nm. The electrical and optical properties of these films are presented to illustrate that at such film thickness they fulfill the requirements for certain applications. The sheet resistance of the $Cu_{2-x}Se$ film was found 700 Ω that for a film thickness of 40 nm indicate an electrical conductivity of 360 $\Omega^{-1}cm^{-1}$.

García *et al.* reported on the structural, electrical and optical properties of thin films of copper selenide obtained from CBD method and the changes brought about in these properties during thermal treatment at 200–400°C in air and vacuum [25,26].

They found the high near infrared reflectance (30-80%) and low transmittance of the films are related to a high p-type electrical conductivity ~ (1-5) x 10^3 $W^{-1}cm^{-1}$.

Padam reported the preparation and characterization method of CBD $Cu_{2-x}Se$ thin films on glass substrates and found that the film showed p-type conductivity [27]. The film also showed the cubic (berzelianite) phase with resistivity ranged from 0.1 to 2×10^{-2} Ω-cm and with a direct optical band gap of 1.20 eV.

Estrada *et al.* present CBD techniques for CuSe thin films using N, N-dimethyleselenourea as a source of selenide ion [28]. Films of 0.1 to 0.3 μm in thickness of CuSe were obtained in 2 to 10h depositions at 50°C and found deposition times higher than 10h resulted in peeling of the films during rinsing. The optical band gap of this film was found ~2.63eV and the sheet resistance ~10^3 Ω/m^2 for ~0.13μm thickness for 3h deposition time.

Lazcano *et al.* reported the deposition of thin films of sulfide and selenide of antimony from chemical baths containing $SbCl_3$ and source of sulfide or selenide ions in presence of legends forming soluble complexes with antimony [29]. As prepared, the films are of poor crystalline and show larger band gaps (e.g., 2.2 eV in the case of Sb_2S_3) than those reported for the material in bulk. However, the films after annealing in nitrogen around 350°C show well-defined peaks in their X rays diffraction patterns.

1.3 AIM OF THE PRESENT RESEARCH WORKS

Thin film modules of various materials are likely going to increase their share of the growing photovoltaic industry. Amorphous silicon modules have been manufactured already for several years but for the high cost deposition techniques have given them somewhat bad reputation. CdTe and $CuInSe_2$ modules are shortly entering the market for low cost and high efficiency.

In this work our aim was to prepare copper selenide thin films using a simple and low cost technique. The results of structural, electrical and optical properties studied on these films are discussed. The clarification of the structure, composition, electrical and optical properties and thermal stability of these thin films is important in the context of its use as a precursor material for forming $CuInSe_2$ thin films, and other multinary materials for thin film technology especially for solar cell application.

Current research efforts are directed towards identifying a low-cost deposition technique for a precursor material from which solar cell grade $CuInSe_2$ can be produced. Such a very simple and low cost chemical bath deposition (CBD) method has been developed in our laboratory and used for the preparation of copper selenide thin film. Here we report the structural, electrical and optical properties of $Cu_{2-x}Se$ and Cu_3Se_2 thin films by CBD technique on microscopic glass substrate.

Surface morphology of the deposited film has been characterized by Atomic Force Microscopy (AFM). Structural properties and chemical compositions have been investigated by X-ray Diffraction (XRD) and X-ray Photoelectron Spectroscopy (XPS), respectively. The electrical properties by I–V characteristics from which resistivity of the materials has been estimated; Hall effect from which Hall coefficient, Hall mobility, types of carrier and carrier concentration have been evaluated; absorption method for direct and indirect energy gap measurements. Transmittance, reflectance and absorption co-efficient measurements were also performed for optical analysis.

1.4 OUTLINE OF THE THESIS

The dissertation is organized below:

Chapter-1. Introduction, which described the introductory concepts of the work; such as the background of the work, review of the previous research work and the aim of the present work.

Chapter-2. Materials and deposition method, which describes the basic fundamentals of copper selenide materials. This chapter contains a brief description about the concept of different deposition techniques.

Chapter-3. Principle of characterization method, various characterizations method such as AFM, XPS, XRD, electrical and optical properties are described.

Chapter-4. Experimental, is on experimental work. It is divided into two broad sections. One deals with the setups used for different experiments whereas the other deals the experimental procedure. Necessary circuit diagrams have been included in this chapter.

Chapter-5. Results and discussion, contains the experimental results with necessary graphs and discussion.

Chapter-6. Conclusion is the final chapter. It contains the summary of the present work with the suggestions for future researchers in this field.

REFERENCES

1. R. W. Birkmire, Compound Polycrystalline Solar Cells. Final Report, Institute of Energy conversion, University of Delware, USA. 16 Feb., 2002.
2. R. S. Thorsen, Microsoft Encarta Encyclopedia 2000.
3. L. D. Partain, Solar cells and their applications. John Wiley & Sons, Inc., 1995.
4. A. L. Fahrenbruch and R. H. Bube, Fundamentals of Solar Cells, Academic Press, New York 1983.
5. D. M. Chapin, C. S. Fullar and G. L. Person, *J. Appl. Physol.*, **55** (1954) 676.
6. D. C. Reynolds, G. Leies, L. T. Antes and R. E. Narburger, *Phys. Rev.*, **96** (1954) 533.
7. M. Lazell, P. O,' Brien, D. J. Olway and J. H. Park, *Mat. Res. Soc. Symp. Proc.*, **127** (2000) 606.
8. H. P. Garg. Treatise on Solar Energy, Volume-**1**, Fundamental of Solar Energy, A Wiley Inter Science Publication, 1982.
9. S. K. Haram and K. S. V. Santhanam, *Thin Solid Films*, **238** (1994) 21.
10. S. G. Ellis, *J. Appl. Phys.*, **38** (1967) 2906.
11. B. Tell and J. J. Wiegand, *J. Appl. Phys.*, **48** (1977) 5321.
12. R. B. Shafizade, I. V. Ivanova and M. M. Kazinets, *Thin Solid Films*, **55** (1978) 211.
13. A. M. Herman and L. Fabick, *J. Cryst. Growth*, **61** (1983) 658.
14. K. Yakamoto and S.Kashida, *J. Solid State Chem.*, **93** (1991) 202.
15. H. Okimura, T. Matsumae and R. Makabe, *Thin Solid Films*, **71** (1980) 53.
16. S. Massaccesi, S. Sanchez and J. Vedel, *J. Electrochem. Soc.*, **140** (1993) 2540.
17. A. Mondal and P. Pramanik, *J. Solid State Chemistry*, **47** (1983) 81.
18. A. Mondal and P. Pramanik, *J. Solid State Chemistry*, **55** (1984) 116.
19. I. Grozdanov, *Synthetic Metals*, **63** (1994) 213.
20. M. Lakshmi, K. Bindu, S. Bini, K.P.Vijaykumar, C. Sudha Kartha, T. Abe and Y. Kashiwaba, *Thin Solid Films*, **370** (2000) 89.
21. M. Lakshmi, K. Bindu, S. Bini, K.P.Vijaykumar, C. Sudha Kartha, T. Abe and Y. Kashiwaba, *Thin Solid Films*, **386** (2001) 127.

22. C. L. Clement, M. N. Spallart, S. K. Haram and K. S. V. Santhanam, *Thin Solid Films,* **302** (1997) 12.

23. P. K. Nair *Solar Energy Materials and Solar Cells*, **52** (1998) 313.

24. P. K. Nair, V. M. Garcia, O Gomez-Daza and M. S.T. Nair, *Semicond. Sci. Technol.*, **16** (2001) 855.

25. V.M. Garcia, L. Guerrero, M.T.S. Nair and P.K. Nair, *Sociedad Mexicana de Ciencia de Superficies y de Vacio,* **9** (1999) 213.

26. V. M. Garcia, P. K. Nair and M. S. T. Nair, *J. Cryst Growth,* **203** (1999) 113.

27. G. K. Padam, *Thin Solid Films*, **150** (1987) L89.

28. C. A. Estrada, P. K. Nair, M. T. S. Nair, R. A. Zingaro and E. A. Meyers, *J. Electrochem. Soc.*, **141** (1994) 802.

29. Y. R. Lazcano, L. Guerrero, O. Gomez Daza, M. T. S. Nair, and P. K. Nair, *Superficies y Vacio* **9** (1999) 100.

CHAPTER 2

MATERIALS AND DEPOSITION METHOD

The properties of copper selenide and various methods of preparation techniques of copper selenide films are described in this chapter.

Copper selenide has been studied with great interest during the past decades because of its potential application in the fabrication of photovoltaic devices. It has many phases and structural forms: stoichiometric α-Cu_2Se, Cu_3Se_2, CuSe, and $CuSe_2$, as well as non-stoichiometric, $Cu_{2-x}Se$. The thermal stability of these compounds varies depending on the composition. Copper selenide is a semiconductor with p-type conductivity, properly useful in the solar cell production. The direct and indirect band gap of about ~2 and ~1.5 eV respectively, being near the optimum value for solar cell applications [1]. These stoichiometric and nonstoichiometric materials could offer a high efficiency of conversion. The use of these films to form a junction with n-type semiconductors either as absorber in heterojunction with CdS or as window material in heterojunction with n-Si has been demonstrated [2-4], showing conversion efficiencies of up to 8.8%. This is the main motivation to study copper selenide thin films.

2.1 PROPERTIES OF COPPER SELENIDE

Among the various compound semiconductor materials, copper selenide show great potential for application to thin film solar cell particularly promising in technology based on $Cu_{2-x}Se$. The major characteristic of $Cu_{2-x}Se$ has a direct and an indirect band gap, high electron mobility, and high electron saturation velocity. These properties make $Cu_{2-x}Se$ technology a practical and even superior alternative to silicon-based solar cell.

Copper selenide is one of many compound semiconductors that have electrical and optical properties for photovoltaic device. These semiconductors, especially $Cu_{2-x}Se$, are used mainly for ternary compound $CuInSe_2$ as a window material for solar cell application. Although we do not know as much about the technology of

compound semiconductors as we do about that of silicon, compound semiconductor technology has advanced partly because of the advances in silicon technology. It is in recent years that $Cu_{2-x}Se$ thin films have excited some interest for solar cell applications, and the literature on these materials is, therefore, sparse. Thin films of $Cu_{2-x}Se$ have been prepared mainly by evaporation [5]. $Cu_{2-x}Se$ exists in several phases and the properties of the films depend very strongly on the stoichiometry, which is governed, by the deposition conditions.

2.1.1 Structural Properties

Bulk material of $Cu_{2-x}Se$ is recorded as cubic structure with lattice constant 5.852 Å and indirect band gap type with E_g=1.4 eV [3]. Shafizade et al. [6] have observed that during heat treatment in vacuum at temperatures below 350°C, CuSe undergoes consecutive phase transformation according to the lattice parameter a of the fcc $Cu_{2-x}Se$ varies in the range 5.68-5.75Å, corresponding to

$$CuSe \xrightarrow{100\text{-}300^\circ C} \underset{\substack{\text{fcc}\\ a=5.68\text{-}5.75\text{Å}}}{Cu_{2-x}Se} \xrightarrow{300^\circ C} \underset{\substack{\text{fcc}\\ a=5.84\text{Å}}}{Cu_2Se} \xrightarrow{\text{cool to room temperature}} \underset{\text{low-temperature modification}}{Cu_2Se}$$

the composition range from $Cu_{1.4}Se$ to $Cu_{1.75}Se$. An ordered low-temperature phase of Cu_2Se exists in the range from $Cu_{1.7}Se$ to Cu_2Se. At temperature above 350°C, CuSe decompose onto two fcc phases with a = 5.84 and 5.65 Å. On cooling to room temperature, two phases are observed to coexist, a low-temperature modification of Cu_2Se and an independent fcc phase with a = 5.63 Å, corresponding to an approximate composition of $Cu_{1.15}Se$. Epitaxial films [7] of the low- temperature modification of Cu_2Se deposited onto NaCl single crystal substrate at 200 and 400°C have been indexed on the basis of a hexagonal lattice with unit cell parameters a =7.07 and c = 6.68 Å. Buldhaupt et al. have reported single phase fcc Cu_2Se thin films at the substrate temperature range of 150 to 275°C [4]. At higher substrate temperatures, the film composition is observed to be less depending on the Se deposition rate (provided that this rate is above a threshold value). The grain size of

the films has been measured to be of the order of 1 μm. Figure 2.1 shows the cubic crystal structure of pure Cu and Fig. 2.2 the *h.c.p* structure of pure Se.

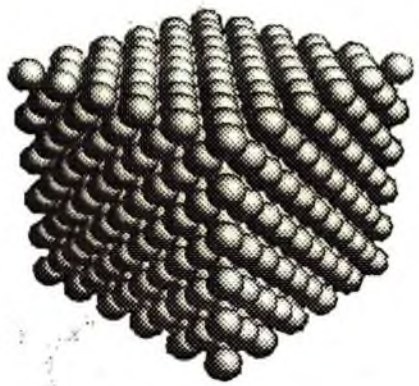

Fig. 2.1. Crystal structure of pure Cu.

Fig. 2.2 Crystal structure of pure Se.

2.1.2 Electrical Properties

Hall and resistivity measurement indicate that Cu_2Se is a *p*-type with a hole mobility of 10 $cm^2V^{-1}s^{-1}$ and a hole concentration of 2×10^{21} cm^{-3}, at a composition of $Cu_{1.8}Se$ [4].

2.1.3 Optical Properties

From the spectral dependence of the absorbance $Cu_{2-x}Se$ films exhibit an indirect band gap of 1.4 eV and direct band gap of 2.2 eV [4]. The clarification of the structure, composition, optical and electrical properties and thermal stability of chemically deposited $Cu_{2-x}Se$ thin films is important in the context of its use as a precursor material for forming $CuInSe_2$ thin films, and other multinary materials for thin film solar cell application [8,9].

2.2 DEPOSITION METHOD

Thin film can be prepared by many physical and chemical techniques. In this section, we describe briefly some of the commonly used methods for depositing large area thin film on a variety of commercially available substrates. The physical

techniques are vacuum evaporation, sputtering, spraying and painting while vapor deposition, oxidation, immersion plating, chemical bath deposition and electroplating are called chemical techniques.

2.2.1 Physical Techniques

2.2.1.1 Vacuum Evaporation Method

In this method material is first thermally vaporized and then condensed on a substrate. Among the numerous deposition parameters substrate temperature, evaporation rate and the vacuum quality affect the microstructure and surface morphology of the coatings. Thermal evaporation technique allows precise control over the film thickness. Hence by sequential evaporation with a good control over thickness multiplayer interface stacks of any complexity can be prepared with great precision.

The evaporation of a material required to be heated at sufficiently high temperature to produce the desired vapor pressure. The rate of free evaporation of vapor atoms from a clean surface of unit area in vacuum is given by the Langmuir–Dushman kinetic theory equation [3]:

$$N_e = 3.513 \times 10^{21} P_e / (MT)^{1/2} \qquad [\text{molecules cm}^{-2}\text{s}^{-1}]$$

where P_e is the equilibrium vapor pressure (in torr) if the evaporant under saturated-vapor conditions at a temperature T, and M is the molecular weight of the vapor species. The vapor atoms traverse the medium and are made to condense on a substrate surface to form a thin film. The rate of condensation/deposition of the vapor atoms depends on the vapor source substrate geometry and the condensation coefficient on the surface under given physical condition.

The temperature of a material for evaporation may be raised by direct or indirect heating. The simplest and most common method is to support the material in a filament or on a boat, which is heated electrically. Many shapes and sizes of filaments and boats of a number of materials are commercially available to suit a range of evaporation materials and applications. The geometrical distribution of vapors from several standard sources is well known and is described in textbooks.

Multiple evaporation sources are essential for multiplayer technology as well as for obtaining controlled composition alloys/semiconductors. Besides controlling the vapor pressure of the constituents, the substrate temperature provides an important control over the relative sticking coefficients and thermodynamic stability of the different vapor species. Thus a multiple source and temperature technique is ideally suited for preparing films of well-defined composition multicomponent semiconductors and has been used extensively for IV-VI, II-VI, and III-V compound films.

Vacuum evaporation requires a system with a known vacuum and its residual gas analysis. A diffusion pump backed by a rotary pump system continues to be the 10^{-6}–10^{-8} torr workhorse in thin film technology largely because of its modest price, simplicity, and high speed. By using special diffusion pump oil (e.g., polyphenyl ether), a cryogenic baffle, and an all-metal system, ultrahigh vacuum (UHV) in the range $10^{-8} - 10^{-10}$ torr are easily obtained.

Vapor species may be created by kinetic ejection from the surface of a material (called target of cathode) by bombardment with energetic and nonreactive ions. The ejection process, known as sputtering, takes place as a result of momentum transfer between the impinging ions and the atoms of the target surface. The sputtered atoms are condensed on a substrate to form a film. The major advantage of this method is that almost any material can be sputter deposited at a high deposition rate compared to evaporation methods. Moreover advantage of the sputtering techniques is that the composition of the sputtered film is nearly the same as that of the method and that the rate of deposition remains constant with time.

2.2.1.2 Spray Pyrolysis

The spray technique involves spraying a solution, usually aqueous, containing soluble salts of the constituent atom of the desired compound onto a heated substrate maintained at elevated temperatures. The sprayed droplet reaching the hot substrate surface undergoes pyrolytic (endothermic) decomposition and forms a single crystallite or a cluster of crystallites of the product. The other volatile byproducts and the excess solvent escape in the vapor phase. The substrate provides the thermal energy for the thermal decomposition and subsequent recombination of the

constituent species followed by sintering and recrystallization of the clusters of crystallites giving rise to a coherent film. This method is cheaper and more convenient.

2.2.1.3 Painting

This is a simple and cheap method of producing selective coating. This can be applied directly on the finished substrate with a brush. The spectral properties of a selective paints depends upon the optical properties of pigments, the particle size and the multiple scattering effect within the pigment binder composite.

2.2.2 Chemical Techniques

2.2.2.1 Chemical Vapour Deposition (CVD)

In this technique, the formation of the films is due to the heterogeneous reaction-taking place at or near the substrate surface. The reactants are in gaseous form and leave a non-volatile product behind. The nature of the film deposited is strongly influenced by the nature of the chemical reaction. The deposition takes place generally at atmospheric pressure. The high temperature of deposition helps in the elimination of stress and delimitation of the coating.

Anodization is an electrolytic oxidation process in which a metal is made the anode in a suitable electrolyte so that when an electric current is passed through the electrolyte, the metal surface is converted to its oxide. Depending upon the solvent action of the selected electrolyte on the anodic oxide and the operating conditions employed a porous anodic oxide film can be grown on the anode. By carrying out electrolysis of this anode film in a metallic salt solution fine metal particles can be embedded in the pores of the anodic oxide film, giving rise to a black colouration to the coating. The operating parameters like composition of the electrolyte, temperature and time have to be optimized to get good selectivity. If a substrate consisting of a noble metal let M_1 is immersed in a solution containing ions of more noble M_2, the more noble metal ions displace the less noble metal at the substrate surface. The reaction likely is

$$M_1 + M_2 \text{ --- } M_2 + M_1$$

The metallic ions taking part in this exchange reaction can partly get oxidized in the presence of suitable oxidizing species in the solution. The optical behavior of the coating is determined by the pH and concentration of the bath and dipping time.

2.2.2.2. Electroplating

Electroplating is one of the most widely used methods to deposit oxide and sulfides on metals. Black nickel and black chrome are the two well-known selective absorbers prepared on commercial scale by electroplating. In the plating process, parameters like pH of the solution, temperature of the bath, current density and plating time effect the micro structure topology and composition of the coatings. By varying the current while plating one can obtain a stack of numerous finely divided layers with a continuous gradient of composition resulting in a continuous gradient of refractive index.

2.2.2.3 Electrodeposition

The occurrence of chemical changes owing to the passage of electric current through an electrolyte is termed electrolysis and the deposition of any substance on an electrode as a consequence of electrolysis is called electrodeposition.

The phenomenon of electrolysis is governed by the following two laws, first enunciated by Faraday in 1833: (i) the magnitude of chemical change occurring is proportional to the quantity of electricity passed and (ii) the masses of different species deposited at or dissolved from electrodes by the same quantity of electricity are in direct proportion to their chemical equivalent weights [10].

The two laws can be combined and expressed mathematically as

$$W = IE_t/F$$

where W is the mass (in grams) of the substance deposited, I is the current (in amperes), E is the chemical equivalent weight (in grams), and t is the reaction time (in seconds). F is a constant called the Faraday, equal to 96500 C and is the amount of charge required to deposit one equivalent of any ion from a solution.

In a laboratory, a low cost electrodeposition method can be easily developed and used for the preparation of copper selenide thin film. This method is not only simple but also has optimum material utilization rate and low energy consumption.

Since the materials are dissolved in a solution and the deposition process is carried out at a relatively low temperature, potential safety hazard during the deposition in minimized. In addition, the deposition system can be easily scaled up for large area film deposition.

2.2.2.4 Chemical Bath Deposition (CBD)

Chemical bath deposition (CBD) is a method of growing thin film of certain materials on a substrate immersed in an aqueous bath containing appropriate reagents at temperatures ranging from room temperature to 100°C. The CBD technique was first used in 1946 [11] to prepare PbS films for infrared applications. It is only recently [12–15] that large-area and large-scale applications of this technique to obtain doped and undoped multicomponent semiconductor films of usual, unusual, and metastable structures have necessiated an understanding of the Physics and Chemistry of the process involved. This full-fledged technique, of great future promise, is the subject of this section.

According to the solubility product principle, in a saturated solution of a weakly soluble compound, the product of the molar concentrations of its ions (each concentration term being raised to a power equal to the number of ions of that kind shown by the formula for the compound), called theionic product, is a constant at given temperature. For example, $CuCl_2$ when added to water will hydrolyze according to the reaction

$$CuCl_2 \longrightarrow Cu^{2+} + 2Cl^-$$

Selenide films [16,17] are obtained by replacing thiourea by selenourea or its other derivatives. Kainthla et al. have generated Se^{2-} ions by dissolving inorganic sodium selenosulfate in an alkaline solution [14] as given by the following reaction:

$$Na_2SeSO_3 + 2OH^- \longrightarrow Na_2SO_4 + H_2O + Se^{2-}$$

This method has the advantage that sodium selenosulfate can be easily synthesized by dissolving Se in Na_3SO_3 solution. On the other hand, selenourea and

derivatives are difficult to synthesize and further, their aqueous solution have to be stabilized using antioxidants like Na_2SO_3.

The technique of CBD involves the controlled precipitation from solution of a compound on a suitable substrate. The technique offers many advantages over the more established vapor phase synthetic routes to semiconductor materials, such as CVD, MBE and spray pyrolysis. Varying the solution pH, temperature and reagent concentration allies' factors such as control of film thickness and deposition rate by varying the solution pH, temperature and reagent concentration with the ability of CBD to coat large areas, in a reproducible and low cost process. In addition, the homogeneity and stoichiometry of the product are maintained partly by the solubility product (Ksp) of the material in question. In CBD, two processes are traditionally used for film growth: single dip, where the substrate is immersed in the reaction bath only once, and multiple dips, where the same substrate is repeatedly coated to obtain thicker film. In our case we use single dip for depositing film.

Typical CBD processes for selenides employ an alkaline media containing the chalcogenide source, the metal ion and added base. A chelating agent is used to limit the hydrolysis of the metal ion and impart some stability to the bath, which would otherwise undergo rapid hydrolysis and precipitation. The technique under these conditions relies on the slow release of Se^{2-} ions into an alkaline solution in which the free metal ion is buffered at a low concentration.

A major drawback of the CBD process is the inefficiency of the process, in terms of the utilizations of starting materials and their conversion to thin films. The extent of the heterogeneous reaction on the substrate surface is limited by two major factors, the competing homogeneous reaction in solution (which results in massive precipitation in solution) and deposition of material on the CBD reactor walls. We are developing CBD processes for the preparation of $Cu_{2-x}Se$ thin films for using as window materials in for solar cell application. The large-scale exploitation of these devices is partly dependent on a reduction of the potential environmental impact of the technology. In the $Cu_{2-x}Se$ thin film for CIS solar cell are deposited with chemical bath deposition. The chemical bath deposition or electroless technique is based on the reaction of a copper salt, a complexing agent and a selenide compounds in an aqueous solution. The process therefore relies on slow release of Cu^{2+} ions and Se^{2-} ions in

solution. The formation of $Cu_{2-x}Se$ takes place heterogeneously on a suitable substrate placed in the bath and homogeneously in the solution.

REFERENCES

1. J. J. Loferski, *J. Appl. Phys.*, **27** (1956) 777.
2. H. Okimura, T. Matsumae, and R. Makabe, *Thin Solid Films*, **71** (1980) 53.
3. K. L. Chopra and S. R. Das, *Thin Film Solar Cells*, Plenum Press, New York (1983).
4. L. F. Buldhaupt, R. A. Mickelson, J. M. Stewart, and W. S. Chen, Emerging Materials Systems for Solar Cell Applications $Cu_{2-x}Se$, Boeing Aerospace Company, Final Report DE-AC04-79Et-23005 (April 1980).
5. A. L. N. Stevels and F. Jellinek, *Recueil*, **111** (1971) 273.
6. R. B. Shafizade, I. V. Ivanova and M. M. Kazinates, *Thin Solid Films*, **55** (1978) 211.
7. R. B. Shafizade, I. V. Ivanova and M. M. Kazinates, *Thin Solid Films*, **35** (1976) 169.
8. P. K. Nair, M. T. S. Nair, V. M. García, O. L. Arenas, Y. Peña, A. Castillo, I. T. Ayala, O. Gomezdaza, A. Sánchez, J. Campos, H. H. R. Suárez, and M. E. Rincón, *Sol. Energy Mater. Sol. Cells*, **52** (1998) 313.
9. R. N. Bhattacharya, J. E. Granata, W. Batchelor, F. Hasoon, H. Wiesner, K. R. Ramanathan, J. Keane, and R. Noufi, *Proc. SPIE*, **90** (1997) 2531.
10. S. Massaccesi, S. Sanchez and J. Vedel, *J. Electrochem. Soc.*, **140** (1993) 2540.
11. R. J. Cashman, *J. Opt. Soc. Am.*, **36** (1946) 356.
12. N. C. Sharma, D. K. Pandya, H. K. Sehgal and K. L. Chopra, *Mater. Res. Bull.*, **11** (1976) 1109.
13. N. C. Sharma, R. C. Kainthla, D. K. Pandya and K. L. Chopra, *Thin Solid Films*, **60** (1979) 55.
14. R. C. Kainthla, D. K. Pandya and K. L. Chopra, *J. Eletrochem. Soc.*, **127** (1980) 77.
15. I. Kaur, D. K. Pandya and K. L. Chopra, *J. Eletrochem. Soc.*, **127** (1980) 943.
16. A. B. Lundin and G. A. Kitaev, *Inorg. Mater.*, **1** (1965) 2107.
17. D. O. Skovlin and R. A. Zingaro, *J. Eletrochem. Soc.*, **111** (1964) 42.

CHAPTER 3

PRINCIPLES OF CHARACTERIZATION METHODS

In the present experiment, samples were characterized by

a. Atomic Force Microscopy (AFM)
b. X-ray Photoelectron Spectroscopy (XPS)
c. X-ray Diffraction (XRD)
d. Resistivity measurement
e. Hall effect measurement
f. Transmittance, reflectance and absorption coefficient measurements
g. Direct and indirect energy band gaps

The principles of these above methods are briefly explained below.

3.1 SURFACE MORPHOLOGY AND STRUCTURAL CHARACTERIZATION

The optical and electrical properties of thin films are very sensitively influenced by the crystallographic and microstructural characteristics of the film. Similarly, the structural features of the interface at the film also affect the electronic behavior of the photovoltaic materials. Several techniques have been developed which provide image of the morphological, crystallographic, and defect structure of materials component.

3.1.1 Atomic Force Microscopy (AFM)

Scanning probe microscopy (SPM) refers to a class of instruments, which provide very high resolution, three-dimensional surface topography on an increasing variety of samples. The first such microscope was the scanning tunneling microscope (STM) which was invented by Ginnig et al. in 1982 [1]. Hansma et al. wrote a review article on STM [2]. The development of the STM was followed by the invention of the atomic force microscope (AFM) in 1985 [3]. In atomic force microscopy (AFM) it is commonly the repulsive force between the tip (located at the end of a cantilever)

and sample that is measured, on the basis of the cantilever deflection. In this contact-mode AFM, the spatial variation of the tip-sample repulsive force is universal, AFM is applicable to conducting as well as insulating materials. In general, AFM enables one to detect surface morphology, nanoscale structures, and molecular- and atomic-scale lattices [4].

Several forces typically contribute to the deflection of an AFM cantilever. The force most commonly associated with atomic force microscopy is an interatomic force called the van der Waals force. The dependence of the van der Waals force upon the distance between the tip and the sample is shown in Fig. 3.1 [5]. Two distance regimes are labeled on Fig. 3.1: 1) the contact regime; and 2) the non-contact regime. In the contact regime, the cantilever is held less than a few Angstroms from the sample surface, and the interatomic force between the cantilever and the sample is repulsive. In the non-contact regime, the cantilever is held on the order of tens to hundreds of Angstroms from the sample surface, and the interatomic force between the cantilever and sample is attractive (largely a result of the long-range van der Waals interactions).

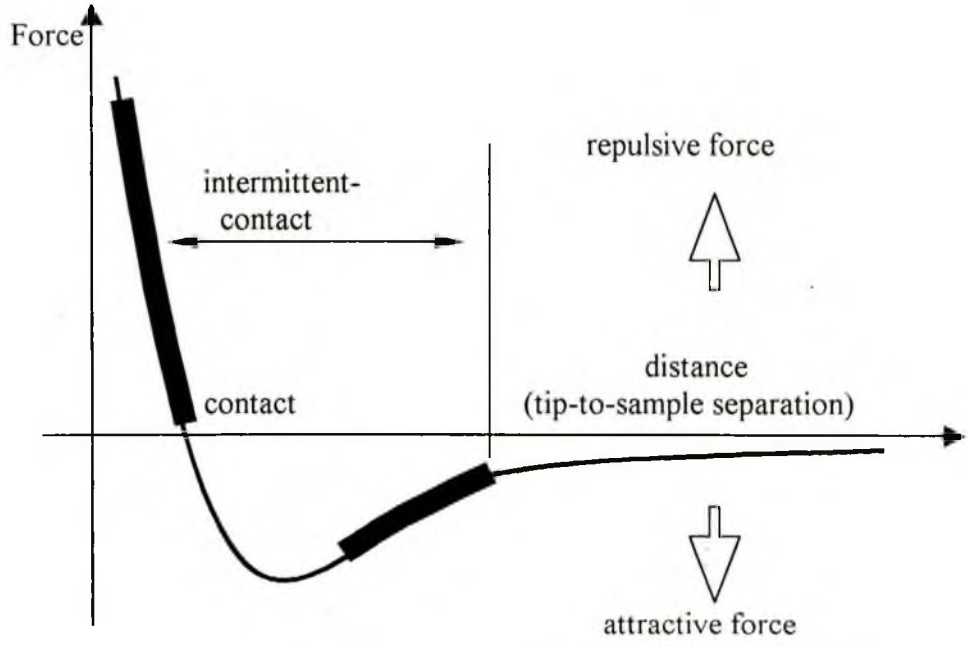

Fig. 3.1. Interatomic force vs. distance curve [5].

In contact-mode AFM, also known as repulsive mode, an AFM tip makes soft "physical contact" with the sample. The tip is attached to the end of a cantilever with a low spring constant, lower than the effective spring constant holding the atoms of the sample together. As the scanner gently traces the tip across the sample (or the sample under the tip), the contact force causes the cantilever to bend to accommodate changes in topography. To examine this scenario in more detail, refer to the van der Waals curve in Fig 3.1.

At the right side of the curve the atoms are separated by a large distance. As the atoms are generally brought together, they first weakly attract each other. This attraction increases until the atoms are so close together that their electron clouds begin to repel each other electrostatically. This electrostatic repulsion progressively weakens the attractive force as the interatomic separation continues to decrease. The force goes to zero when the distance between the atoms reaches a couple of angstroms, about the length of a chemical bond. When the total van der Waals force becomes positive (repulsive), the atoms are in contact.

The slope of the van der Waals curve is very steep in the repulsive or contact regime. As a result, the repulsive van der Waals force balances almost any force that attempts to push the atoms closer together. In AFM this means that when the cantilever pushes the tip against the sample, the cantilever bends rather than forcing the tip atoms closer to the sample atoms.

In addition to the repulsive van der Waals force described above, two other forces are generally present during contact-AFM operation: a capillary force exerted by the thin layer often present in an ambient environment, and the force exerted by the cantilever itself. The capillary force arises when water wicks it way around the tip, applying a strong attractive force (about 10^{-8} N) that holds the tip in contact with the surface. The magnitude of the capillary force depends upon the tip-to-sample separation. The force exerted by the cantilever is like the force of a compressed spring. The magnitude and sign (repulsive or attractive) of the cantilever force depends upon the deflection of the cantilever and upon its spring constant.

As long as the tip is in contact with the sample, the capillary force should be constant because the distant between the tip and the sample is virtually incompressible. It is assumed that the water layer is reasonably homogeneous. The

variable force in contact AFM is the force exerted by the cantilever. The total force that the tip exerts on the sample is the sum of the capillary plus cantilever forces, and must be balanced by the repulsive van der Waals force for contact AFM. The magnitude of the total force exerted on the sample varies from 10^{-8} N to the more typical operating range of 10^{-7} to 10^{-6} N.

3.1.2 X-ray Photoelectron Spectroscopy (XPS)

Surface analysis by X-ray photoelectron spectroscopy (XPS), more commonly known as electron spectroscopy for chemical analysis (ESCA), is accomplished by irradiating a sample with monoenergetic soft X-rays and analyzing the energy of the electrons emitted. Mg Kα X-rays (1253.6 eV) or Al Kα X-rays (1486.6 eV) are ordinarily used. These photons have limited penetration power in a solid, of the order of 1-10 micrometers. They interact with atoms in this surface region by the photoelectric effect, causing electrons to be emitted. The emitted electrons have kinetic energies given by:

$$KE = h\nu - BE - \varphi_S$$

where $h\nu$ is the energy of the photon, BE is the binding energy of the atomic orbital from which the electron originates, and φ_S is the spectrometer work function.

The binding energy may be regarded as ionization energy of the atom for the particular shell involved. Since there are a variety of possible ions from each type of atom, there is a corresponding variety of kinetic energies of the emitted electrons. Moreover, there is a different probability, or cross-section, for each process.

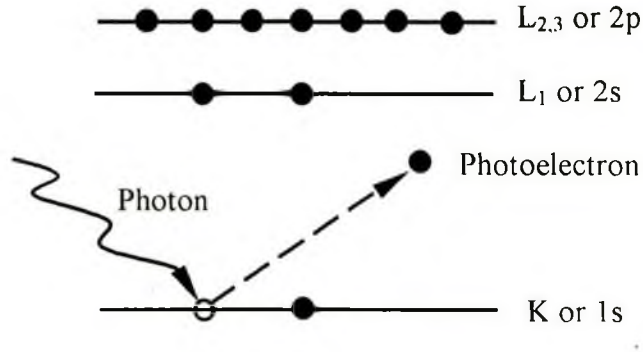

Fig. 3.2. Diagram of the photoelectric process.

In addition to the photoelectrons emitted in the photoelectric process, Auger electrons are emitted due to relaxation of the energetic ions left after photoemission. This Auger electron emission occurs roughly 10-14 seconds after the photoelectric event. In the Auger process, shown in Fig. 3.2, an outer electron falls into the inner orbital vacancy, and a second electron is emitted, carrying off the excess energy. The Auger electron possesses kinetic energy equal to the difference between the energy of the initial ion and the doubly-charged final ion, and is independent of the mode of the initial ionization. Thus, photoionization normally leads to two emitted electrons, a photoelectron and an Auger electron. Of course, the energies of the electrons emitted cannot exceed the energy of the ionizing photons.

Probabilities of interaction of the electrons with matter far exceed those of the photons, so while the path length of the photons is of the order of micrometers, that of the electrons is of the order of tens of Angstroms. Thus, while ionization occurs to a depth of a few micrometers, only those electrons that originate within tens of Angstroms below the solid surface can leave the surface without energy loss. It is these electrons, which produce the peaks in the spectra and are most useful. Those that undergo loss processes before emerging from the background.

3.1.3 X-ray Diffraction (XRD)

X-ray diffraction [6,7] is the most precise technique for studying the crystal structure of solids, generally requiring no elaborate sample preparation and is essentially nondestructive. Thin surface films, up to about 1000 Å thick, can be investigated using X-ray diffraction [8,9]. Thicker films can be characterized by reflection high-energy electron diffraction (RHEED). Analysis of the diffraction patterns obtained by these techniques and comparison with standard ASTM data can reveal the existence of different crystallographic phases in the film, their relative abundance, the lattice parameters, and any preferred orientations. From the width of the diffraction line, it is possible to estimate the average grain size in the film [6].

The term structure encloses a variety of concepts, which describe on various scales, the arrangement of the building blocks of materials. On an atomic scale, one deals with the crystal structure, which is defined by the crystallographic data of the unit cell. These data contain the shape and dimensions of the unit cell and the atomic

position within its Bravias structure. They are obtained by diffraction experiments. On a coaster scale, one deals with the microscopic observations of the microstructure, which characterizes the size, shapes and mutual arrangements of individual crystal grains. It also includes the morphology of the surface of the materials. Microstructure and surface morphology observation of coatings, which are too thick for direct transmission also depend heavily on the high resolving power of electron microscopy. Suitable technique is surface replication and scanning electron microscopy [9-12]. Frequently one has to determine whether a given deposit is a single crystal or polycrystalline either with a random distribution of orientation with respect to the coating plane. For a single crystal coating, it is important to know its orientation relationship with respect to the substrate [13]. X-ray diffraction is a suitable tool to determine the crystal structure of any unknown materials, whether the sample is a single crystal or polycrystals [6], either with a random distribution of orientations or with a preferred orientation with respect to the film plane.

3.2 ELECTRICAL CHARACTERIZATION

Electrical characterization of a semiconductor involves determination of the resistivity ρ, mobility of carriers (μ_n or μ_p), the carrier concentration (n or p), the Hall coefficient (R_H).

The techniques for measuring ρ, μ, and n are quite well known and have been documented in the literature [14,15]. The measurement methods commonly employed include: (i) two-point method for resistivity, (ii) linear four-probe method for resistivity, (iii) spreading resistance method for resistivity (iv) Vander Pauw technique for resistivity; (v) Hall effect measurements, Hall coefficient, and Hall mobility, and (vi) Haynes-Shockley method for mobility.

3.2.1 Dark Conductivity

In order to record the change in conductivity before and after the illumination of the sample, conductivity must be measured before illumination, preferably in dark. The method of measurement of conductivity depends on many factors, such as size of the sample, thickness of the sample and shape of the sample. Among few important

methods that are used in the laboratory, here we describe only the direct method in brief.

Direct Method / Two Electrode Method

In this method, a voltage V is applied to the sample of known geometry and the resultant current I is measured in the external circuit. It gives the conductivity from the formula

$$\sigma = \left(\frac{I}{V}\right)\frac{l}{A} \qquad (3\text{-}1)$$

Where A is the cross sectional area and L is the length of the sample. But the value of σ is obtained may not be the characteristic of the material between the electrode for two reasons:

(i) A resistance at the interface between the sample and the electrode will result in the voltage drop across the sample being less than the applied voltage. So, σ will be lower than the true value. Either a poor mechanical contact or a rectifying junction at the electrode sample interface will produce this effect.

(ii) Contacts can also affect the results if the electrodes inject holes or electrons into the sample. Eq. (3-1) thus applies strictly only when σ is determined solely by the bulk resistivity of the sample.

In a relatively uniform specimen, to nullify the effect of contact resistance two point probe method is usually used. The simple circuit diagram is shown in Fig: 3.3. To avoid heating of the sample current in the circuit must be kept low, the voltmeter must have high-input impedance.

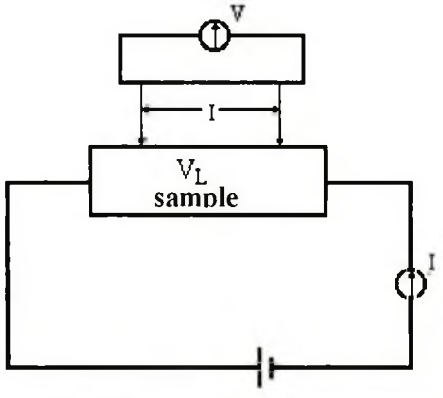

Fig. 3.3. Two-point probe method for conductivity measurement.

Measurements should be made away from the contacts so that minority carriers may be recombined before they reach probes.

The resistance of the sample of length L is

$$R_L = \frac{V_L}{I} \qquad (3\text{-}2)$$

From where resistivity may be evaluated if the area of cross section of the sample is known.

3.2.2 Hall Effect

The Hall effect principle states that when a current carrying conductor is placed in magnetic field, a voltage will be generated perpendicular to the direction of the field and the flow of current. Consider Figure 3.4 in which a constant current is passed through a thin sheet of semiconducting material to which are attached output connections at right angles to the current flow. With zero magnetic fields current distribution is uniform and there is no potential difference at the output contacts.

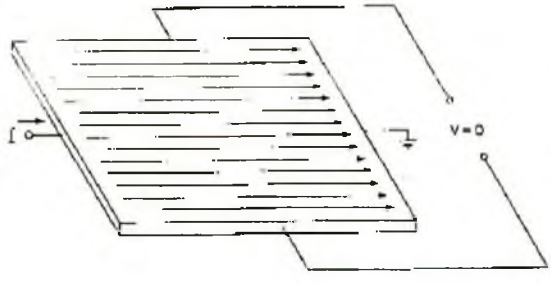

Fig. 3.4 A constant current is passed through a thin semiconductor

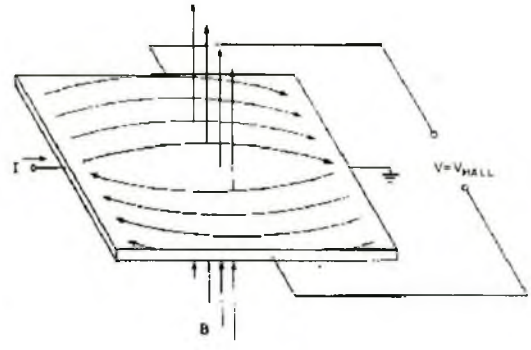

Fig. 3.5 A magnetic field is passed perpendicular to the direction of the constant current

When a perpendicular magnetic field is present, as illustrated in Figure 3.5, the current flow is distorted. The uneven distribution of electron density creates a potential difference across the output terminals. This voltage is called the Hall voltage.

3.2.2.1 Hall Voltage and Hall Coefficient

Hall effect has long been one of the principal means of characterization of semiconductors to measure carrier concentration and/or carrier mobility. When a magnetic field is applied at right angles to the direction of current flow, an electric field is set up in a direction perpendicular to both the direction of the current and of the magnetic field. If we assume electric field i.e. current density E≡X, B≡Z, then the Hall electric field E_H may be expressed as

$$E_H = R_H\left(\frac{IB}{A}\right) = R_H JB \qquad (3\text{-}3)$$

where, J = current density = $\frac{I}{A} = \frac{I}{wd}$

B = magnetic field

R_H = the constant of proportionality called Hall coefficient.

w = the width of the material.

d = thickness of the film.

For a rectangular type of specimen, the field E_H appears across the faces along y-axis. The corresponding Hall voltage developed across the face is

$$V_H = Ew \qquad (3\text{-}4)$$

Where, E is the field created along the width of the material due to the drift of charge carriers.

In terms of drift velocity (V), E is given by,

$$E = V B$$

$$= \frac{J}{qp_0}B = R_H JB \qquad (3\text{-}5)$$

$$R_H \equiv \frac{1}{qp_0} \qquad (3\text{-}6)$$

Thus the Hall field is proportional to the product of the current density and the magnetic flux density. The proportionality constant R_H is called the Hall coefficient. A

measurement of the Hall voltage for a known current and magnetic field yields a value for the carrier concentration.

$$p_0 = n_0 = \frac{1}{qR_H} = \frac{JB}{qE} = \frac{(I/wt)B}{q(V_H w)} = \frac{IB}{qtV_H} \qquad (3\text{-}7)$$

Since all of the quantities in the right hand side of the above equation can be measured, the Hall effect can be used to give quite accurate values for carrier concentration.

Since the conductivity $\sigma = 1/\rho$ is given by $q\mu_p p_o$, the mobility is the ratio of the Hall coefficient and the resistivity:

$$\mu_p = \frac{\sigma}{qp_o} = \frac{1/\rho}{q(1/qR_H)} = \frac{R_H}{\rho} \qquad (3\text{-}8)$$

In the present work, Hall effect measurement has been performed on copper selenide material to determine the above parameters. The experimental setup and the results have been discussed in the chapter 4.

3.2.2.2 Carrier Concentrations

If an electric field **E** is established across a conductor, the current density **J** through the material is proportional to the electric field

$$\mathbf{J} = \sigma\mathbf{E} \qquad (3\text{-}9)$$

where σ is termed as conductivity of the material, which is related to carrier concentration n and another important parameter called mobility μ:

$$\sigma = ne\mu \qquad (3\text{-}10)$$

here μ is the mobility expressed in the unit of $cm^2/V\text{-}s$. Mobility is a very important parameter that describes the ease with which charge carriers drift in the material.

In the case of intrinsic semiconductors where charge carriers are both electrons and holes, the conductivity is then given by

$$\begin{aligned} \sigma &= ne\mu_n + pe\mu_p \\ &= e(n\mu_n + p\mu_p) \\ &= n_i e(\mu_n + \mu_p) \end{aligned} \qquad (3\text{-}11)$$

where μ_n is called electron mobility and μ_p is the hole mobility. The parameters determining mobility are m* (effective mass of electron or holes as the case may be) and mean free time τ of the carriers.

The effective mass is a property of material's band structure

$$m^* = \frac{\hbar^2}{d^2E/dk^2} \qquad (3\text{-}12)$$

The other parameter τ is the mean time between scattering events. This is determined primarily by temperature and impurity concentration in semiconductor.

For n-type material and p-type material, conductivity would primarily be determined by the electron concentration and electron mobility or hole concentration and hole mobility respectively.

The carrier concentration and the conductivity are the two basic parameters, which have been evaluated for copper selenide in this work. The detail experimental results for these parameters will be discussed in the chapter 4.

3.2.2.3 Mobility

The carrier mobility is an important device parameter. It influences the device behavior through its frequency response or time response in two ways. The carrier velocity is proportional to the mobility for low electric fields. Hence, a higher mobility material is likely to have a higher frequency response.

There are several mobilities in use. The fundamental mobility is the *microscopic mobility*, which is calculated from basic concepts and describes the mobility of the carriers in their respective band. The *conductivity mobility* is the mobility that determines the conductivity or the resistivity of a semiconductor material. The *Hall mobility* is determined from the Hall effect and differs from the conductivity mobility by a factor dependent on the scattering mechanisms. The *drift mobility* is the mobility measured when minority carriers drift in an electric field. It is a device oriented mobility and therefore very useful. But it is not as easy to measure as the Hall mobility and is not used as extensively for that reason. The geometry has a major influence on the mobility in some devices. For example, the effect of surface scattering has a major influence in reducing the mobility in MOSFETs. The resulting mobility, determined from the device current-voltage characteristic, is termed the

effective mobility. In addition there are considerations that causes further division between *majority mobility* and *minority carrier mobility*.

In this experiment Hall mobility has been calculated and the mathematical expressions for Hall mobility will be discussed in chapter-4.

3.3 OPTICAL CHARACTERIZATION

A large variety of experimental technique has been employed to determine the optical constants (n and k) of thin films. A critical discussion of these techniques is given by Chopra [17]. The most commonly employed method involves separate determination of n and k from reflectance and transmittance measurement on the same film. Under the condition that the film thickness is such that the effects of multiple reflections are suppresses, the transmittance T of a film of index n_1-ik_1 and thickness t is given by

$$T = \frac{16n_0(n_1^2 + k_1^2)\exp(-4\pi k_1 t/\lambda)}{[(n_1+1)^2 + k_1^2][(n_0+n_1)^2 + k_1^2]} \qquad (n_1 > n_0) \qquad (3\text{-}13)$$

where n_0 is the index of the substrate and the ambient is assumed to be air. A plot of logT vs. t would then yield the value of k_1 from the intercept as well as the slop. If interference and multiple reflections are neglected, T and R are related by $T = (1-R)\exp(-4\pi k_1 t/\lambda)$. When reflection at the film/substrate interface is taken into account, $T = (1-R)^2 \exp(-4\pi k_1 t/\lambda)$ for $n_0 < n_1$, $k_0 = 0$. Since the absorption coefficient α is equal to $4\pi k_1 t/\lambda$, measurement of R and T data on the same film offers the most convenient method for determining of α.

The value of α can be determined at different wavelengths using a spectrophotometer. The spectral variation of α can be fitted to equation $\alpha = A(h\nu - E_g)^{1/2}$ to determine the nature (direct of indirect) of the optical transition and the value of the optical gap E_g.

3.3.1 Band Theory of Solids

In crystalline solids the atoms are so near to one another that their valence electron wave functions overlap. As a result, the Pauli's exclusion principal comes into M_1 play and as the atoms are brought together – the split energy levels form

continuous bands of energies. The electrons now more in a periodic potential and this leads to formation of energy bands separated by forbidden regions. The functions E (k) are periodic in k. The energy bands of a solid, the gaps between them, and the extent to which they are filled by electrons not only govern the electrical behavior of the solid but also have important bearing on others of its properties.

In the isolated atomic structure there are discrete (individual) energy levels associated with each orbiting electron. Each material will, in fact, have its own set of permissible energy levels for the electrons in its atomic structure. The more distant the electron from the nucleus, the higher the energy state, and any electron that has left its parent atom have a higher energy state than any electron in the atomic structure.

The energy band structure depends on the orientation of the atoms relative to each other i.e. crystal structure and also upon the atomic number. Solutions of Schrödinger wave equation are rather very complicated and only in few cases appropriate solution exist. If the forbidden gap is large – the system is an insulator. The material for which the gap is reliably small (~1eV) is called semiconductor. On the other hand a partly filled band state is called metal.

In a solid, many atoms are brought together, so that the split energy levels form essentially continuous bands of energies. As the distance between atoms approaches the equilibrium interatomic spacing, this band splits into two bands separated by an *energy gap* E_g.

In typical calculations, a single electron is assumed to be in the form of a plane wave moving, for example, in the x direction with propagation constant k, also called a wave vector. Solving the Schrodinger equation, the space-dependent wave function (from this, the average position, energy, and momentum of the particle can be found) for the electron is

$$\psi_k(x) = U(k,x)e^{-jk_x x} \qquad (3\text{-}14)$$

Where the function $U(k,x)$ modulates the wave function according to the periodicity of the lattice.

In such a calculation, allowed values of energy can be plotted versus the propagation constant k. Theoretically for semiconductors three methods, orthogonalized plane-wave, the pseudopotential and the k. p method are studied for

the energy bands of solids. Since the periodicity of most lattices is different in various directions, the (E, k) diagram must be plotted for the various crystal directions, and the full relationship between E and k is a complex surface, which should be visualized in three dimensions.

Measurement Methods

The following two methods are used to determine the energy gap:

1. Electrical method: Conductivity method [17]
2. Optical method: Absorption method [18]

3.3.1.1 Conductivity Method

The electrical conductivity of an intrinsic semiconductor is given by

$$\sigma = n_i e(\mu_n + \mu_p)$$

Here the concentration n_i increases exponentially with temperature as equation

$$n_i = 2\left(\frac{2\pi kT}{h^2}\right)^{3/2} (m_n^* m_p^*)^{3/4} e^{-E_G/2kT}$$

If we combine these equations, we may write the conductivity in the form

$$\sigma = 2e(\frac{2\pi kT}{h^2})^{3/2}(m_n^* m_p^*)^{3/4}(\mu_n + \mu_p)e^{-E_g/2kT} \qquad (3\text{-}15)$$

or,

$$\sigma = f(T)e^{-E_g/2k_BT} \qquad (3\text{-}16)$$

where $2e(\frac{2\pi kT}{h^2})^{3/2}(m_n^* m_p^*)^{3/4}(\mu_n + \mu_p) = f(T)$ is a function, which weakly depends on temperature, i.e., as a polynomial. Thus conductivity increases exponentially with temperature because of the exponential factor in (3-16).

At T=0, the conductivity is zero and the sample behaves as an insulator. At this temperature the resistance of the sample is high. From eq. (3-16) we can write

$$R_T = R_o\, e^{E_g/2k_BT} \qquad (3\text{-}17)$$

where

R_T = The resistance of the semiconductor at temperature T K.

$R_o = 1/f(T)$ = The resistance of the semiconductor at temperature 0 K.

At a certain temperature T_o the equation (3-17) becomes

$$R_{T_0} = R_o\, e^{E_g/2k_BT_0} \qquad (3\text{-}18)$$

Using equations (3-17) and (3-18) we can get

$$LnR_T = LnR_{T_0} + \frac{E_g}{2k_B}\frac{1}{T} \qquad (3\text{-}19)$$

A plot of $\ln R_T$ versus $1/T$ therefore yield a straight line whose slope, $\frac{E_g}{2k_B}$, determines the band gap energy, E_g.

In the early days of semiconductors this was the standard procedure for determining the energy gap. Now a days, however, optical method is used to measure the energy gap.

3.3.1.2 Optical Method: Absorption Method

Ionic crystals exhibit strong absorption and reflection in the infrared region as a result of the interaction of light with optical photons. Because of the partially ionic character of their bonds, compound semiconductors such as GaAs, GaP, etc., should and do, exhibit these properties.

In fundamental absorption, an electron absorbs a photon (from the incident light), and jumps from the valence band into conduction band. The photon energy must be equal to the energy gap, or larger. The frequency must therefore be

$$\nu \geq E_g/h \qquad (3\text{-}20)$$

The frequency $\nu_0 = E_g/h$ is referred to as the absorption edge.

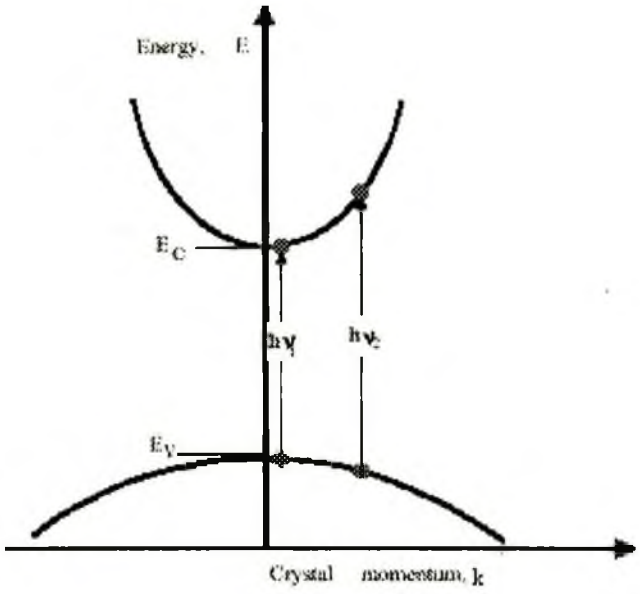

Fig. 3.6 The fundamental absorption process in semiconductors

In the transition process (photon absorption), the total energy and momentum of the electron-photon system must be conserved. Therefore

$$E_f = E_i + h\nu \qquad (3\text{-}21)$$

and $$k_f = k_i + q \qquad (3\text{-}22)$$

where E_i and E_f are the initial and final energies of the electron in the valence and conduction bands, respectively, and k_i, k_f are the corresponding electron momenta. The vector q is the wave vector for the absorbed photon. The wave vector in the optical region is negligibly small. The momentum therefore reduces to

$$k_f = k_i \qquad (3\text{-}23)$$

That is, the momentum of the electron alone is conserved. This selection rule means that only vertical transitions in k-space are allowed between the valence and conduction bands (Figure 3.6).

Calculating the absorption coefficient for fundamental absorption requires quantum manipulations. Essentially, these consists of treating the incident radiation as a perturbation which couples the electron state in the valence band to its counterpart in the conduction in the conduction band, and using the technique of quantum perturbation theory. One then finds that the absorption coefficient has the form.

$$\alpha_d = A(h\nu - E_g)^{\gamma} \qquad (3\text{-}24)$$

where A is a constant involving the properties of the bands ½ is a parameter, and E_g is the energy gap.

The absorption coefficient increases parabolically with the frequency above the fundamental edge (Fig. 3.7a). The absorption coefficient for GaAs and CuSe in Figure 3.7b is consistent with this analysis.

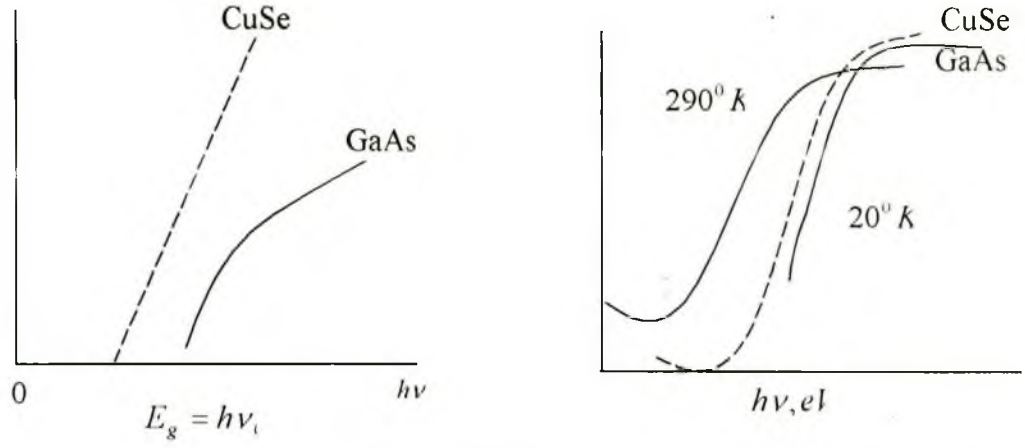

Fig. 3.7 (a) The absorption coefficient α versus $h\nu$ in a semiconductor. (b) The absorption coefficient α versus $h\nu$ in a GaAs and CuSe.

Thus at the frequency edge, ν_0, $E_g = h\nu_0$.

The absorption coefficient associated with fundamental absorption is large, about $10^4 cm^{-1}$.

The absorption process occurs in the so-called direct-gap semiconductors. Here the bottom of the conduction band lies at k=0, and hence directly above the top of the valence band. Electrons near the top of the valence band are able to make transitions to states near the bottom of the conduction band, consistent with the selection rule. Examples of such substrates are GaAs, InSb, and many other III-V and II-VI compounds.

In indirect-gap semiconductors,

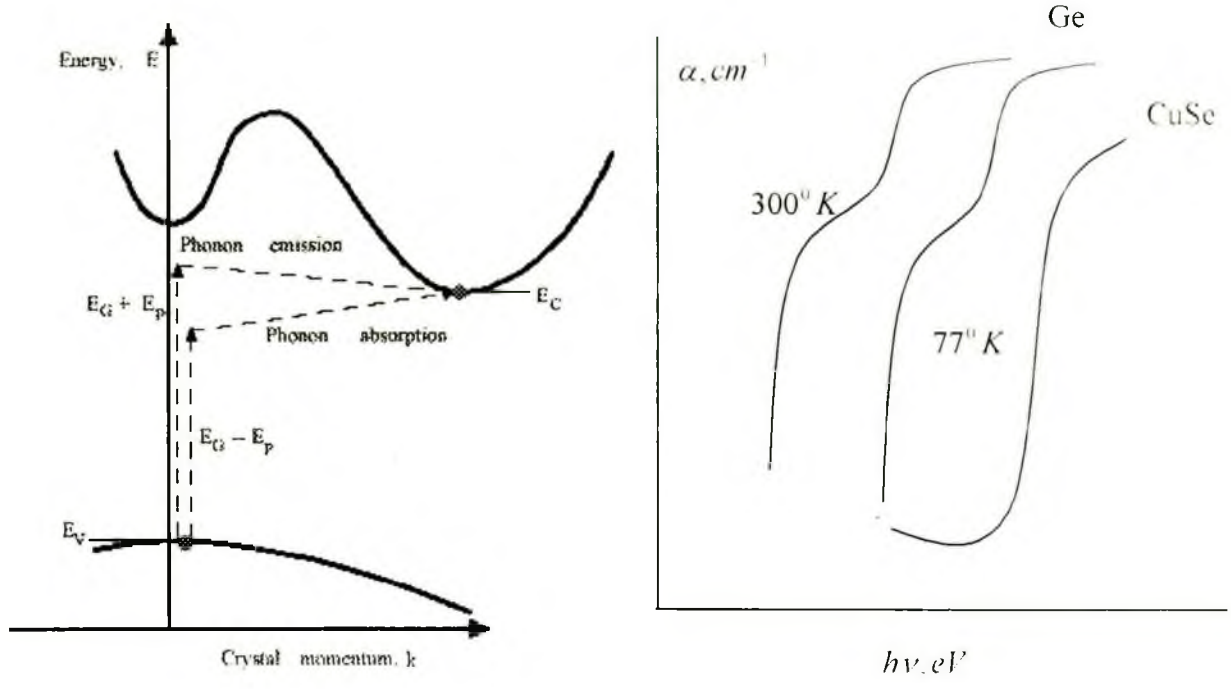

Fig. 3.8 (a) An indirect-gap semiconductor, (b) The absorption coefficient versus $h\nu$ in Ge and CuSe.

The electron cannot make a direct transition from the top of the valence band to the bottom of the conduction band because this would violets the momentum conservation rule. Such a transition still take place, but as a two-step process. The photon supplies the energy, while the phonon supplies the required momentum.

Calculation of the energy gap is found using the formula, given by the same reference, is

$$\alpha_i = A'(T)(h\nu - E_g)^2 \qquad (3\text{-}28)$$

where $A'(T)$ is a constant containing parameters pertaining to the bands and the temperature. Examples of such substrates are Si and Ge.

3.3.2 Spectrometric Measurement

3.3.2.1 Absorption Phenomenon

When light is incident on a crystalline solid, different optical phenomenon such as reflection, refraction, absorption, transmission, etc. may occur.

Optical absorption may occur in two processes: intrinsic and extrinsic. Intrinsic absorption in fig-3.9 (a) corresponds to the raising of an electron from the valence band to the conduction band.

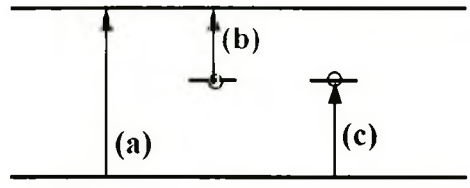

Fig-3.9. (a) Intrinsic transition,
(b) & (c) Extrinsic transition.

Extrinsic optical absorption corresponds to the raising of an electron from the imperfection to the conduction band as in fig: 3.9(b), or the raising of an electron from the valence band to an imperfection in fig: 3.9(c) [19].

Optical absorption in solid is the result of any of the following five processes.

1. Excitation of crystal vibration,
2. Formation of excitations,
3. Excitation of free electrons and holes within the allowed band,
4. Excitation of free electron and holes from one band to another of the same type,
5. Excitation of electrons across the gap from the valence band to conduction band. Of the five absorption processes, only the last gives rise to photoconductivity.

3.3.2.2 Excitation of Electrons

The necessary condition for the absorption for the absorption of a photon and the formation of a electron-hole pair is the condition $h\nu \geq \Delta E$ where ΔE is the width of the forbidden energy gap in the semiconductor. The conversion of energy must be satisfied. If the electron with momentum p is transferred from balance band to conduction band of momentum p' by absorbing a photon of momentum $(h\nu/c)s$, then,

$$p' - p = (h\nu/c)s \qquad (3\text{-}26)$$

where, s is unit vector in the direction of motion of the photon. The photon momentum is negligible and so equation can be written as,

$$p' - p = 0 \qquad (3\text{-}27)$$

i.e. only those transitions are allowed where momentum of the electron undergoing transition remain fixed. Allowed transitions correspond to vertical or direct transition.

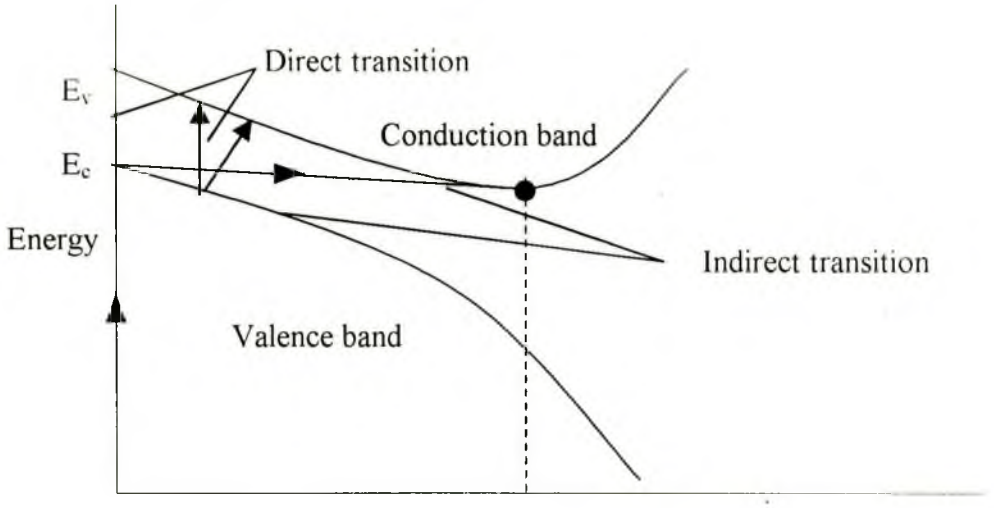

Fig. 3.10 Direct and indirect transition

If k and k' are the wave vectors of the electron at valence band and of the electron transferred to the conduction band, equation (1) becomes

$$\hbar k - \hbar k' = 0$$

$$\text{i.e. } k' = k \qquad (3\text{-}28)$$

In addition to the vertical optical transition where momentum does not change we have the non-vertical of indirect transition where wave vector k changes.

Indirect transition is impossible with a collision only between two bodies (i.e. the photon energy and the electron), because the law of conservation of wave number will be violated. So, it is assumed that there is a probability of three-body collision involving a photon, an electron and a photon. In this interaction the electron absorbs the main part of the photon energy and changes the wave number at the expense of photons, i.e., by interacting with lattice.

The process described above may be expressed as follows:

$$k = k \pm K\phi \qquad (3\text{–}29)$$

Where K is the phonon absorbed or released during the transfer process. The relations that governs the intrinsic band edge are

$$\hbar\omega_{It} = \Delta E_o^{\circ}$$

$$\hbar\omega_{It} = (\Delta E_o^{T} \pm \hbar\omega_{phonon}) \qquad (3\text{–}30)$$

where, ΔE_o°, band gap determined from spectrophotometric measurement, ΔE_o^{T}, band gap determined from thermal measurement, $\hbar\omega_{phonon}$, energy corresponding absorbed of emitted phonon during the process.

It has been shown that the absorption coefficient α near the intrinsic absorption edge is approximately given by,

$$\alpha \propto (\hbar\omega - \Delta E_o)^{x}$$

$$\alpha = \text{constant}\ (\hbar\omega - \Delta E_o)^{x} \qquad (3\text{-}31)$$

For direct transition (allowed) x = ½

For direct transition (forbidden) x = 3/2

For indirect transition (allowed) x = 2

For indirect transition (forbidden) x = 3 [20].

3.3.2.3 Absorption by Charge Carriers

When light penetrates into a semiconductor material the interaction between the incoming and the charge carriers (holes and electron) may lead to absorption of light. The carriers are accelerated, thereby their energy increases at the expose of the lattice – converting then light energy ultimately to heat energy (lattice vibration). The phenomenon can be derived by chemical electro-dynamics. The absorption coefficient for such interaction is given by

$$\alpha = 4\pi/cn\sigma \qquad (3\text{-}32)$$

where, n = refractive index of the material,

c = velocity of light,

σ = conductance of the material,

α is frequency dependent parameter.

3.3.2.4 Absorption Spectrum

The attenuation of light transmitted through a distance x of a material is

$$I(x) = I(0)\, e^{-\alpha x} \qquad (3\text{-}33)$$

Where I (x) is the intensity of light after it passes a distance x of the medium, k is the absorption coefficient.

The dependence of absorption coefficient on the frequency $\alpha(\omega)$ or on the wavelength $\alpha(\lambda)$ is known as the absorption spectrum of solid. The absorption coefficient, measure of probability of photon absorption cross-section $\rho(\omega)$ and by the concentration of absorption centers N:

$$\alpha(\omega) = \rho(\omega)\, N \qquad (3\text{-}34)$$

For a semiconductor containing absorption centers of different nature with its own effective cross-section

$$\alpha_i(\omega) = \rho_i(\omega)\, N_i \qquad (3\text{-}35)$$

The obtain absorption o-efficient is the sum of partial absorption co-efficient

$$\alpha = \Sigma\alpha_i(\omega) = \Sigma\rho_i(\omega)\, N_i = \alpha(\omega) \qquad (3\text{-}33)$$

If R is the reflectivity ($R=I_R/I_o$) then equation (3-31) becomes

$$I(x) = I_o(1-R)\, e^{-\alpha x} \qquad (3\text{-}37)$$

where, I_R is the intensity if the reflected ray.

We define transmission T as $T=(I_T/I_o)$ where, IT is the intensity if transmitted beam. If there is no reflection the intensity of transmitted beam after a distance x is,

$$I(x) = I_o\, e^{-\alpha x}$$

$$\text{or, } T = (I_T/I_o) = [I(x)/I_o] = e^{-\alpha x}$$

$$\text{or, } \ln(1/T) = \alpha x = A \qquad (3\text{-}38)$$

where, A is called the absorptance.

If we have the reflectivity R, then the modified equation of absorptance would be

$$A = \alpha x = \ln 1 + (1 + 4c^2R^2/2c)^{1/2} \qquad (3\text{-}39)$$

where, $c = T/(1-R)^2$ and $T = I(x)/I_o$

REFERENCES

1. G. Binnig, H. Rohrer, Ch. Gerber and E. Weibel, *Phy. Rev. Lett.*, **49** (1982) 57.
2. P. K. Hansma and J. Tersoff, *J. Appl. Phys.*, **61** (1987) R1.
3. G. Binnig, C. Quate and Ch. Gerber, *Phy. Rev. Lett.*, **56** (1986) 930.
4. S. N. Magonov and M. H. Whangbo, Surface Analysis with STM and AFM-Experimental and Theoretical Aspects of Image Analysis, (VCH, 1996).
5. R. Howland and L. Benatar, *A Practical Guide to Scanning Probe Microscopy*, (Park Scientific Instruments, 1997).
6. B. D. Cullity, *Elements of X-ray Diffraction*, Addison-Wesley Publishing Company, Inc., USA, 1959.
7. B. K. Gupta and O. P. Agnihotri, *Phil. Mag.*, **37** (1978) 631.
8. V. D. Vankar, S. R. Das, P. Nath and K. L. Chopra, *Phys. Stat. Sol.*, (a), **45** (1978) 665.
9. L. Stturkey, Symposium on Advances in Techniques in Electron Metallography, American Society for Testing Materials, 1963.
10. C. S. Barrett and T. B. Massalski, *Structure of Metals*, McGraw-Hill Book Company, New York, 1966.
11. L. I. Maissel and R. Glang, *Handbook of Thin Film Technology*, McGraw-Hill Book Company, New York, 1970.
12. P. B. Hirsch, A. Howie, R. B. Nilcholson, D. W. Pashly and M. J. Whelan, *Electron Microscopy of Thin Crystals*, Butterworths, Washington D. C., 1965.
13. B. K. Vainshtein, *Structure Analysis by Electron Diffraction*, The Macmillan Company, New York, 1970.
14. H. K. Charls, Jr., R. J. King and A. P. Ariotedjo, *Solar Cells*, **1** (1979) 327.
15. E. H. Putey, *The Hall Effect and Semiconductor Physics*, Dover Publications, Inc., New York 1960.
16. K. L. Chopra, *Thin Film Phenomena*, McGraw-Hill Book Company, New York (1969).
17. M. Ali Omar, *Elementary solid state physics*, Addision-wesley, 1993.
18. F. J. Blatt, *Physics of Electronic Conduction in Solids*, New York, McGraw-Hill, 1968.
19. H. Richared Bube, *Photoelectronic properties of Semiconductors*, Cambridge, University Press, 1992.
20. J. Johnson, *Semiconductor and semimetals*, **3** (1967) 153.

CHAPTER 4

EXPERIMENTAL APPARATUS AND EXPERIMENTAL PROCEDURE

In this chapter we deal with the various experimental apparatus and experimental procedure that are used for the structural, electrical and optical characterization of copper selenide thin film. Sample preparation was carried out by two techniques:

1) chemical bath deposition technique and 2) vacuum evaporation technique. All the measurements (except XPS) were carried out in air. AFM and XPS were carried out in Surface Science Laboratory (SSL), Department of Materials Science, TU Darmstadt, Germany. XRD measurement was performed at the Bangladesh Council for Scientific and Industrial Research (BCSIR), Dhaka.

4.1 EXPERIMENTAL APPARATUS

4.1.1 Apparatus For Sample Preparation

4.1.1.1 Chemical Bath Deposition (CBD) Technique

The experimental set up for deposition thin film using CBD method is shown in fig. 4.1. The technique is very simple and does not require any special set-up. It is convenient for both small and large substrates. For example a 50 ml beaker can be used for small substrates and a large bath container for large substrates. In this work glass container of up to 400 ml total volume have been used to insert 4-5 substrates the size of standard microscopic glass slide.

In this method the reacting solutions were kept in the reaction bath (generally in a beaker), which is stirred continuously with a magnetic stirrer. A contact thermometer that forms a part of feed back circuit controlling the heater to maintain a constant temperature (monitors by digital display) of the bath. When the ionic product (IP) of the metal and chalcogen ions exceeds the solubility product (SP) of the corresponding chalcogenide, a metal chalcogenide film is formed on the substrate by an ion-by-ion condensation process [1].

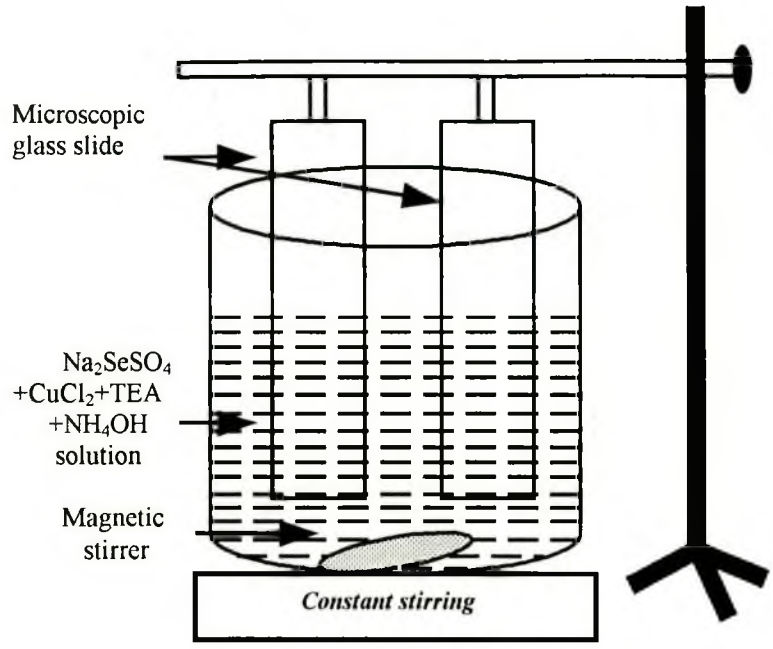

Fig. 4.1. Chemical bath deposition system

The kinetic of growth of a thin film in this process is determined by the ion-by-ion deposition of the chalcogenide on nucleating sites on the immersed surfaces. Initially, the film growth rate is negligible because an incubation period is required for the formation of critical nuclei from a homogeneous system onto a clean surface. Once nucleation occurs, the rate rises rapidly until the rate of deposition equals the rate of dissolution i.e., ionic product equals to solubility product (IP=SP). Consequently, the film attains a terminal thickness. On a presensitized substrate surface, no incubation period for nucleation is observed, since nucleation centers already exist in the substrate. Also, when the substrates are suspended in the solution, film thickness increases in a manner similar to that of the sensitized surface, thereby showing that the nuclei for the formation of the film are provided by the solution itself [1].

4.1.1.2 Vacuum Evaporation System

In our laboratory, samples were also prepared by vacuum evaporation method (Edward, England) with base pressure 1×10^{-5} Torr. This is a completely coating unit consisting of a rotary pump and oil diffusion pump capable of producing a vacuum down to a pressure of 10^{-5} Torr or less. The chamber was equipped with a double-pass glass shield. The diffusion pump is separated from the main chamber by gate valve. In

our experiment, we use both oil pump, like rotary and diffusion pump. For both pumps we use fluids and flowing cooling water. It need warming-up period and cannot be normally into operation simply by switching on.

It is known that incident atoms and /or molecules are gathered onto the substrate. But it does not mean that they form thin film. If they gather randomly on the substrate without any alignment, they will form amorphous. But depending on the alignment of incident atoms and molecules, thin film may growth as polycrystal and single crystal. Generally, incident atoms on the substrate perform surface migration, such as interaction between atoms, interaction between atoms and substrate, effect of substrate temperature. As a result, depending on the different types of migration, structures of the growth films will be varied. There are three types of growth modes of thin film [2]. These are given below.

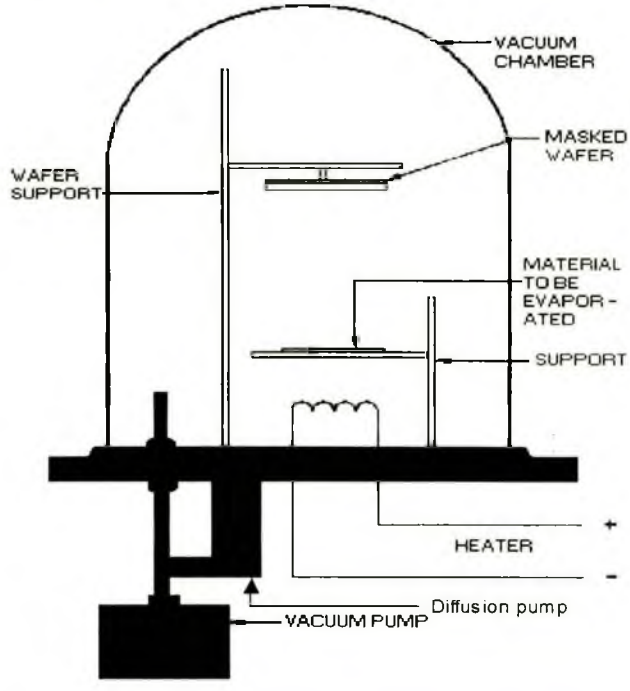

Fig. 4.2. Vacuum evaporation system

(1) Nucleation and Growth: Atoms evaporate from the evaporation source are assembled together and form nucleus on the substrate. Then films are growth three-dimensionally from initial stage. These three-dimensional islands gather continuously as films. This of type growth mode is called Volmer-Weber (VW) Mode [3] and shown in Fig. 4.3(a). Crystallization of film of this mode depends on the three-

dimensional nucleus, density and direction of islands of the initial growth. In this mode, interaction between incident atoms is stronger than that of between incident atoms and substrate atoms.

(2) Layer-by-Layer Growth: In this mode, substrate surfaces are covered uniformly with incident atoms and films are growth two-dimensionally with primitive layer-by-primitive layer. This type of growth mode is called Frank-van der Merwe (FM) Mode [4] and shown in Fig. 4.3(b). It is easy to grow the film in this mode, if the interaction between substrate atoms and incident atoms become strong. For the better substrate quality, better quality of films can be grown, which is practically important.

(3) Layer Growth and Nucleation: In this mode, at first, from unit layer to several layers form onto the substrate, and then growth process completes as three-dimensional nucleus onto the former film. This type of mode is called Stranski-Krastanov (SK) Mode [5] and shown in Fig. 4.3(c). Growth of large number of metals, such as Ag, In, Sn, Au, etc. onto semiconductor surfaces (Si, Ge) follows the SK mode

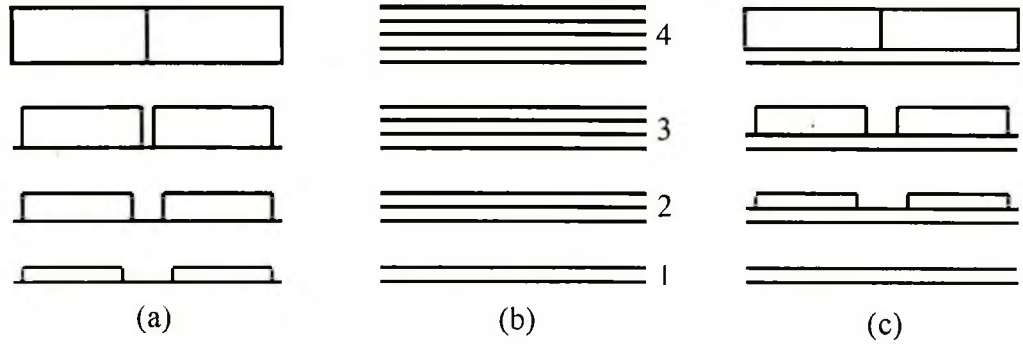

Fig. 4.3. The basic growth mechanisms: (a) Volmer-Weber mechanism; (b) Frank-van der Merwe mechanism; (c) Stranski-Krastanov mechanism.

It has been reported that the $Cu_{2-x}Se$ thin film grown with two different morphologies [6]. The first layer nearer the substrate consists of crystals whose arrangement is compact. They exhibit sharp edges. On top of this layer a second layer consists of crystals arranged in a less compact manner. The presence of two layers indicates that, the thin film growth is characterized by a two-step growth process.

4.1.2 Apparatus For Structural Characterization

4.1.2.1 AFM Apparatus

Surface morphology was studied using an atomic force microscope (AFM) system from Thermomicroscopes. The measurement was performed in air to observe the surface morphology of the $Cu_{2-x}Se$ thin film. Contact-mode AFM is used in the present study.

4.1.2.2 XPS Apparatus

The XPS experiments were performed in a VG ESCALAB MkII photoelectron spectrometer whose ultra-high vacuum (UHV) chamber is directly connected to a home made deposition chamber by sample transfer system (base pressure ~ 10^{-9} mbar). The samples were analysed after different preparation steps by X-ray photoelectron spectroscopy (XPS). For XPS measurements, electrons were excited with an X-ray source (Mg Kα: hν=1253.6 eV). Since XPS measurement was performed in an ultrahigh vacuum so we shall describe the X-ray source in short.

X-ray Source

Choice of a material for a soft X-ray source in XPS depends on two considerations. Firstly, the line width must not limit the energy resolution required in the technique and, secondly, the characteristic X-ray energy must be high enough that a sufficient range of core electrons can be photoejected for an unambiguous analysis. It is easy to see the relationship governing the interaction of a photon with a core level, viz.

$$E_K = h\nu - E_B - e\varphi \qquad (4.1)$$

where E_K = kinetic energy of ejected photoelectron

$h\nu$ = characteristic energy of X-ray photon

E_B = binding energy of core level

$e\varphi$ = work function term

that the line width of E_K will depend on the line width of $h\nu$, since that of the core level is narrow and $e\varphi$ is a virtual constant in any case. Now in XPS, chemical information is extracted by detailed analysis of individual elemental spectra, including

resolution of contributions from the various chemical states present, from which it follows that the best energy resolution should be used compatible with the signal-to-noise ratio in the particular spectrum. Thus, to avoid limitation of the resolution by the line width of the source, it is necessary to use materials whose characteristic X-ray lines have widths less than 1.0 eV. In XPS the two materials used universally as anodes in soft X-ray sources are Mg and Al. In our present experiment, we have used the Mg K_α X-ray source.

X-rays are generated in a Mg target by bombardment with electrons of sufficient energy. For a particular X-ray line, photoemission starts at the ionization threshold of the core level involved and increases rapidly as the electron energy is increased, eventually saturating at some energy very much higher than the threshold. Fig. 4.4 shows the block diagram of the X-ray source.

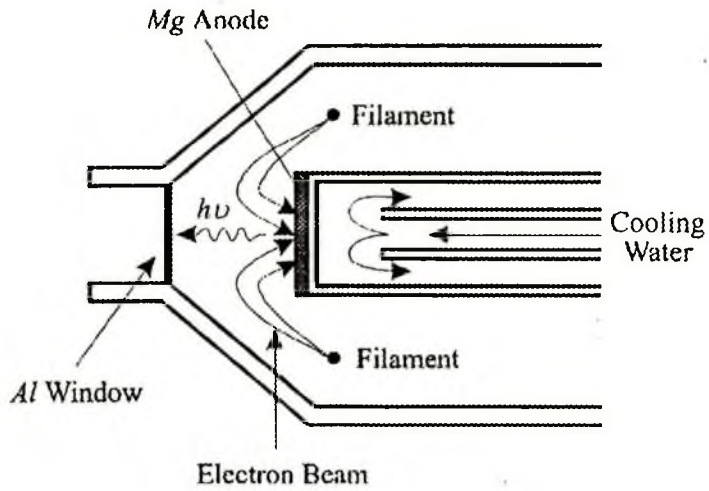

Fig. 4.4. Block diagram of X-ray source.

Soft X-ray emission from any material does not consist merely of a characteristic X-ray line. The spectrum from an unmonochromatized source is quite complex. Certainly most of the intensity goes into the principal characteristic line, which for Mg is the $K\alpha_{1,2}$ line (hν= 1253.6 eV), but there are satellite lines such as the $K\alpha_3$ (hν= 1262.0 eV), $K\alpha_4$ (hν= 1263.8 eV) and the $K\beta$ (hν= 1302.1 eV) lines, as well as other very minor ones, such as $K\alpha_5$ (hν= 1271.1 eV) and $K\alpha_6$ (hν= 1273.6 eV) lines.

4.1.2.3 XRD Apparatus

A Philips X'Pert X-ray diffractrometer (XRD) was used to get X-ray data for the samples at the Bangladesh Council for Scientific and Industrial Research (BCSIR), where the diffraction technique was used with a primary beam power of 40kV and 30mA for Cu radiation. A nickel filter was placed before the sample to reduce CuK_β radiation and finally $CuK\alpha$ radiation was only used as the primary beam. A (θ-2θ) scan was taken from 20 to 120° to get possible fundamental peaks for each sample with the sampling pitch of 0.02° and time for each step data collection was 0.6 sec. The XRD machine was totally computer controlled and all the data were stored in the hard disk memory of the computer for further analysis.

4.1.3 Apparatus For Electrical Characterization

4.1.3.1 Apparatus For Measurement of I–V Characteristics

The block diagram of the current voltage characteristic curve is shown in Fig. 4.5.

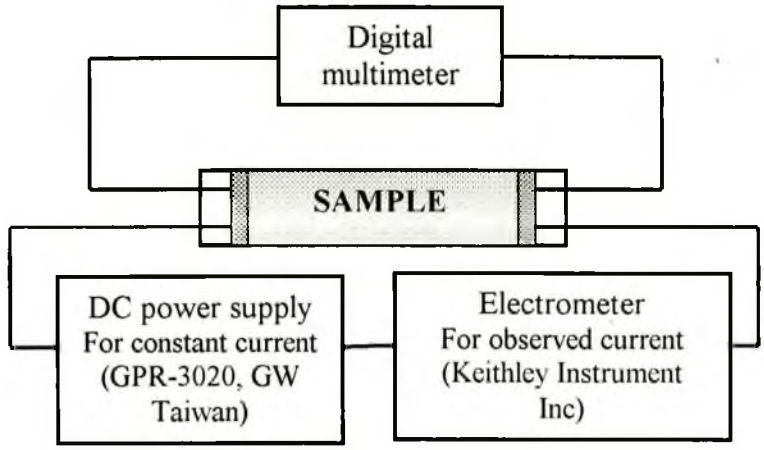

Fig. 4.5. Block diagram of I–V characteristics.

Contact problem is one of the most significant problems in thin film research. To get ohmic contact fine Cu-wires were connected to the film with silver paste. In our experiment, we used direct method to study I–V characteristics of the films. On two ends of the film a relatively thick silver films have deposited that act as an electrode. Steady voltage was applied from few mV to several volts across the

electrodes by a laboratory dc power supply (GPR-3020, GW Taiwan); the current through the sample was measured by an electronic electrometer (Keithley Instrument Inc). The voltage was measured with a digital multimeter (GDM 345P).

4.1.3.2 Apparatus for Resistivity Measurement

We use direct two-point probe method for measurement of resistivity i.e. a voltage V is applied to the thin film and the resultant current I is measured in the external circuit (Fig 4.6). The resistivity of the thin film can be obtain by the formulae

$\rho=\frac{VA}{Il}$ where, A is the cross-sectional area and l is the length of the sample. From I–V curve as mentioned above we find the slope of the curve and estimated the value of $\frac{V}{I}$. Using the above equation we evaluated the resistivity.

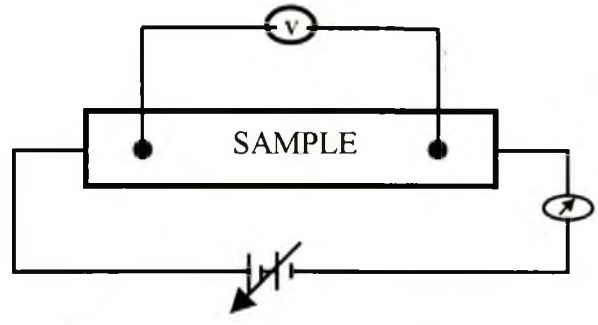

Fig. 4.6. Circuit diagram of resistivity measurement

4.1.3.3 Apparatus for Hall Effect Measurement

The measurement of Hall effect was performed in our Solid State Physics laboratory, Department of Physics, D.U. It is a complete Hall effect measurement set and can produce magnetic field upto 1 tesla. The photograph and arrangement of the Hall Effect measurement setup are shown in Figs. 4.7-4.9

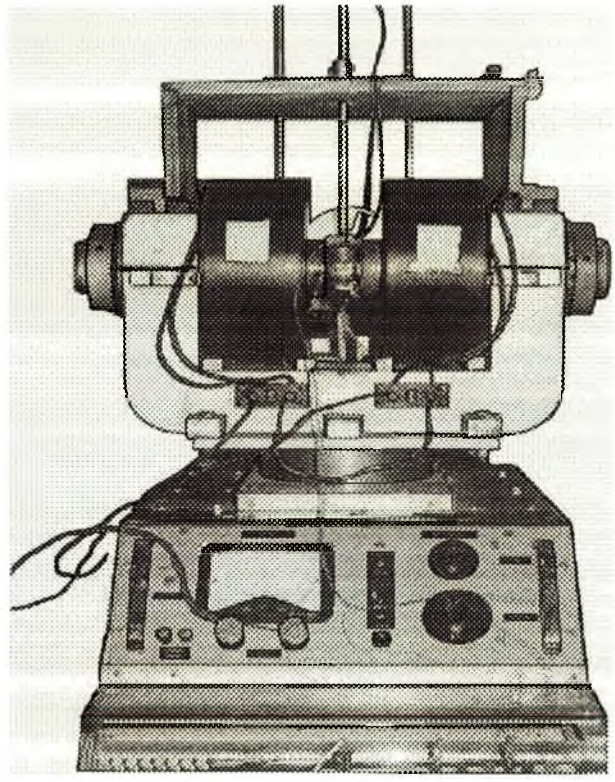

Fig. 4.7. Photograph of Hall measurement set up

This part describes the Hall effect apparatus, as well as the procedures for data collection.

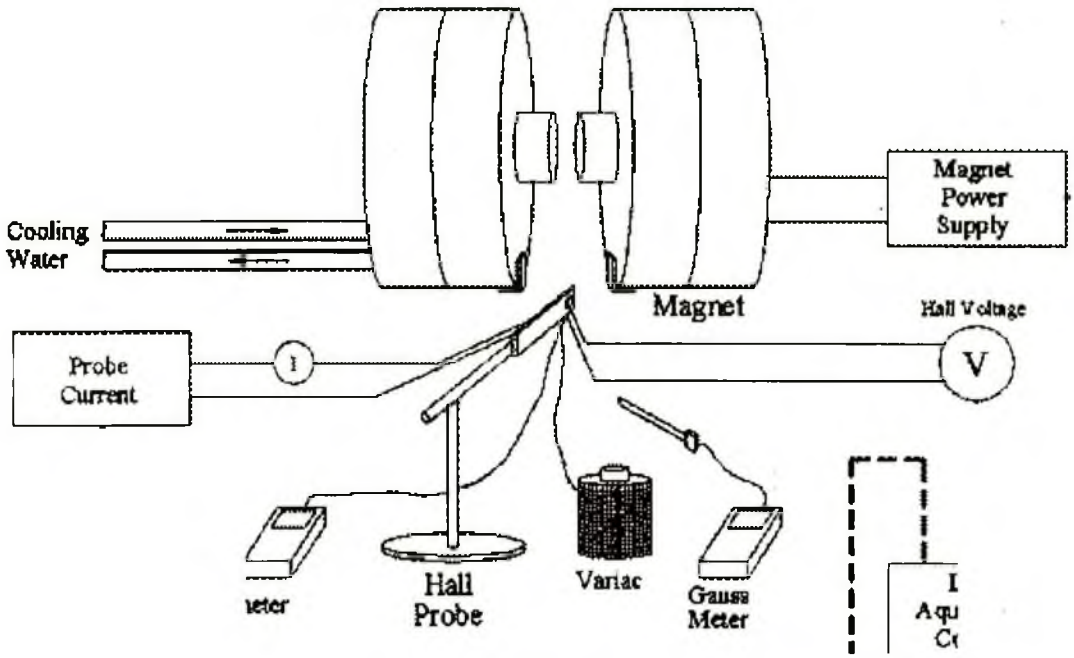

Fig. 4.8. The experimental set up for Hall Effect.

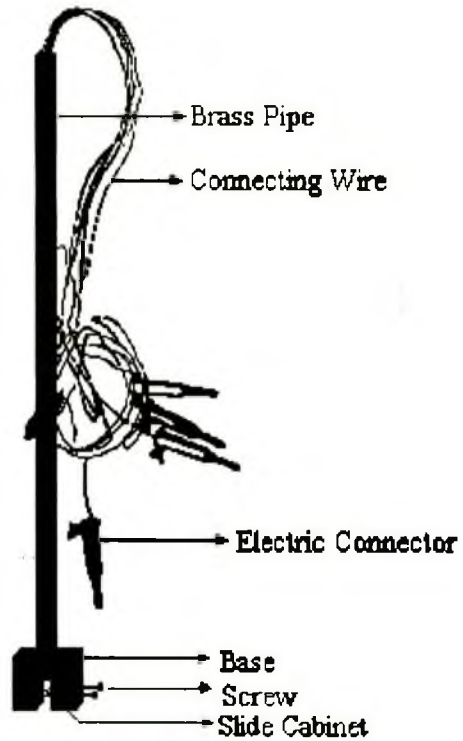

Fig. 4.9. The Hall Probe

Equipment

1. Alpha water-cooled magnet and power supply. (Do not exceed 10 A magnet current).
2. Hall Probe. Extra Hall Probe for examination, with stand.
3. DC Power Supply to furnish current to Hall probe; adjust only the "voltage" control; probe current not to exceed 0.4 A.
4. Ammeter, to measure Hall probe current.
5. Voltmeter, high input impedance, to measure Hall voltage.
6. Gaussmeter to measure magnetic field.

Procedure

The steps listed below outline the procedure for taking the data to investigate the Hall effects. Complete sets of data should be taken at room temperature. For each magnetic current, we use the gaussmeter to determine the magnetic field. In order to make the field measurements, the Hall probe must be removed and replaced by the gaussmeter probe. Using MKSC units consistently. Magnetic fields should be expressed in Teslas (T = Ns/mC = kg/Cs). The physics literature often expresses magnetic fields in gauss, with 1 T = 10,000 gauss.

4.1.3.4 Apparatus for Carrier Type Determination

Although for determination of carriers is the same one normally used for Hall effect measurement, we attempt to determine this parameter by another special technique. So we arrange a simple experiment to measure the thermo e.m.f between the two ends of the sample. The experiment consists of an arrangement shown in fig.4.10. If the thermal voltage between the hot and cold end of the sample is found to positive on digital voltmeter, then the sample is *n*-type; whereas if the voltage is negative, then the sample is *p*-type.

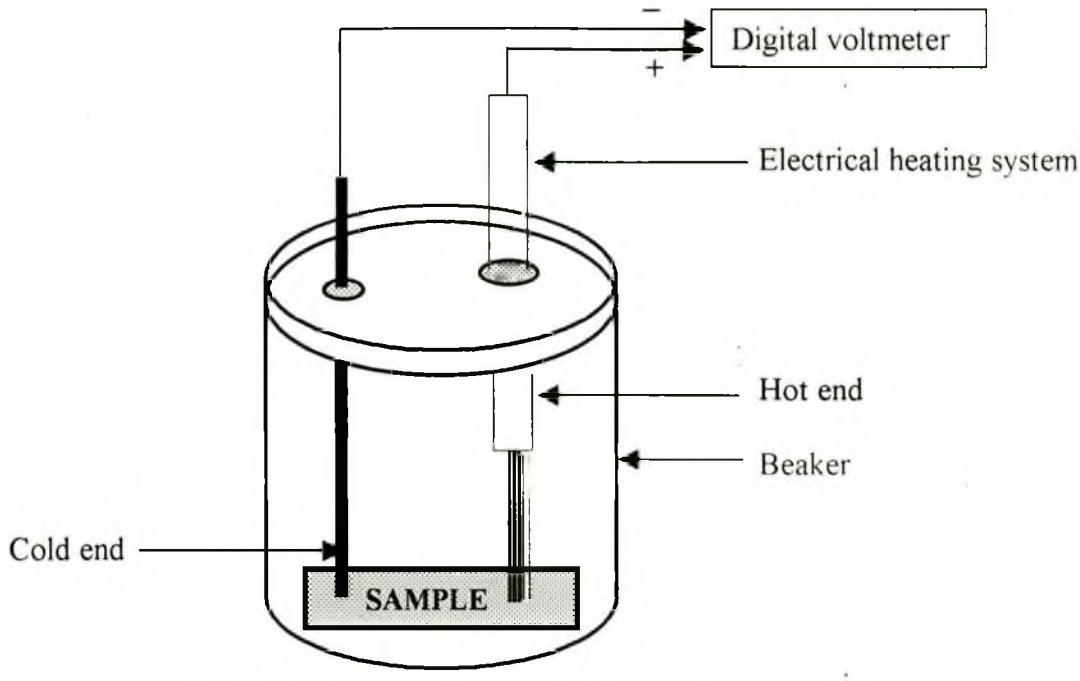

Fig.4.10. Experimental set-up for identifying the carrier type (hot probe method)

4.1.4 Apparatus For Optical Characterization

4.1.4.1 Apparatus for Spectrophotometric Measurements

The optical measurements were performed using a UV-1201V spectrophotometer (Shimadzu Corp., Japan) in our Semiconductor Technology Research Center. D.U. Fig. 4.11 shows the construction of a typical spectrophotometer (UV-1201V, Shimadzu. Corp., Japan) and Fig. 4.12 shows the optical system. This attachment is used to measure the relative specular transmittance and reflectance at an incident angle of 5°. A sample is to be placed horizontally on the stage facing downward, being illuminated from the bottom. The optics on the sample side and that on the reference side are almost symmetrical.

In this apparatus a monochromatic light beam entering the sample compartment is first reflected by the mirror M_1 and then by the plane mirror M_2 mounted at 45° upwards, and thus the beam comes upwards. Then, it strikes the standard mirror or unknown sample at an incident angle of 5°, and reflected light beam comes down.

After that, the beam is again reflected by the mirror M_2 to go in the horizontal direction to the mirror M_3, thus passing through the exit of the sample compartment to the detector.

However, the reference-side sample face is 10 mm lower than that on the sample side. The reason is that a larger sample can be mounted in the sample side while the standard mirror is mounted on the reference side.

Firstly remove the standard rectangular cell holder from the sample compartment, and instead, install the specular reflectance attachment main body, fitting it to the positioning pins, and fixing it securely with fixing screws. At this time, the sample side of the attachment should be in the front side of the sample compartment. Then mount the mirror assemblies (for reflectance standard) on the respective sample stage [(10) and (11) in fig. 4.11], with their mirror faces down. By closing the sample compartment the system run to make a baseline correction for the required wavelength range. After finishing the baseline correction, remove the sample-side reflecting mirror, and instead set an unknown sample. After that, start a measurement of the relative specular reflectance of this sample. Similar procedure was followed for transmittance measurement. Using the optical spectra, the band gap values for the films were estimated as described below.

The transmittance spectra that found from the spectrophometer have been corrected for the loss due to reflections by following the equation $T_{corr.} = \{T(\%)/(100 - R(\%))\} \times 100$. We assume that the predominant component in the reflected intensity is due to the air-film interface. The absorption coefficients (α) for band-to-band transition across the gap at different wavelengths are calculated using the corrected transmittance values: $\alpha = (1/t)ln(100/T_{corr.})$, where t is the film thickness [7,8].

The direct and indirect band gap values are obtained from the plots of $(\alpha h\nu)^2$ and $(\alpha h\nu)^{1/2}$ respectively, against photon energy $h\nu$ (eV). Extrapolating the straight-line part of the curve in these graph to the energy axis, where $(\alpha h\nu)^2=0$, gives the values of band gap for direct transitions ($E_{g.dir}$) and to where $(\alpha h\nu)^{1/2}=0$ gives the values of band gap for indirect transitions ($E_{g.indir}$). The thickness of the films was also determined by using data pack in spectrophotometer.

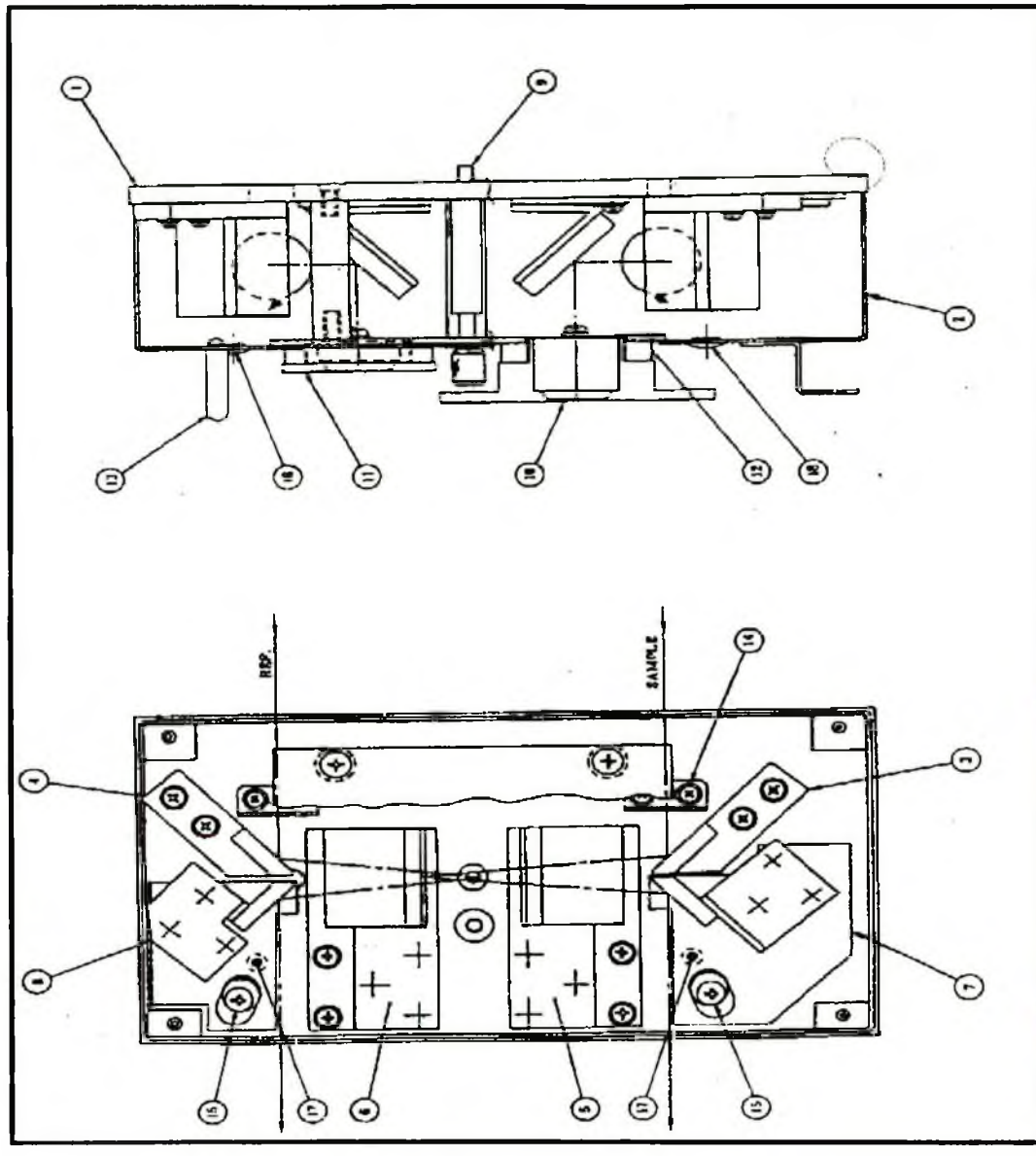

1. Base
2. Cover
3. Mirror 1 ASSY (S)
4. Mirror 1 ASSY (R)
5. Mirror 2 ASSY (S)
6. Mirror 2 ASSY (R)
7. Mirror 3 ASSY (S)
8. Mirror 3 ASSY (R)
9. Main body fixing screw
10. Sample stage (with aperture, S side)
11. Sample stage (with aperture, R side)
12. Sample stage positionar
13. Knob
14. Mask
15. Adjusting screw (S)
16. Adjusting screw (R)
17. Mirror 3 fixing screw
18. Cap

Fig. 4.11. Construction of Specular Reflectometry Attachment (With Incident Angle 5°)

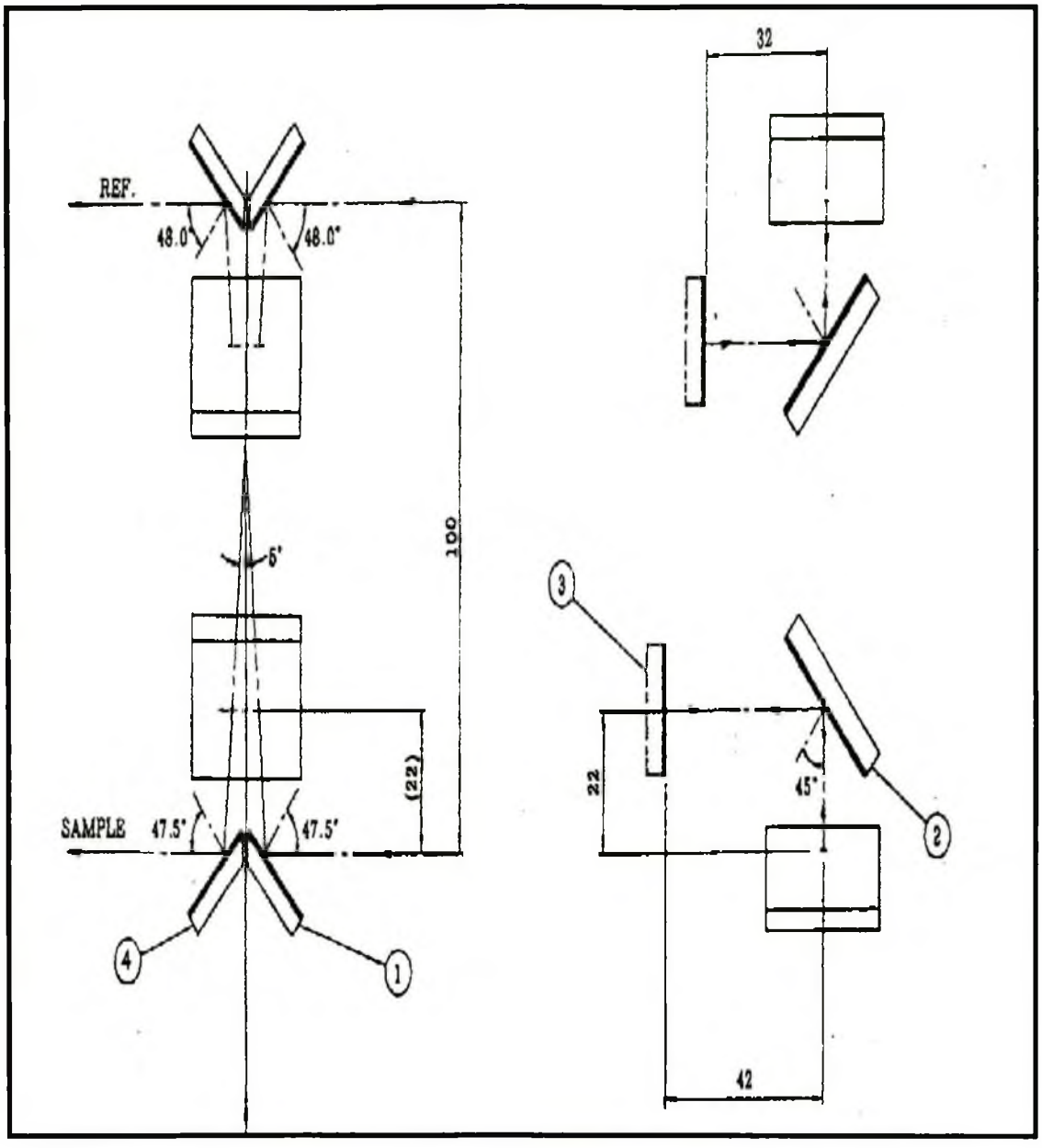

1. and 2. Plane mirrors
3. Reflectance standard mirror or unknown sample
4. Concave mirror

Fig. 4.12. Optical System of Specular Reflectometry Attachment (With Incident Angle 5°)

4.1.4.2 Apparatus for Thickness Measurement

The variation of optical transmittance (T) and absolute specular reflectance (R) of the films with wavelength of light incident on them were measured using a UV-121V recording spectrophotometer (Shimadzu Corp., Japan) in the wavelength range of 300-1100nm.

An integrating sphere detected light signals coming from the samples. The thickness of the thin film was measured with the infrared interference method using the reflectance characteristics of the films having interference pattern. From the reflection spectra we have estimated the thickness of the film under study from the following formula

$$t = N\lambda_1\lambda_2/2(\lambda_2 - \lambda_1)(n^2-\sin^2\theta)^{1/2}$$

where, n=refractive index of the material of the film,

λ_1=location of the wavelength of a peak of the spectra,

λ_2= location of the wavelength of another peak of the spectra, and $\lambda_2 > \lambda_1$

N=number of complex cycles between λ_2 and λ_1,

θ=incident angle of the light beam, in our experiment $\theta=5^\circ$ and usually n=2 for thin film.

4.2 EXPERIMENTAL PROCEDURE

The overall experimental procedure is depicted in Fig. 4.13.

4.2.1 Preparation of the Substrates

Poor adhesion and non-uniform films are common problems when depositing films on smooth substrates by chemical deposition. Therefore, special attention was paid to cleaning and activating the substrate surface. In our experiment Microscopic glass slide of 76 mm × 26 mm × 1 mm were use as substrate. To remove the grease and dust particles, ultrasonic cleaning of the substrate was performed by using acetone, deionized water, methanol and then finally again deionized water. Every stage of cleaning was done for 5 minutes. After cleaning, substrate was kept into a drier at room temperature to dry the substrate naturally.

4.2.2 Deposition of the Films Using CBD

For preparation of copper selenide thin film by chemical bath deposition technique the chemicals, used for the preparation of thin films, were LR grade (Merck) cupric chloride di-hydrate ($CuCl_2$, $2H_2O$), selenium powder of 99.99% purity, sodium sulfite (Na_2SO_3), tri-ethanol amine (TEA) and ammonium hydroxide (NH_4OH). At first, selenium was used for the preparation of sodium selenosulfate. It was prepared in our laboratory by refluxing fine selenium powder (as indicated molecular weight Se for required phase) with sodium sulfite solutions for about 30 minutes at ~120°C by stirring in a beaker. A constant stirring machine with a constant temperature bath was used for reaction. Secondly, $CuCl_2$ $2H_2O$ solution (as indicated molecular weight ratio of copper and selenium for required phase) was mixed with $NaSeSO_3$ at constant stirring. 10 ml TEA (0.1 M) was added to this solution. NH_4OH was used to adjust the pH of the reaction bath. The substrates were then immersed vertically into the deposition bath against the wall of the beaker containing the reaction mixture. The deposition was allowed to proceed at room temperature for different time durations from 15 to 180 minutes. After deposition, the glass slides were taken out from the bath, washed with distilled water and were dried in blowing air. A lot of samples were prepared by varying different bath temperature, pH value, and concentration of NH_3, $NaSeSO_3$ and deposition time. These results are presented in chapter-5.

4.2.2.1 Chemical Bath Composition

Six different bath compositions were used to deposit the copper selenide thin films, by mixing the chemical solution specified for each bath for CBD.

Bath 1-6: 150 ml of a freshly prepared solution of Na_2SeSO_3, 50 ml of $CuCl_2$. $2H_2O$, 1 ml of 1M triethanolamin (TEA), 2-10 ml of 30% NH_3 (aq.) to fixed the pH value ~9. The all parameters are same for samples 1-6 used in our study by CBD except the concentration of Na_2SeSO_3 and $CuCl_2$. $2H_2O$. The change of these concentration according to the desired phase describe in Table-4.1.

Table-4.1: Various concentration and phases of copper selenide thin films.

Bath or Sample No	Weight of Se (gm) with 12.604 gm Na_2SO_4 and 200 ml water	Weight of $CuCl_2.2H_2O$ (gm) with 50 ml water	Required phase of copper selenide thin film
1	0.7896	2.557	$Cu_{1.5}Se$
2	Same	2.727	$Cu_{1.6}Se$
3	Same	2.898	$Cu_{1.7}Se$
4	Same	3.068	$Cu_{1.8}Se$
5	Same	3.239	$Cu_{1.9}Se$
6	1.579	5.114	Cu_3Se_2
7	0.566 and 0.263 gm of Cu and Se deposited by vacuum evaporation technique.		

4.2.2.2 Chemical Reaction For CBD

Deposition of copper selenide thin films involves the controlled release of copper ions from the triethanolamin complex and the ion-by-ion condensation along with the selenium ions present in the solution, on to the glass substrate [9]. In the reaction bath there exist the possibility of reduction of Cu (II) to Cu (I) due to the presence excess sodium sulfite [7].

$$SO_3^{2-} + 2OH^- \rightarrow SO_4^{2-} + H_2O + 2e^- \qquad (4\text{-}1)$$

$$Cu^{2+} + e^- \rightarrow Cu^{1+} \qquad (4\text{-}2)$$

The final reaction

$$2Cu^{1+} + SeSO_3^{2-} + 2OH^- \rightarrow Cu_2Se + SO_4^{2-} + H_2O \qquad (4\text{-}3)$$

leads to the formation of Cu (I) selenide (more specifically $Cu_{2-x}Se$ in our case). The final phase of this reaction was found to be temperature independent. Hence $Cu_{2-x}Se$

preparation could be carried at room temperature. Out of convenience, we preferred room temperature deposition for $Cu_{2-x}Se$ films [10].

Although the mechanism of formation of the selenide has not been established [6], it may be considered as being formed by the following step [11].

$$2Cu(TEA)^{+} + 2SeSO_3^{2-} + 4OH^{-} \Rightarrow Cu_2Se + 2TEA + 2SO_4^{2-} + Se + 2H_2O \qquad (4\text{-}4)$$

A kinetically slow reaction may also occur:

$$3Cu_2Se + SeSO_3^{2-} \Rightarrow 2Cu_3Se_2 + SO_3^{2-} \qquad (4\text{-}5)$$

The rate of deposition and the terminal thickness both depend on the number of nucleation centers, super saturation of the solution (define as the ratio between IP to SP), and stirring. The growth kinetics depends on the concentration and growth process on the immersed surface. The effects of various deposition conditions on these parameters are discussed in chapter 5.

4.2.3 Deposition of the Films Using Vacuum Evaporation Technique.

For the preparation of copper selenide thin film by vacuum evaporation technique dried glass substrate were mounted on the sample holder at a distance of ~ 8 cm from the tungsten filament. Small pieces of metallic copper wire (99.99% pure) were fitted into the tungsten filament that is connected with a high current source for directly evaporated into the vacuum chamber. When necessary pressure 10^{-5} Torr in vacuum is attained, the metallic copper is then heated by passing a current gradually through the tungsten filament. Before the deposition was started, the source temperature for copper was maintained at 1100°C for 4-5 minutes to obtain stable melting conditions. After gradual increase of temperature copper was evaporated from a tungsten heater and copper is found to deposited on glass substrate. After copper deposition the film is taken away from the vacuum chamber and arrangement was made for selenium deposition on it.

For the deposition of selenium on copper film as sandwitch we use molybdenum boat as an additional part with spiral tungsten filament instead of tungsten wire. A small amount of selenium powder (99.99%) is placed on molybdenum boat just below the spiral tungsten filament. By following the same procedure, as mentioned above selenium was evaporated by applying current through

the filament and the source temperature for selenium was maintained at 400 C for evaporation. The evaporated films of copper selenide were brown; the thickness of these films was found almost in the range of 200-600 nm. Silver paste established an ohmic contact.

4.2.4 Sample Identification

Name: Copper Selenide Thin film. **Molecular Weight**: 206.05

Synonym: Copper II Selenide; Cuprous Selenide. **Molecular Formula**: $Cu_{2-x}Se$, Where x=0.1-0.5

Preparation Method: Chemical bath deposition and vacuum evaporation technique.

Melting Point: 1113°C, **Specific Gravity**: 6.75

Solubility in H_2O: Insoluble, **Physical States**: thin solid film

Inhalation: Acute: Danger-Poison. May cause a metallic taste in the mouth, congestion of nasal mucous membranes, irritation to the respiratory tract and acute selenium poisoning [12].

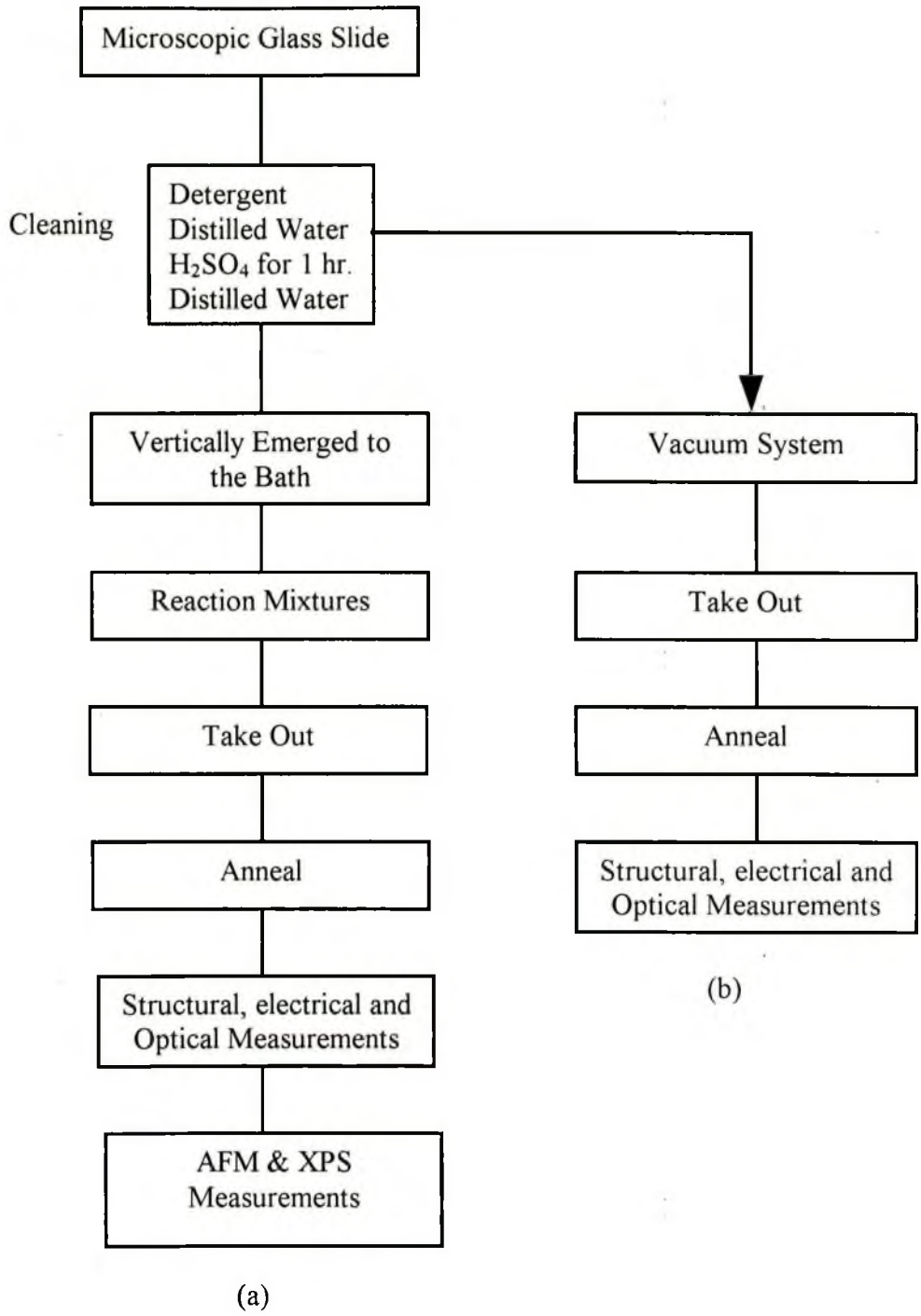

Fig. 4.13. Block Diagram of Experimental Procedures: (a) CBD; (b) vacuum evaporation techniques.

REFERENCES

1. K. L. Chopra and S. R. Das, *Thin Film Solar Cells*, Plenum Press, New York (1983).
2. E. Bauer and H. Poppa; *Thin Solid Films* **12** (1972) 167.
3. M. Volmer and A. Weber; *Z. Phys. Chem.* **119** (1926) 205.
4. F. C. Frank and J. H. van der Merwe; *Proc. Roy. Soc.* A **198** (1949) 205.
5. I. N. Stranski and L. Krastanov; *Ber. Akad. Wiss. Wien* **146** (1938) 797.
6. C. L. Clement, M. N. Spallart, S. K. Haram and K. S. V. Santhanam, *Thin Solid Films,* **302** (1997) 12.
7. V. M. Garcia, P. K. Nair and M. S. T. Nair, *J. Cryst Growth,* **203** (1999) 113.
8. G. Hodes, A. A. Yayor, F. Decker and P. Motisuke, *Physical Review B*, **36** (1987) 4215.
9. K. L. Chopra, R. C. Kainthla, D. K. Pandya, and A. P. Thakoor, *Physics of Thin Films* ed. G. hass et al, Academic Press, New York, **12** (1982) 201.
10. M. Lakshmi, K. Bindu, S. Bini, K.P.Vijaykumar, C. Sudha Kartha, T. Abe and Y. Kashiwaba, *Thin Solid Films,* **370** (2000) 89.
11. S. K. Haram and K. S. V. Santhanam, *Thin Solid Films,* **238** (1994) 21.
12. www.espimetals.com/msds's/copperselenidecu2se.pdf Issued By: S. Dierks Dated: September 1995.

CHAPTER 5

RESULTS AND DISCUSSION

The results regarding structural, electrical and optical properties of $Cu_{2-x}Se$ and Cu_3Se_2 thin films deposited by CBD method have been presented in this chapter. The annealing effect of the film has also been discussed. A comparative study has also been performed between the films prepared by CBD and vacuum evaporation technique.

5.1 GROWTH OF THE FILMS USING CBD

5.1.1 Growth of the Films By Varying Bath Parameters

It has been observed that amount of film deposition as a function of duration of deposition for different ammonia and triethanolamin (TEA) concentrations at room temperature is shown in Fig. 5.1. It is seen that at low concentration of ammonia or TEA, the terminal thicknesses of the films are less, which gradually increase with increasing concentrations and then drop down at still higher concentrations. The same behavior was found for CBD CdSe thin films [1,2]. Both ammonia and TEA are bases and liberate OH^- ions in solution, i.e., they increase the pH of the solution. Again, they form complexes with Cu^{2+} ions. Hence, on addition of TEA or ammonia to the reaction solution, two processes starts simultaneously. Firstly Cu^{2+} ions form the complexes thereby retards the rate of formation of thin films and secondly, the increased pH of the solution enhances the rate of formation of copper selenide thin films. Results show that optimum amounts of both the reagents present in the reaction solution lead to a controlled reaction yielding the maximum terminal thickness of the film. Moreover, it has been found that complexing the Cu^{2+} ions with TEA first, and then addition of ammonia yields better results than the reverse process. Hence in all the experiments TEA has been added before ammonia.

The effect of various concentration of the selenosulfate solution on the film thickness at room temperature has been plotted in Fig. 5.2. An optimum amount of the selenosulfate solution is required to deposit the thickest film. The deposition process may be explained as follows: At low selenosulfate concentration, the number of Se^{2-} ions being insufficient to combine with all the available Cu^{2+} ions, the terminal

thickness is observed to be less. As selenosulfate concentration increases, more Se^{2-} ions become available to form copper selenide thin films, leading to greater film thickness (curve b). Above a certain concentration, when rate of reaction becomes very fast, precipitation dominates over film formation, leading again to lower terminal thickness (curve c).

The temperature dependence of film formation as a function of duration of deposition shown in Fig. 5.3. With increasing temperature, the rate of deposition of thin films increases due to increase in the kinetic energy of the reacting ions, i.e., an increase in frequency of collision among the ions. This is reflected in the curve b obtained at 65°C, which has a higher deposition rate than that obtained at 30°C. Deposition at still higher temperature, i.e., at 85°C, however, again lead to lower deposition rate on the substrate surface. Here the rate of precipitation becomes much faster than the rate of deposition at the surface. However, deposition at 85°C yields greater terminal thickness than that at 65°C (not shown in figures). This is because a total loss of complexation of the Cu^{2+} ions occurs at 85°C yielding a colorless solution. While up to 65°C, the solution remains dip-blue even after the experiments were over. This extra release of Cu^{2+} ions at 85°C helps to attain greater terminal thickness. One disadvantage that crops up with increase on the deposition temperature is that the adherence property of the film decreases gradually. The films start peeling off the substrates at higher temperatures of deposition. Moreover, at higher temperatures, the deposition is not uniform. Hence, room-temperature deposition is always preferred at any circumstances.

Film deposition was also carried out under stirring condition at room temperature. As expected, the rate of deposition in this case was greater than that obtained for the unstirred solution. This is due to the faster arrival of the ions on the substrate surface. However, in case of the stirred solution, an adherent deposit of the precipitate was found to develop gradually at particular positions over the film after the deposition for about 3 to 4 hr. This gives rise to nonuniform film deposition.

In all the experiments it has been found that an initial induction period of about 5-10 minutes was required after which film deposition starts. This may be due to the fact that the complexing of Cu^{2+} ions with TEA and ammonia being quite strong, the release of Cu^{2+} ions from the complexes after the addition of selenosulfate solution is a

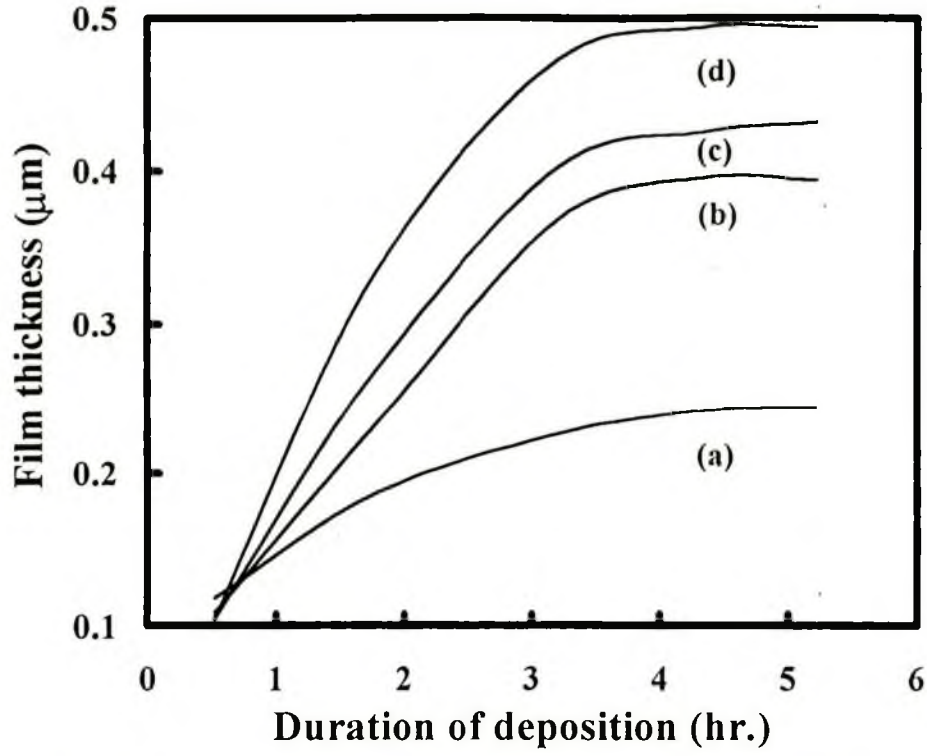

Fig. 5.1. Variation of $Cu_{2-x}Se$ film thickness with duration of deposition for different ammonia concentrations: curve (a) without NH_3, (b) 2 ml of 0.5% NH_3 (c) 4 ml of 0.5% NH_3 (d) 6 ml of 0.5% NH_3.

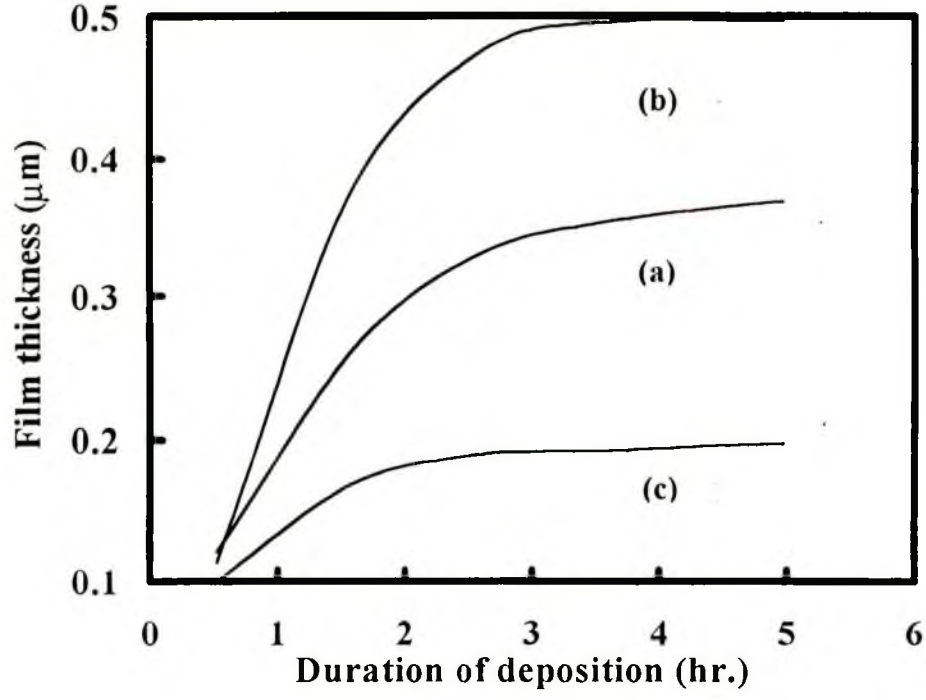

Fig. 5.2. Variation of $Cu_{2-x}Se$ film thickness with duration of deposition for different selenosulfate concentrations: curve (a) 100 ml 0.1 M Na_2SeSO_3, (b) 150 ml 0.1 M Na_2SeSO_3, (c) 200 ml 0.1 M Na_2SeSO_3.

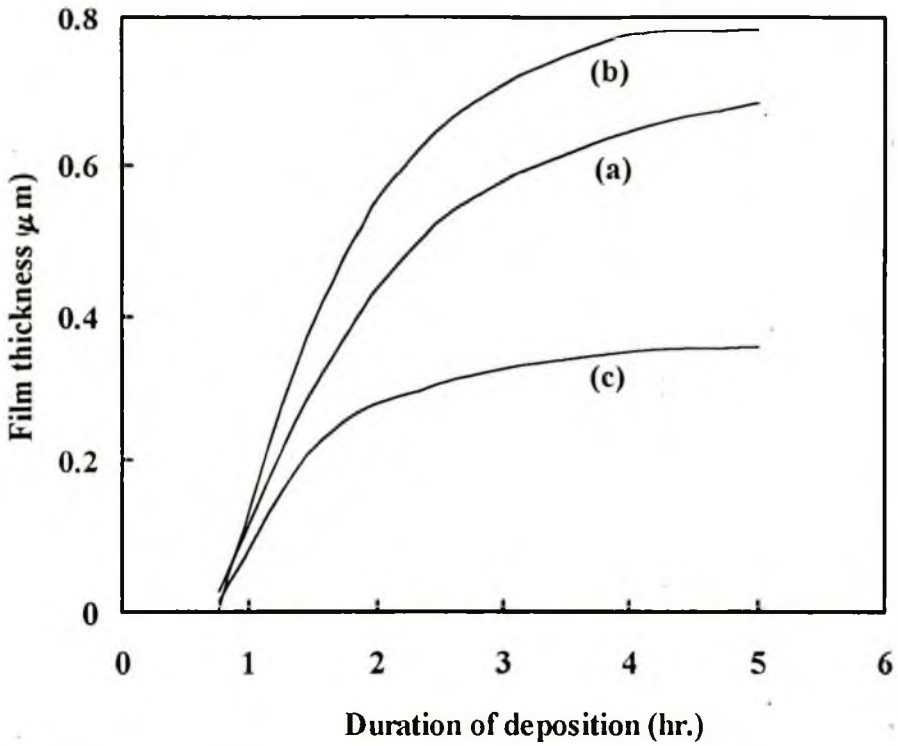

Fig. 5.3. Variation of $Cu_{2-x}Se$ film thickness with duration of deposition time at different temperatures: curve (a) deposition at room temperature (30°C), (b) deposition at 65°C, (c) deposition at 85°C.

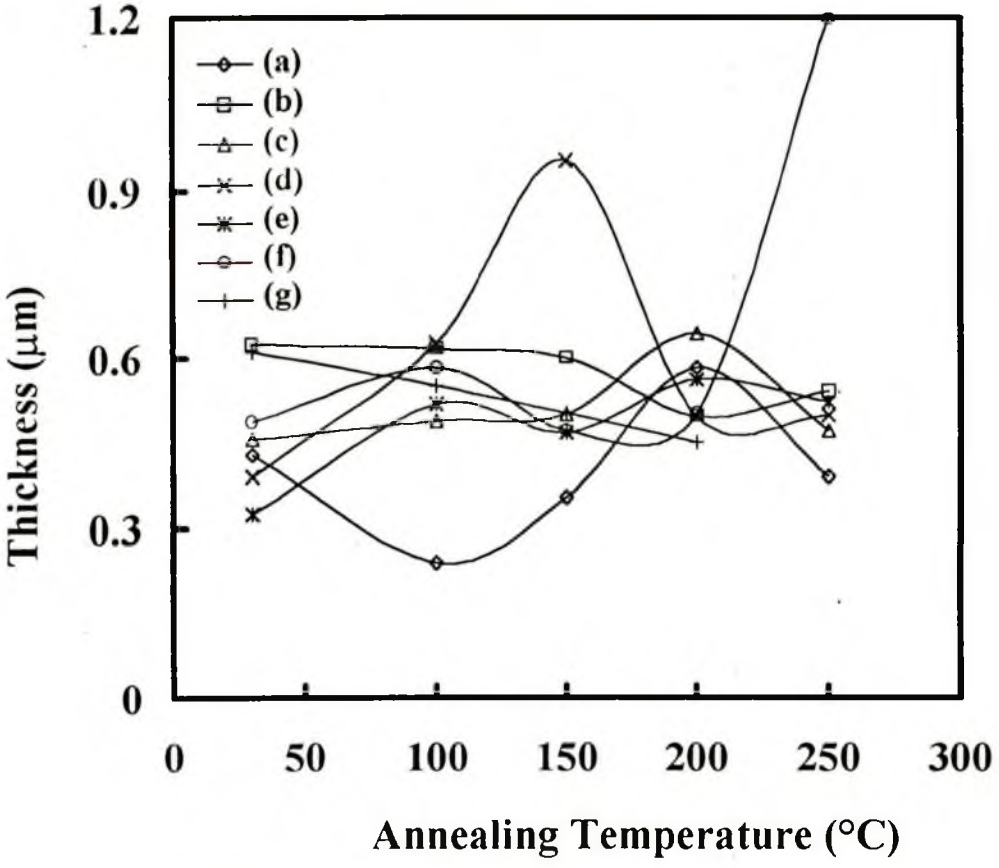

Fig. 5.4. Thickness variation with annealing temperature: (a-g) for sample 1-7.

time-consuming process leading to a longer time for the ionic product of copper selenide to exceed its solubility product. Garcia *et al.* [3] reported that the thickness increases even after the deposition for 20 hrs, whereas in our case, the thickness does not change with the increase of time duration after 4 hrs. Thus it is unable to detect the terminal thickness for each deposition process. Powdery deposits and lack of specular reflection usually accompany higher deposition rate and higher film thickness. In the present work, some good samples of copper selenide thin film deposited for 1 hour at room temperature of thicknesses between 0.2 and 0.6 μm with the various ratios between Cu and Se were characterized, and these parameters are same for all the samples used in the present study.

5.1.2 Thickness Variation with Annealing Temperature

Figure 5.4 shows the variation of film thickness with different annealing temperatures for all samples. From these plot it seems that for all samples prepared by CBD the thickness increases with the annealing temperature upto 200°C, this may be due to the increases of grain size. After annealing above 200°C the film thickness gradually decreases, this may be due to the same reason for oxygen disorption upto 200°C and above 200°C, Se starts peeling off from the substrate, which will be discussed later in XPS and XRD measurement. For vacuum deposited thin film the thickness gradually decreases with temperature, this may be due to reduction of multilayer (Cu and Se layer) into a single layer of copper selenide thin film.

5.2 SURFACE MORPHOLOGY BY AFM MEASUREMENTS

The surface morphology of copper selenide films deposited onto glass substrate was studied by Atomic Force Microscopy (AFM). AFM images of as-deposited CBD copper selenide thin film are shown in Figs. 5.5 and 5.6 for the scan areas of 2×2 μm^2 and 4×4 μm^2, respectively. In the figures, (a) and (b) are the two- (2D) and three-dimensional (3D) images, respectively. It seems that the overall film surface is almost smooth. The film surfaces contained small islands, and many continuous islands are overlapping on the glass substrate. It is observed from the profile diagram of the AFM image that the mean roughness and mean height are in the range 2.9-3.4 Å and 11-15

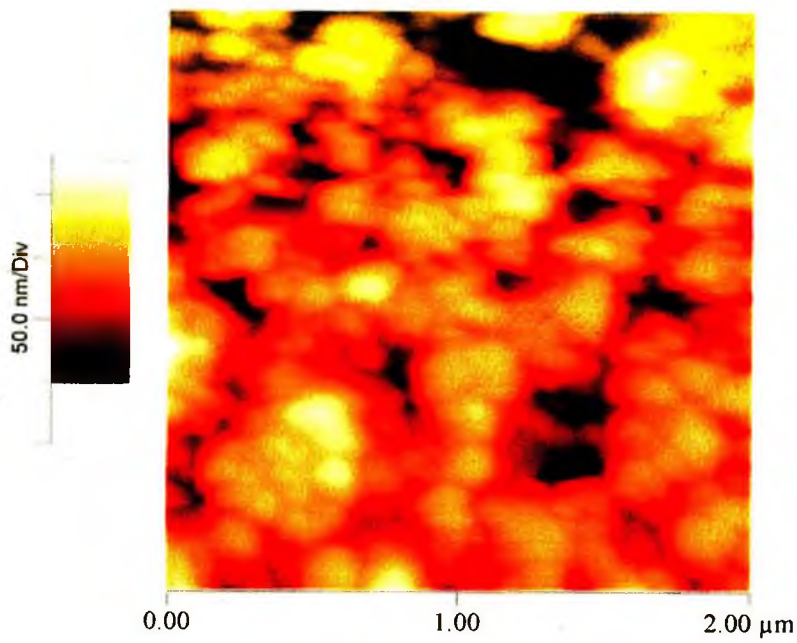

Fig. 5(a). 2D AFM image of as-deposited CBD copper selenide thin film with the scan area 2×2 μm^2.

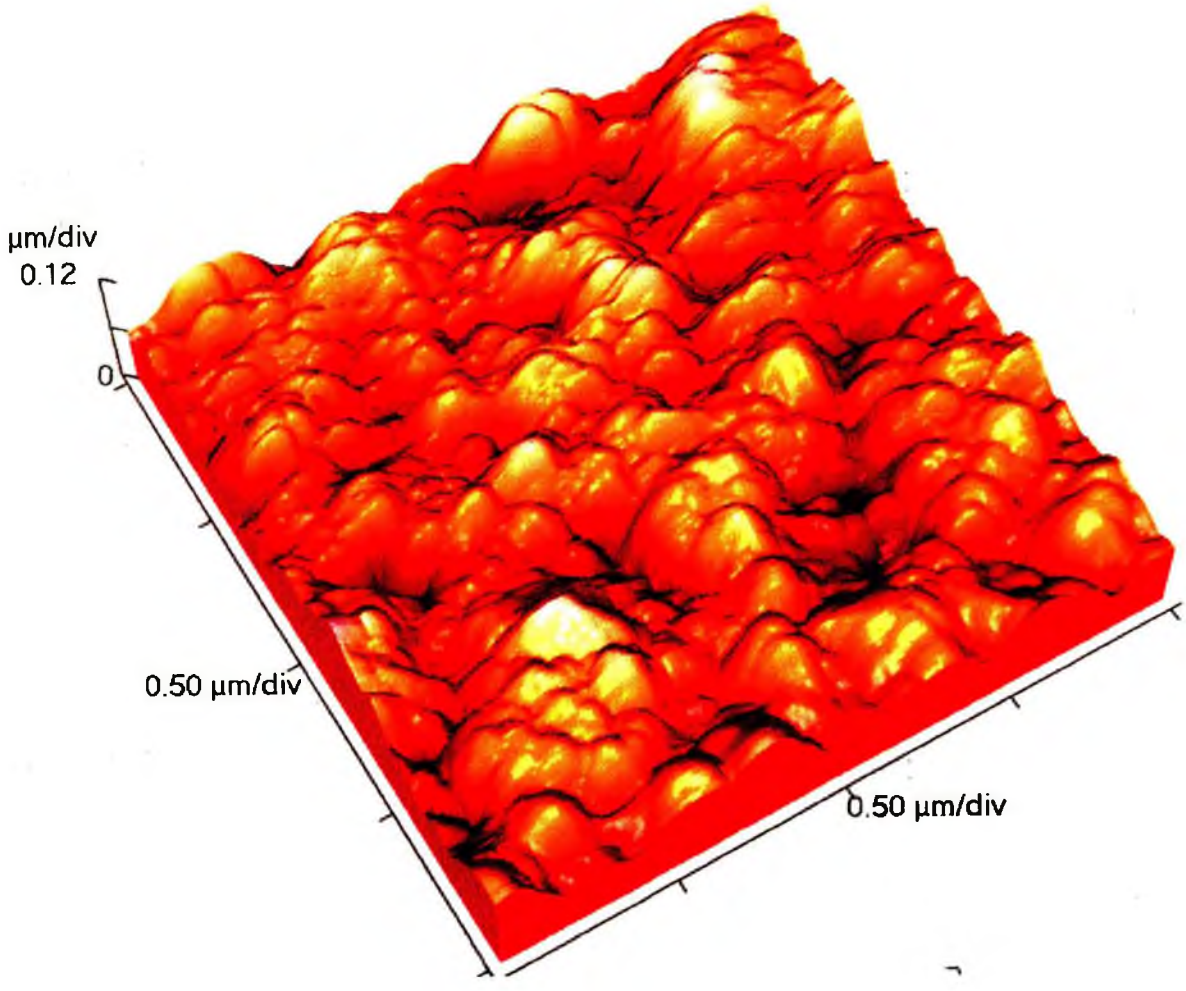

Fig. 5(b). 3D AFM image of as-deposited CBD copper selenide thin film with the scan area 2×2 μm^2.

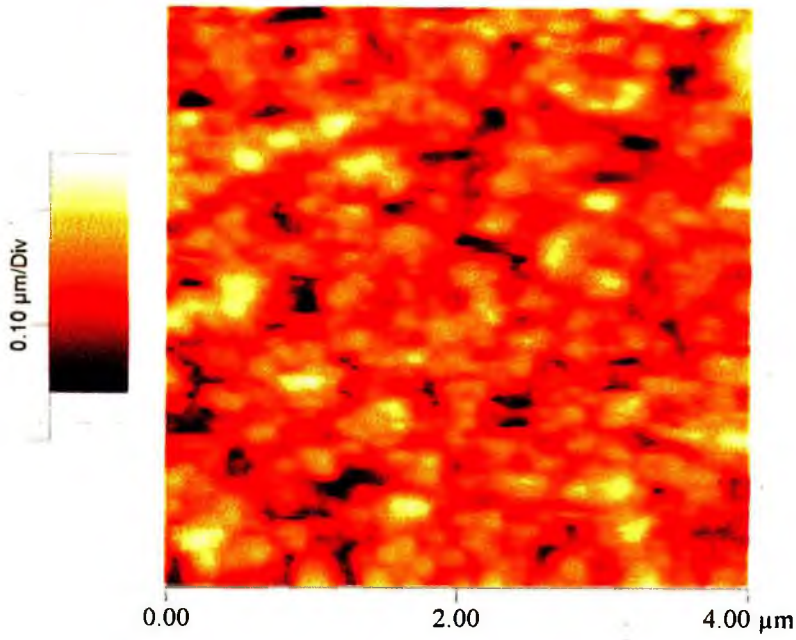

Fig. 6(a). 2D AFM image of as-deposited CBD copper selenide thin film with the scan area 4×4 μm^2.

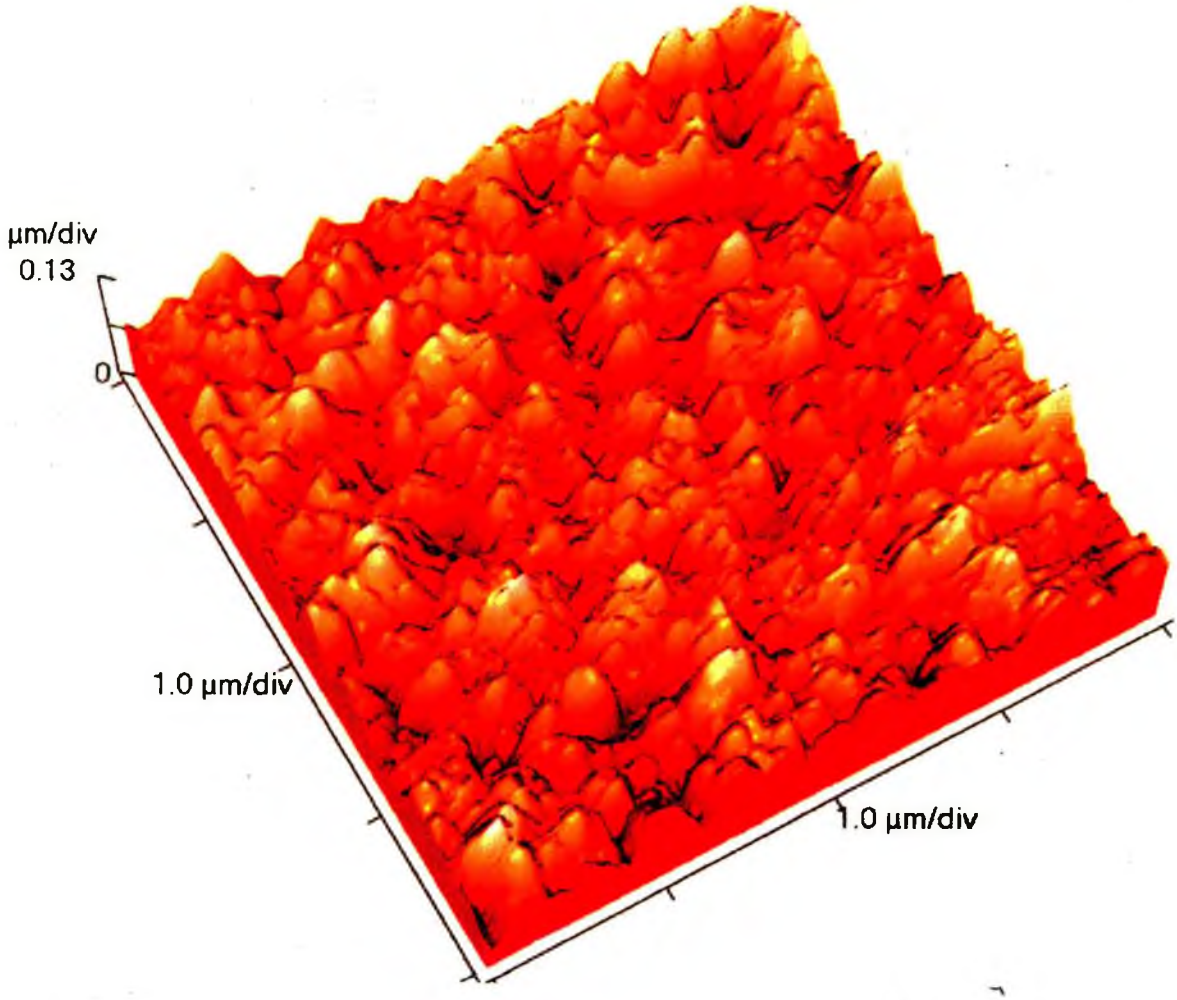

Fig. 6(b). 3D AFM image of as-deposited CBD copper selenide thin film with the scan area 4×4 μm^2.

Å, respectively. The observed value of mean height well agrees with the film thickness of as-deposited films as observed by other methods.

5.3 XPS MEASUREMENTS

The XPS spectra of different copper selenide thin film of sample-4 presented in Fig-5.7. In the figure, spectrum-a represents for as-deposited sample, spectrum-b represents for the sample annealed at 200°C for 30 min in UHV and spectrum-c represents for the sample annealed at 250°C for 30 min in UHV. It is observed that the as-deposited film is mostly covered with oxygen (at 531eV) and carbon (at 285eV) (spectrum-a). Whereas, the peak intensity of Cu and Se are very weak. It is usual that the chemically-deposited sample may be contaminated with oxygen and carbon from the environment as the sample is exposed to environment during preparation. It is seen that the peaks corresponding to Cu and Se become prominent in the sample annealed at 200°C (spectrum-b) and after annealing at 250°C, the intensity of Cu and Se peaks become more prominent, thereby indicating lowering of contamination owing to annealing at 250°C (spectrum-c). Further annealing around 300°C, Se starts to desorb from the surface, (data are not shown), which means that copper selenide film remains stable below 300°C. It is also observed that color of the film was changed from greenish to orange due to annealing. It means that as-deposited film is contaminated by oxygen and oxygen contamination starts to remove due to annealing. The amount of oxygen decreases significantly but Se is also started to decrease due to annealing at above 300°C. The color becomes greenish orange on annealing at 200°C, and at 250°C, the color changes to fully orange, which does not change on annealing above 300°C.

The core level spectra of Cu 2p and Se 3d are shown in Fig. 5.8. In the figure, (a) is the Cu 2p core level spectra and (b) is the Se 3d core level spectra for as-deposited sample, and the sample annealed at 200°C and 250°C for 30 min. The peaks of as-deposited sample are very weak due to the contamination. Both the Cu 2p and Se 3d peaks become prominent owing to annealing, showing reduction of contamination on annealing. The binding energy of Cu $2P_{1/2}$ and Se 3d peaks of as-deposited sample are observed to be 932.0 and 55.4 eV respectively. The binding energy of both the Cu $2p_{1/2}$ and Se 3d peaks are changed to 932.4 and 54.4 eV, respectively due to annealing

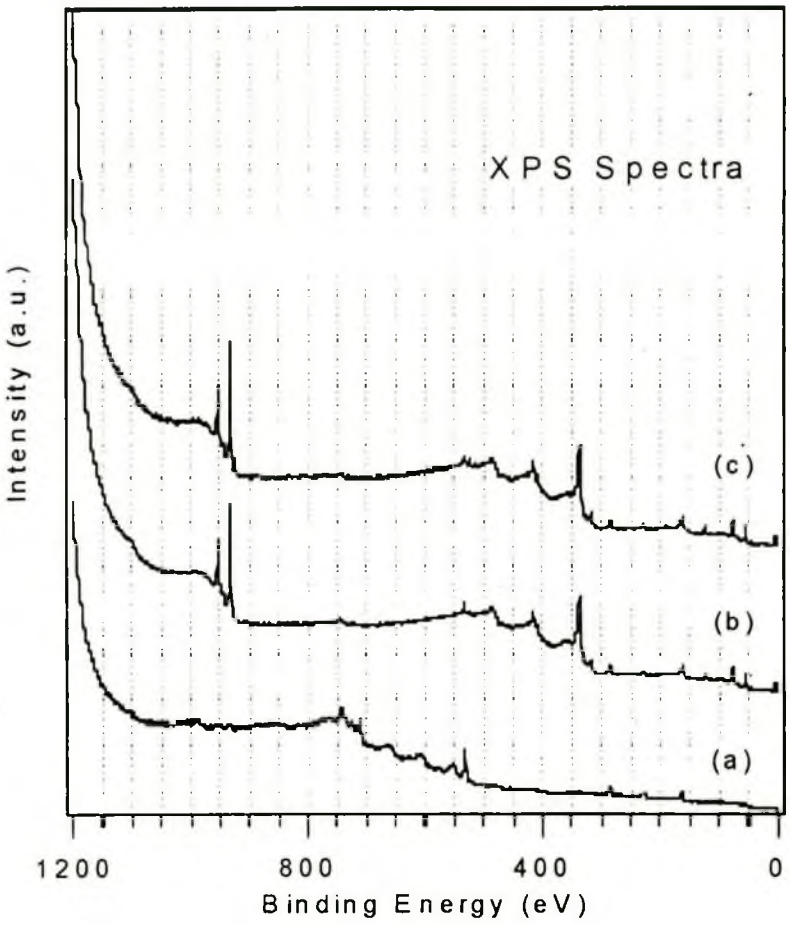

Fig. 5.7. XPS spectra of $Cu_{2-x}Se$ thin film: (a) as-deposited, (b) after annealing at 200°C for 30 min, (c) after annealing at 250°C for 30 min. The annealing is performed in UHV chamber

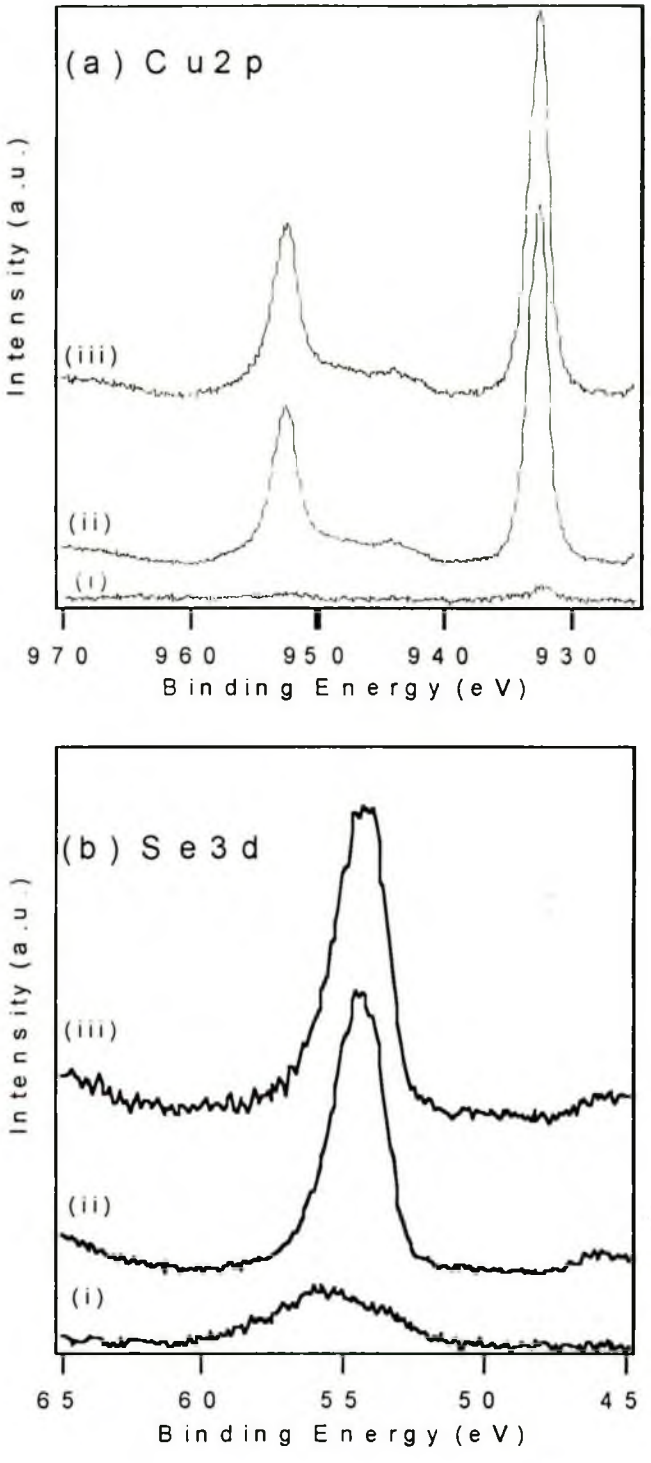

Fig. 5.8. Core-level XPS spectra of $Cu_{2-x}Se$ thin film: (a) Cu $2p_{1/2}$ level (i) as-deposited, (ii) after annealed at 200°C for 30 min, (iii) after annealed at 250°C for 30 min and (b) Se *3d* level (i) as-deposited, (ii) after annealed at 200°C for 30 min, (iii) after annealed at 250°C for 30 min. The annealing has performed in UHV chamber.

at 200°C. The binding energy of Cu $2P_{3/2}$ peak of as-deposited and annealed sample is observed to be at 952.0 (weak peak) and 952.4 eV, respectively. It is also observed that the peak positions of both Cu $2p_{1/2}$ and Se 3d are not changed any more due to annealing at 250°C. The peak area of Cu 2p and Se 3d has been calculated. The Cu/Se ratio is estimated to be 1.8 for sample-4. Similarly different samples have been deposited with different Cu and Se ratio.

5.4 XRD MEASUREMENT

All the X-ray data of the samples were analyzed by using computer to get d values and peak intensities. The spacing d was calculated using Bragg relation,

$$2d \sin\theta = \lambda$$

where λ is the wavelength of the incident radiation and for Cu(Kα), λ=1.54178Å. The XRD pattern was then analyzed using the d values of their main fundamental peaks. The d values and their intensity ratios were compared with the data available in the analytical library of the computer software, which contains JCPDS International Centre for Diffraction Data (PCPDFWIN, V **202**,1999) and the unknown compound and elements were identified.

Figure 5.9 shows the XRD pattern of as-deposited sample. From this pattern it shows that no well-defined peak was found and no plane was obtained in the case of as-deposited films, which means that the as-deposited films were dis-order.

Figure 5.10 shows the XRD pattern of sample-4 followed by annealing at 250°C in air for one hour shows well-defined peaks suggesting that crystalline film is formed after annealing. A comparison of the observed pattern with the standard JCPDS cards shows that the annealed samples with above condition possess a structure matching the cubic (Berzelianite) (JCPDS 26-512) [4], $Cu_{2-x}Se$ with x=0.2 which belongs to the cubic system with lattice parameter a=5.697Å. The crystallinity of the films was observed to improve owing to annealing at 250°C. The observed peak positions are in agreement with those due to reflection from (111), (220) and (311) planes of the reported structure. The same reflection plane and crystal structure was observed for as-deposited $Cu_{2-x}Se$ thin film prepared by $CuSO_4$ and tri-sodium citrate [5] and for as prepared $Cu_{1.85}Se$ thin film of 0.13 μm thickness [3,6]. Figure 5.11 shows the XRD pattern of annealed sample-6 at 250°C in air for one hour. It shows

well-defined peaks matching to Cu_3Se_2 (JCPDS 25-263) which belongs to the tetragonal phase with a=5.63Å and c=11.23Å. The observed peak positions are in agreement with those due to reflection from (112), (204) and (312) planes of the reported structure [7]. It can be concluded that the crystallinity is found very low for as-deposited samples, but this improves upon annealing in air at 250°C.

The crystalline grain size in the films was calculated using the Scherrer formula. The full width at half maxima (FWHM) of the largest peak for as-deposited, samples (4 and 6) annealed at 250°C were found to11.29, 0.38 and 0.40, respectively. The average grain diameter for as-deposited sample was found to be 0.025 nm that increases for annealed samples 4 and 6 to 0.724 and 0.688 nm respectively. Very low grain size is observed for as-deposited samples, which can be increased about 30% owing to annealing. The X-ray diffraction parameters for $Cu_{1.8}Se$ and Cu_3Se_2 are summarized in Tables-5.1 and 5.2.

Table-5.1: X-ray diffraction parameters of Cubic (berzelianite) $Cu_{1.8}Se$ thin film.

***d* (Å) experimentally observed**	***d* (Å) theoretical values**	***hkl***	**Relative Intensity (%)**	**Angle (*2θ*)**	**Peak height (counts/s)**
3.324	3.328	111	100.00	27.43	125.12
1.996	2.038	220	88.08	45.14	110.20
1.743	1.738	311	29.99	53.36	37.52

Table-5.2: X-ray diffraction parameters of tetragonal Cu_3Se_2 thin film.

***d* (Å) experimentally observed**	***d* (Å) theoretical values**	***hkl***	**Relative Intensity (%)**	**Angle (*2θ*)**	**Peak height (counts/s)**
3.245	3.252	112	100.00	27.46	306.43
2.005	1.994	204	81.97	45.19	251.19
1.744	1.734	312	16.68	52.41	51.11

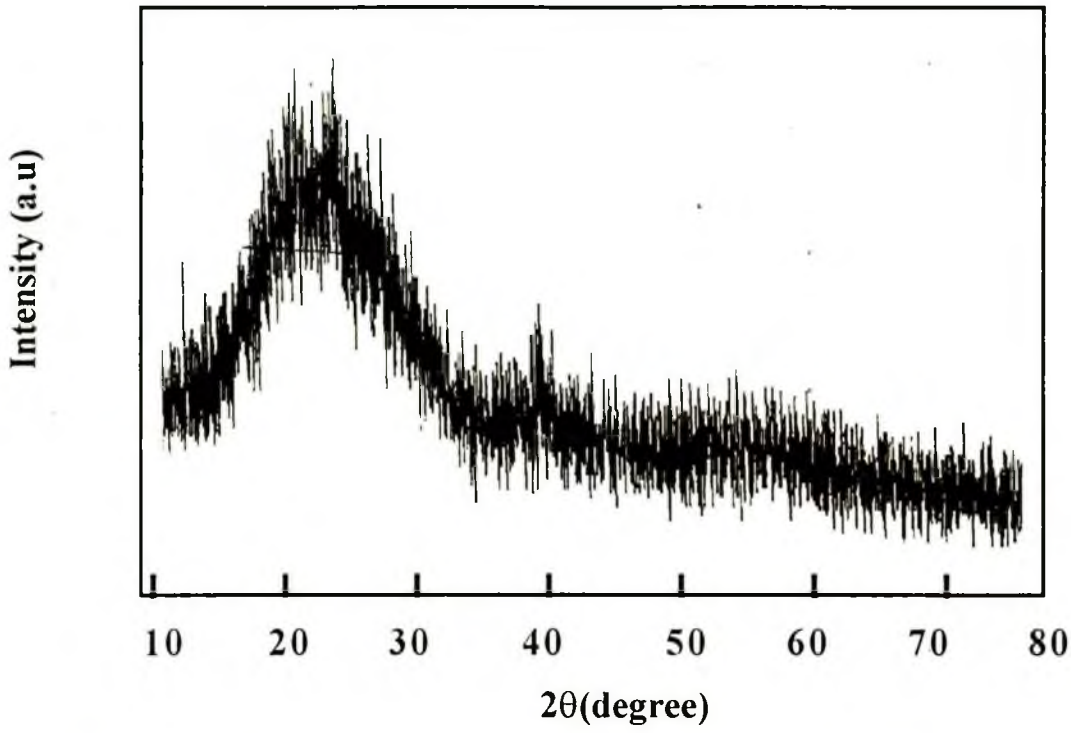

Fig. 5.9. XRD pattern of as-deposited CBD copper selenide thin film.

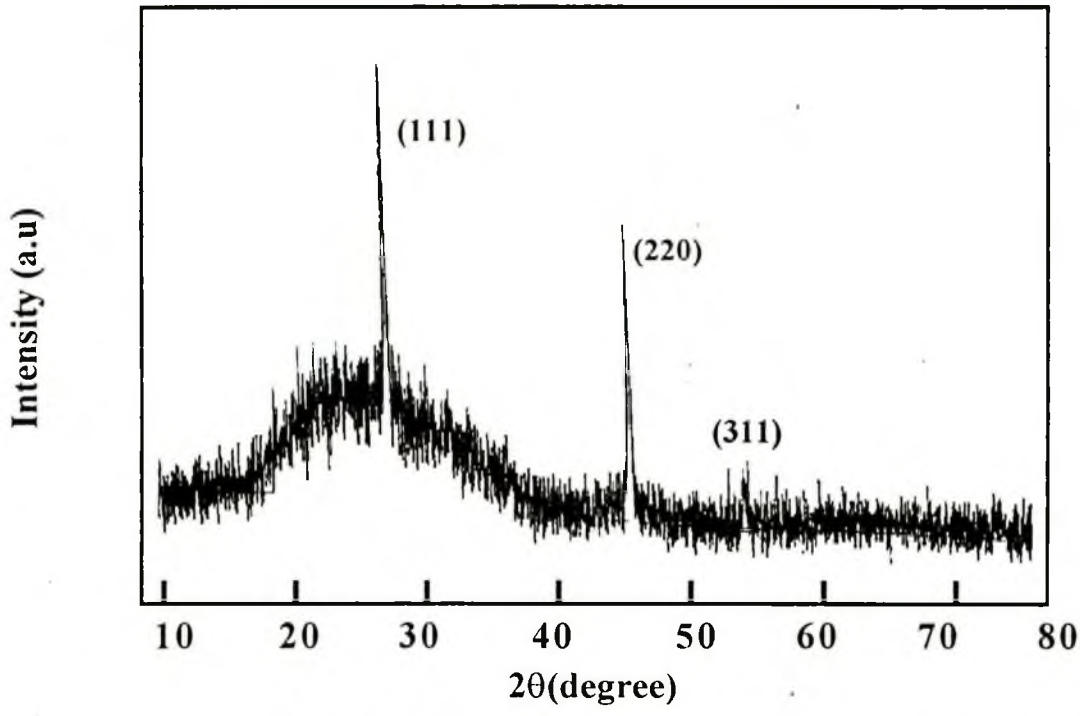

Fig. 5.10. XRD diffraction pattern of sample-4 followed by annealing at 250°C for 1 hr.

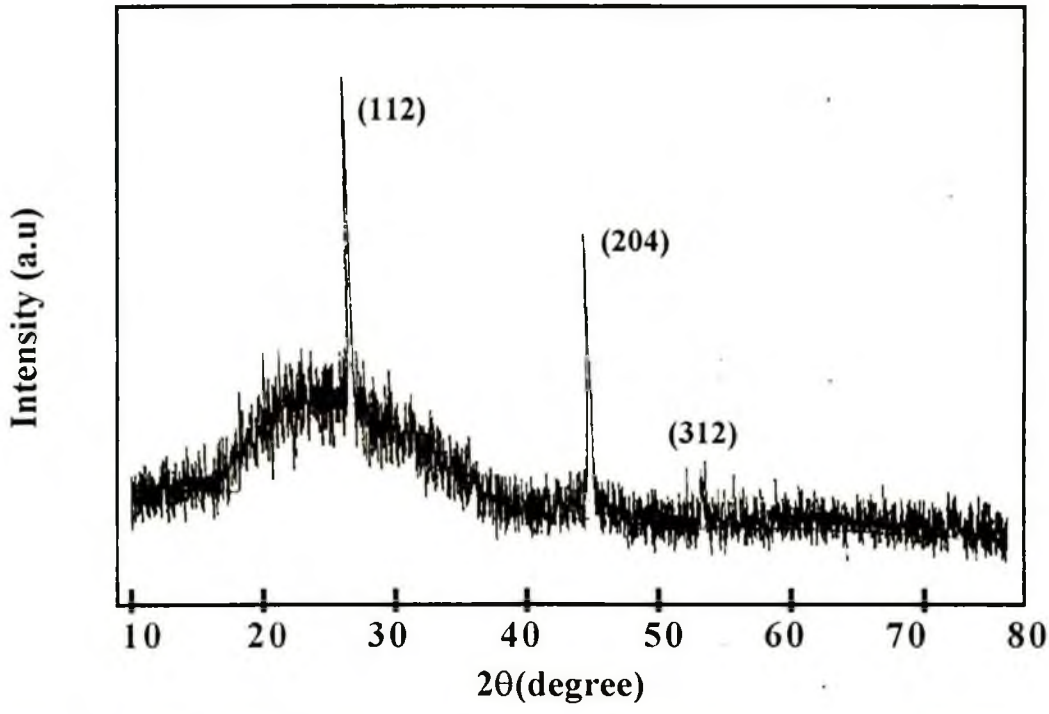

Fig. 5.11. XRD diffraction pattern of sample-6 followed by annealing at 250°C for 1 hr.

5.5 DC ELECTRICAL PROPERTIES

Two points on the surface of the film were made for electrical contact with silver paste. Figures 5.12–5.18 show the I–V characteristic curves for samples 1-7. The I–V characteristics have been studied over the range from 5 mV to 20 V. An ohmic behaviour is observed in as-deposited and annealed samples at all temperature.

We evaluated the resistivity from I–V data. Very low resistivity is observed for CBD thin film lying in the range (2 to 25) × 10^{-3} Ω-cm whereas the vacuum deposited film showed the resistivity in the range 1.5 to 2.3 × 10^{-3} Ω-cm. The resistivity of vacuum deposited thin film was found to be lower than that of CBD deposited film. The CBD resistivity of films deposited at different conditions is summarized in Table-5.3. Figure 5.19 represents the change of resistivity of samples (1–6) deposited at room temperature with the increase of annealing temperature. Initially for CBD samples (1–5) the resistivity decreases slowly with the increase of annealing temperature upto 200°C and then increases rapidly. As observed in XPS, the surfaces of the as-deposited films are mostly covered with oxygen. In as-deposited and samples annealed at lower temperature ionization take place on the surface owing to the presence of oxygen resulting lower resistivity because of participation of ionic current with the electronic current. Whereas, for the sample annealed above 250°C, the ionic contribution becomes less due to desorption of oxygen from the surface. As a result, the resistivity increases rapidly. A gradual decrease of resistivity was observed for sample-6, this may be due to high conductivity of this phase of Cu_3Se_2 thin film. The resistivity increases for vacuum deposited thin film, this may be due to bonding of Se with Cu atom.

Figure 5.20 represents plot of resistivity with various concentration of x at different annealed temperature. From the concentration dependent resistivity, it is seen that the resistivity of the sample in the x = 0.3 shows much been dependent on annealing temperature. All other samples show more dependent on annealing temperature.

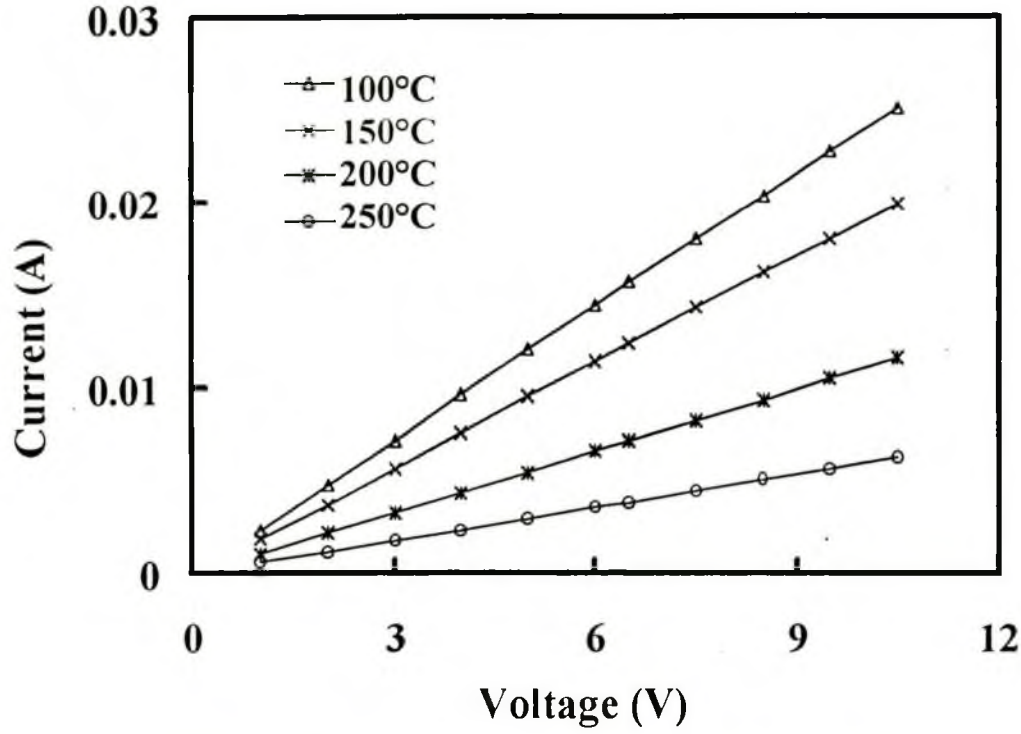

Fig. 5.12. Current-voltage curve for sample-1 at various annealed temperature for 1 hr.

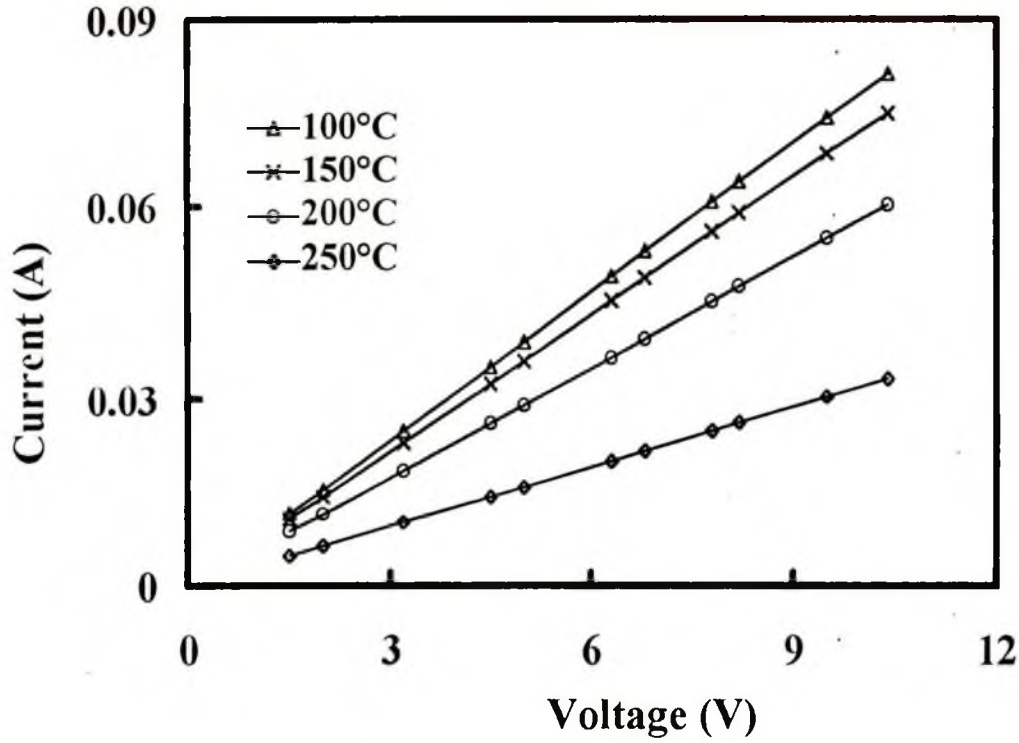

Fig. 5.13. Current-voltage curve for sample-2 at various annealed temperature.

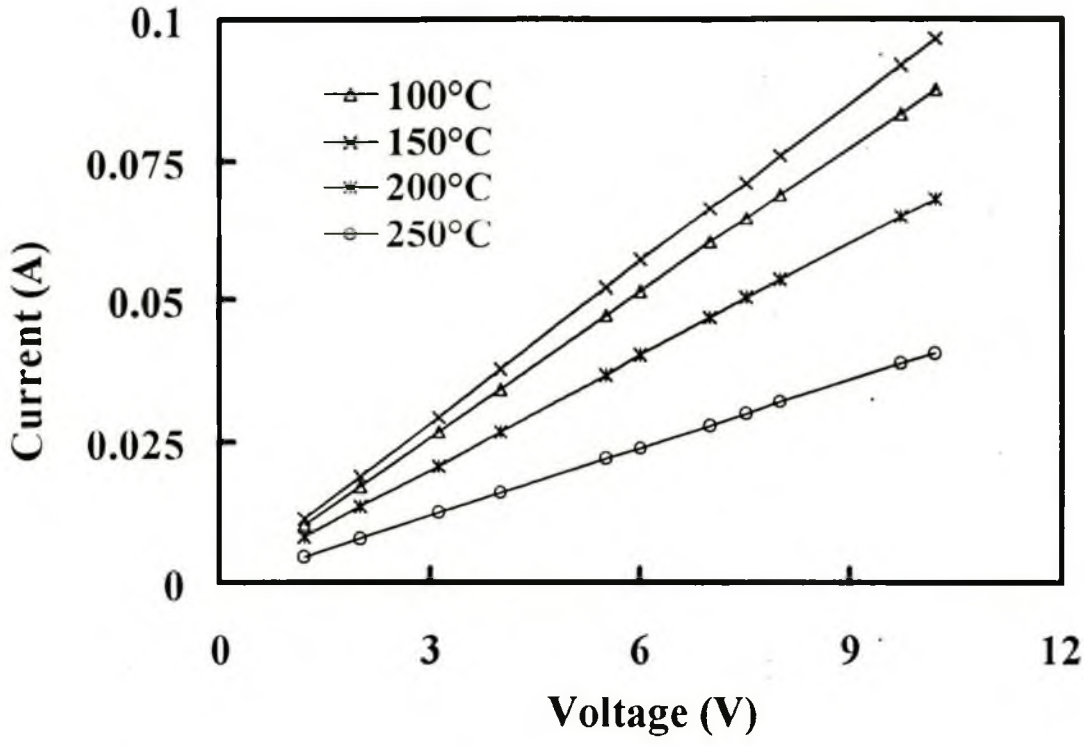

Fig. 5.14. Current-voltage curve for sample-3 at various annealed temperature for 1 hr.

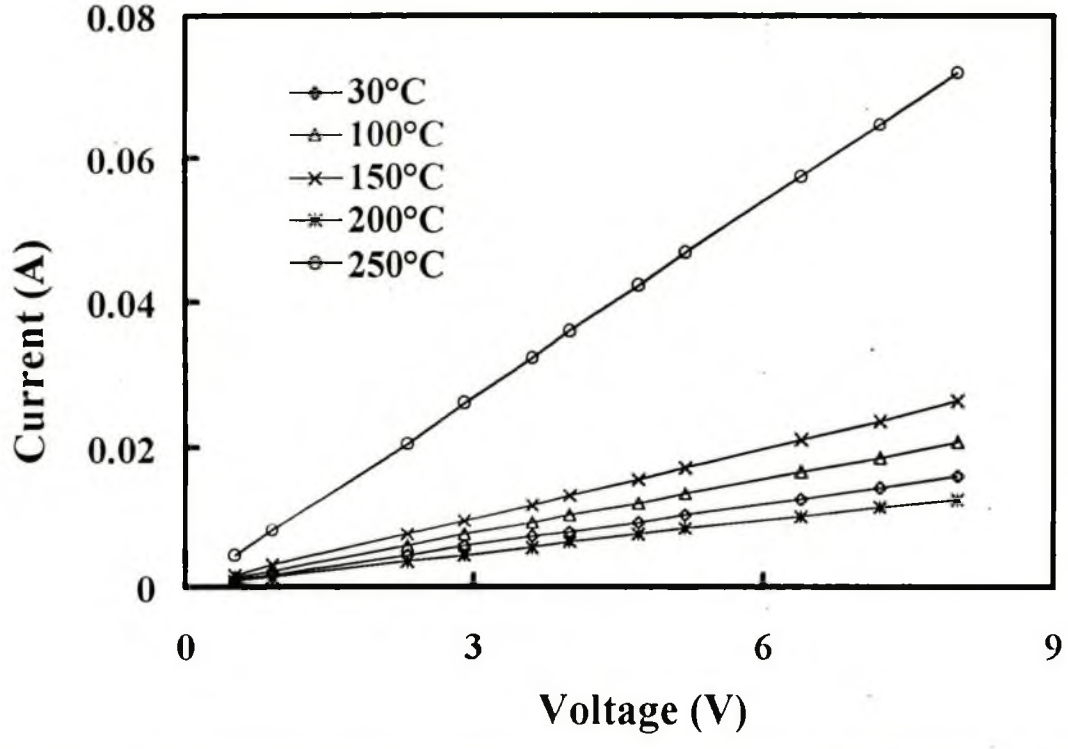

Fig. 5.15. Current-voltage curve for sample-4 at various annealed temperature for 1 hr.

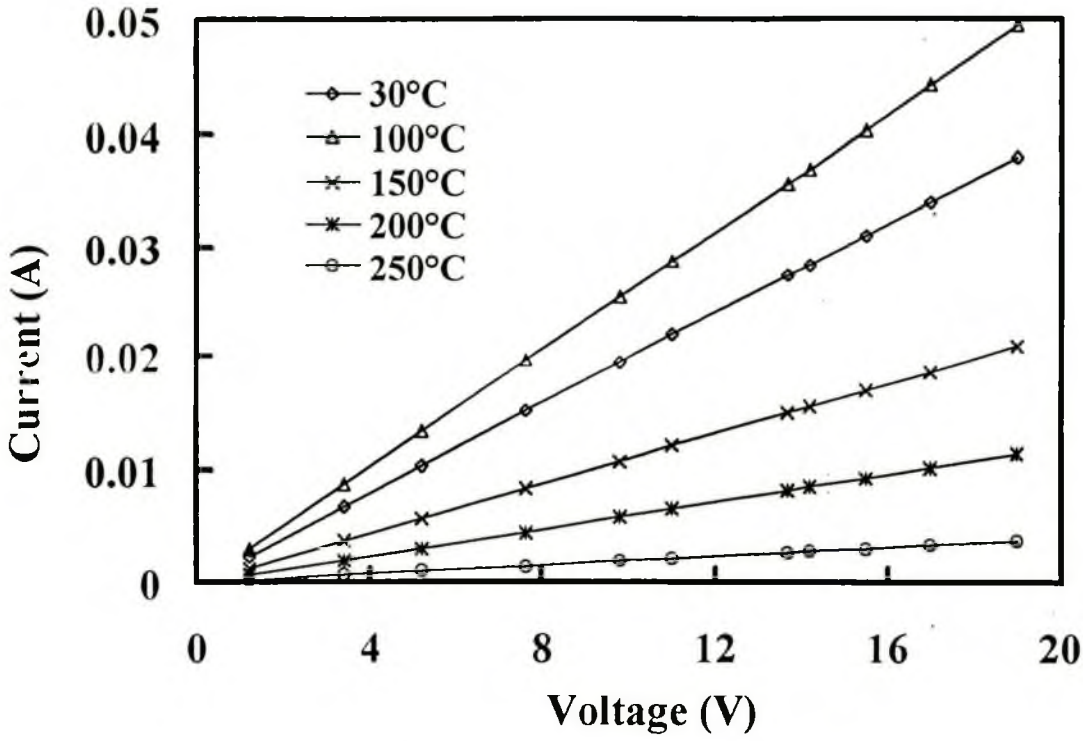

Fig. 5.16. Current-voltage curve for sample-5 at various annealed temperature for 1 hr.

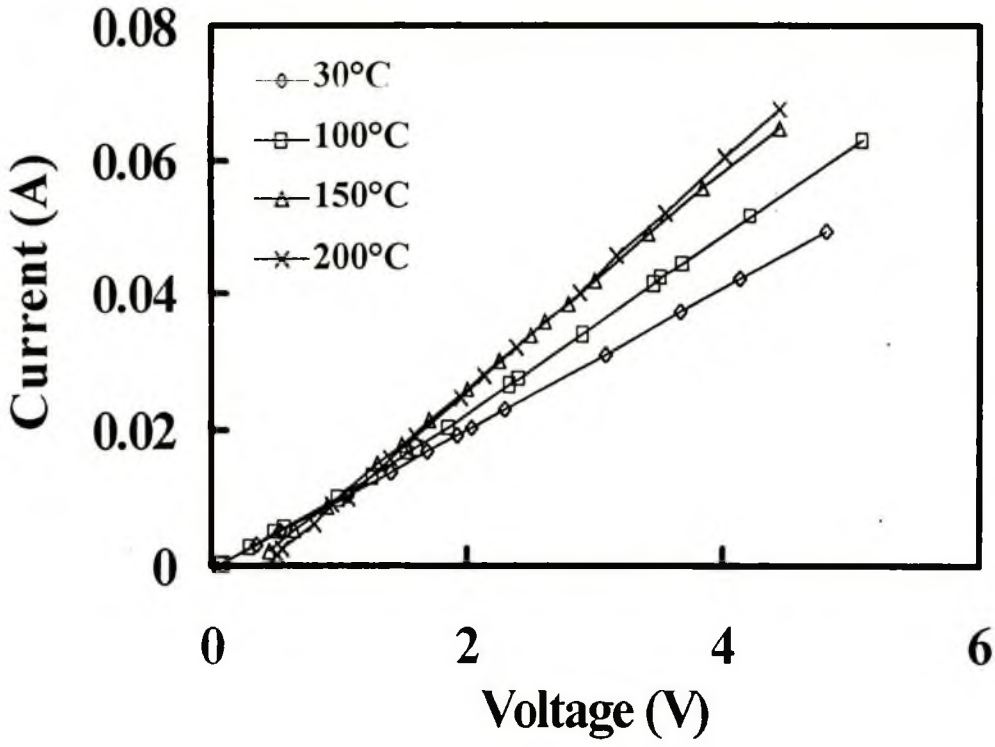

Fig. 5. 17. Current-voltage curve for sample-6 at various annealed temperature for 1 hr.

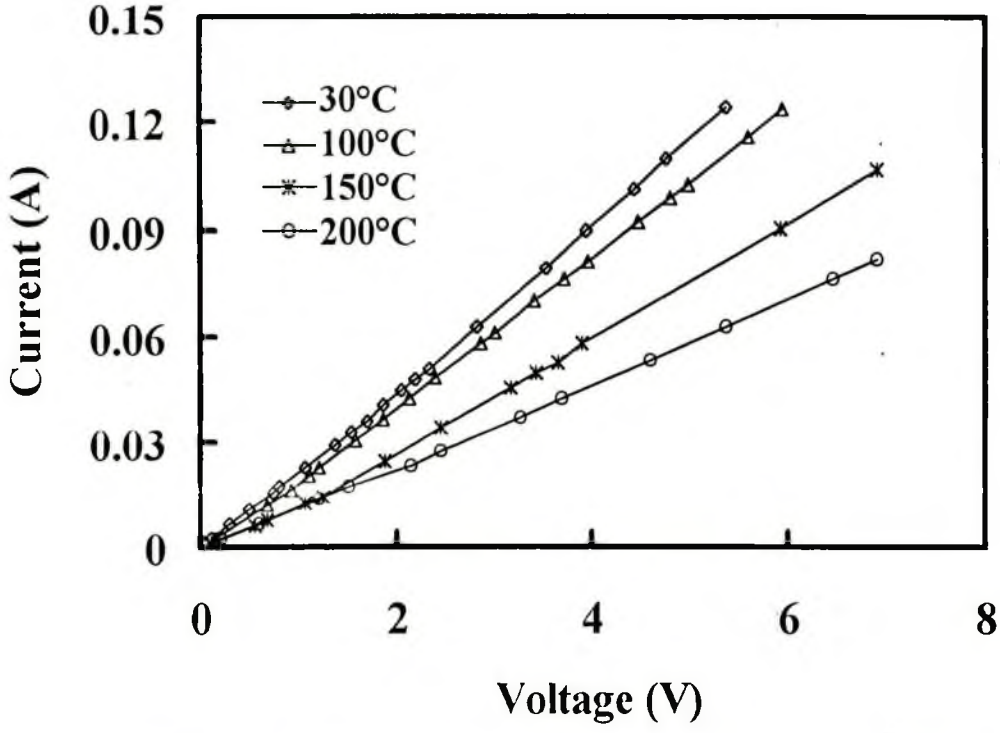

Fig. 5.18. Current-voltage curve for sample-7 at various annealed temperature for 1 hr.

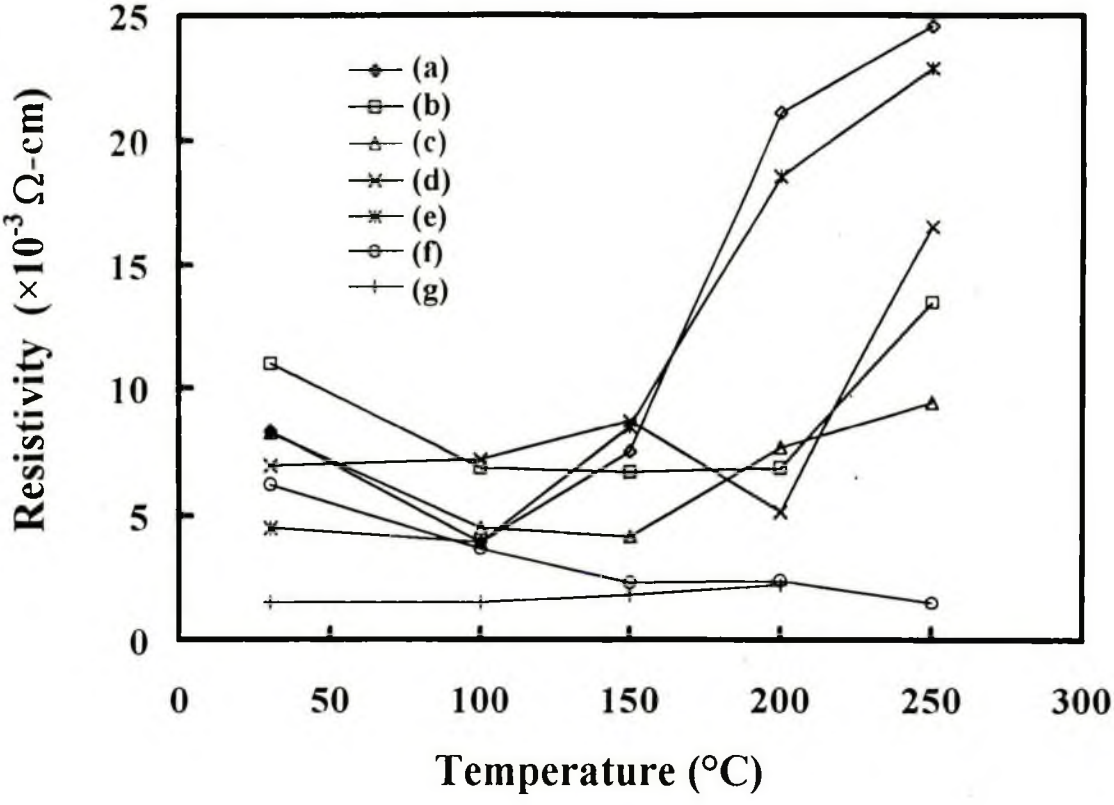

Fig. 5.19. Variation of resistivity with different annealed temperatures of copper selenide thin film: curve (a-f) for CBD sample-(1-6) and (g) for vacuum deposited sample.

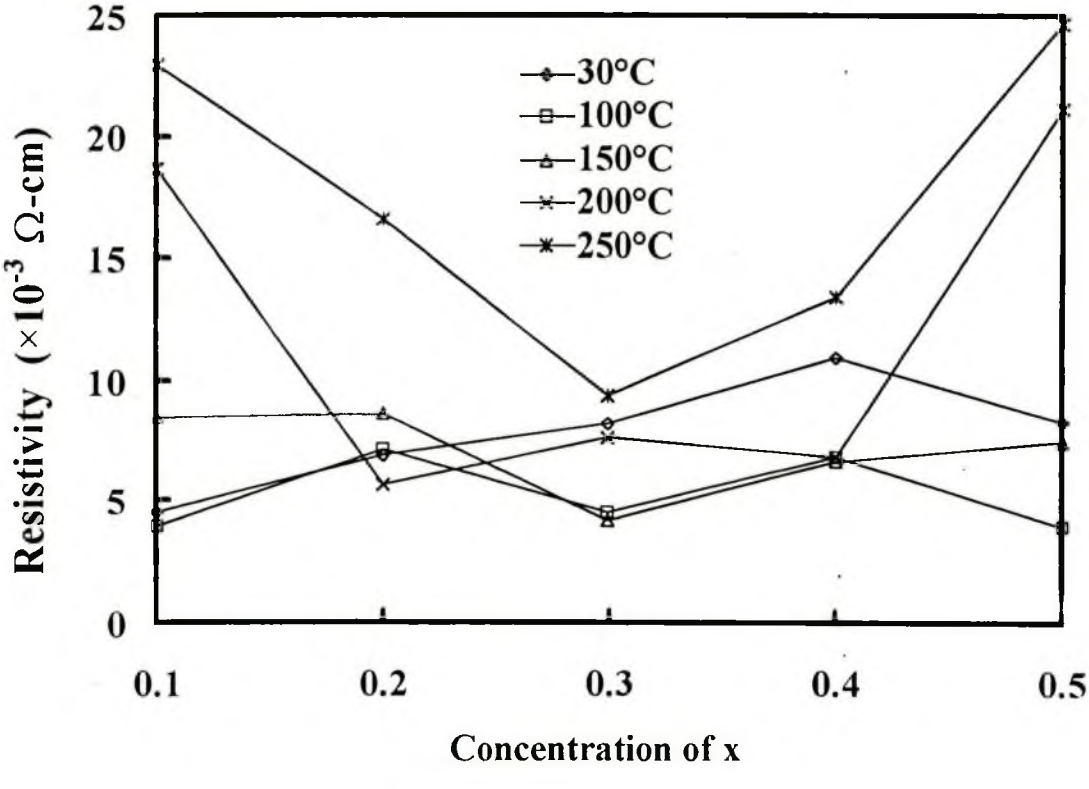

Fig. 5.20. Variation of resistivity with value of x at different annealed temperatures.

Table-5.3. Resistivity of different phase of CBD copper selenide thin film annealed at different temperatures.

	t (°C)	Sample-1	Sample-2	Sample-3	Sample-4	Sample-5	Sample-6	Sample-7
Resistivity (Ω-cm)	30	8.34×10^{-3}	10.99×10^{-3}	8.23×10^{-3}	6.90×10^{-3}	4.55×10^{-3}	3.74×10^{-3}	1.54×10^{-3}
	100	3.98×10^{-3}	6.85×10^{-3}	4.52×10^{-3}	7.20×10^{-3}	3.96×10^{-3}	3.72×10^{-3}	1.55×10^{-3}
	150	7.47×10^{-3}	6.67×10^{-3}	4.20×10^{-3}	8.67×10^{-3}	8.49×10^{-3}	2.36×10^{-3}	1.89×10^{-3}
	200	21.16×10^{-3}	6.82×10^{-3}	7.67×10^{-3}	5.71×10^{-3}	18.65×10^{-3}	2.40×10^{-3}	2.26×10^{-3}
	250	24.65×10^{-3}	13.47×10^{-3}	9.40×10^{-3}	16.59×10^{-3}	22.94×10^{-3}	1.55×10^{-3}	--------

5.6 HALL MEASUREMENTS

The knowledge of the Hall coefficient is very useful since R_H is inversely proportional to the carrier concentration *n*, it follows that we can determine *n* by measuring the Hall coefficient. Hall effect measurements were carried out for copper selenide sample of thickness 0.269 μm in a magnetic field of 50–550 mT. Figure 5.21 shows a plot of B versus V_H at a constant current and Fig. 5.22. shows a plot of I versus V_H at a constant magnetic field. The values of Hall coefficients (R_H) of these samples were estimated to be in the range $(1.2–1.3)\times10^{-5}$ $cm^3A^{-1}S^{-1}$. The smaller Hall coefficient indicates a very high concentration of charge carriers. The carrier concentrations were calculated using the equation $R_H = 1/ne$, where n denotes the carrier density and e the electronic charge. Carrier concentrations were obtained in the range (5–6) × 10^{23} cm^{-3} for these samples, which are very close to that for a bulk material reported by Ogirelec and Selinger [9]. Such a concentration of charge carriers makes the copper selenide thin film to a degenerate material. The Hall mobilities of these samples have been calculated and observed to be $(1–2)\times10^{-3}$ $cm^2/(V\text{-}S)$ which is closed to the reported value for CBD copper selenide thin film of phase CuSe [10].

5.7 ANALYSIS OF THE OPTICAL ABSORPTION

The variations of transmittance T (%) of $Cu_{2-x}Se$ thin film with wavelength λ for as-deposited samples, annealed different temperatures are shown in Figs. 5.23–5.29 for samples 1–7. Transmittance is obtained to be about 3–75% in the wavelength

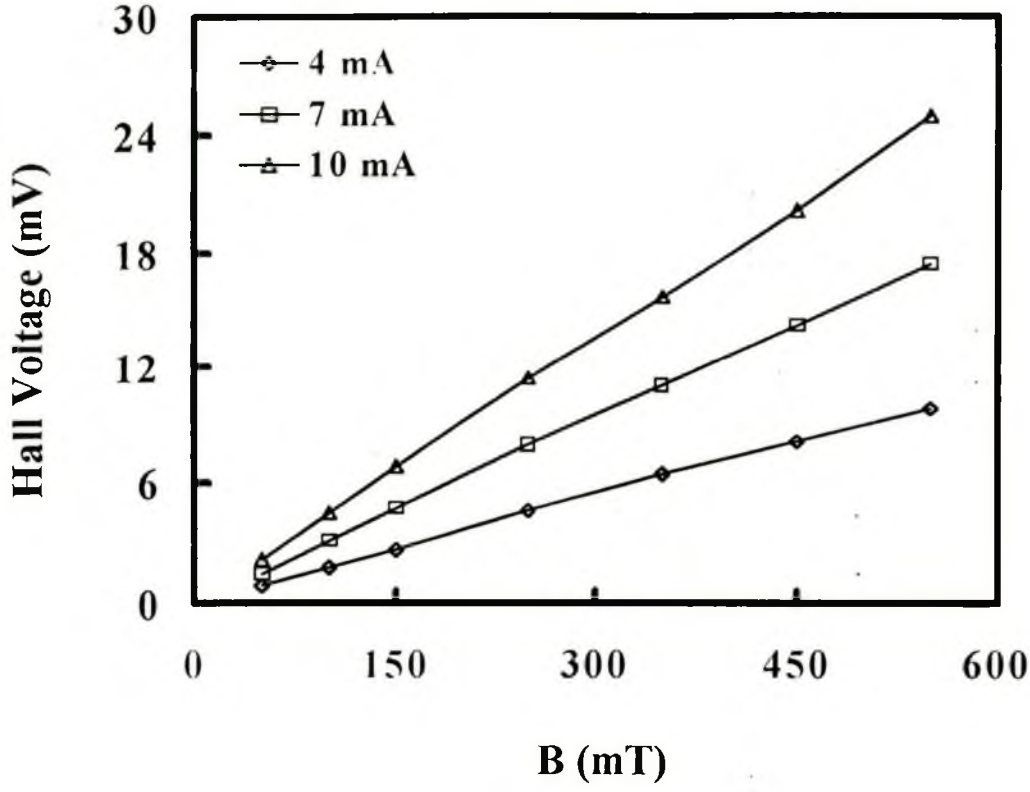

Fig. 5.21. Hall voltage versus magnetic induction curve at various bias current

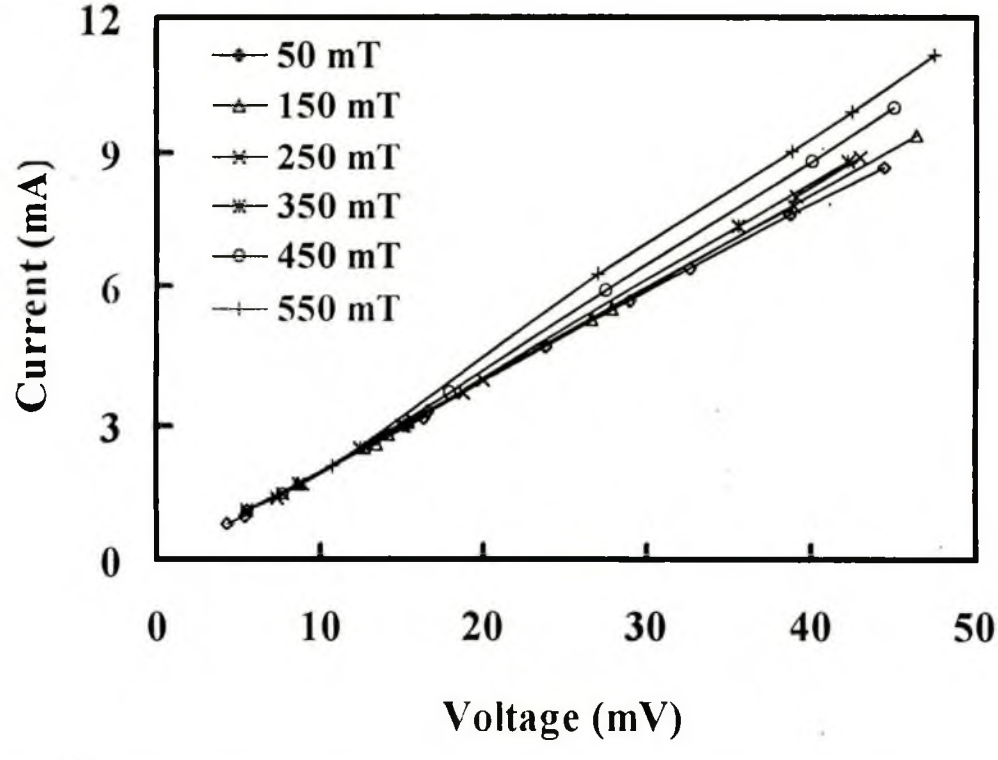

Fig. 5.22. Variation of current with voltage at different applied magnetic field

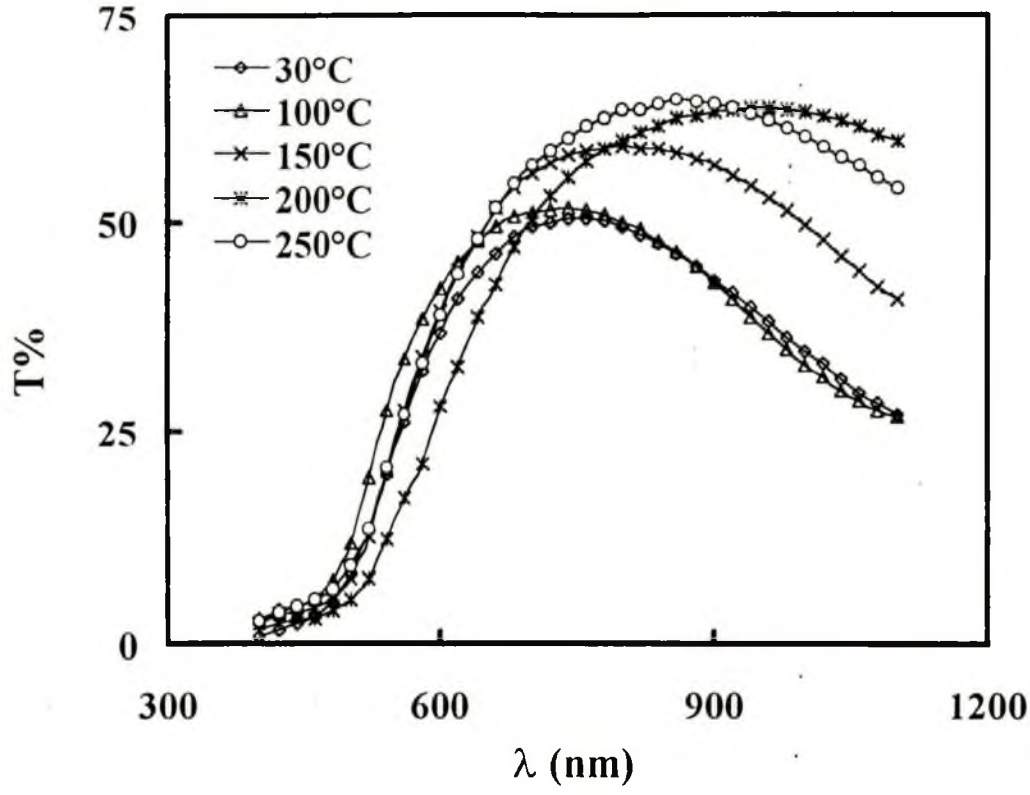

Fig. 5.23. The optical transmittance spectra of $Cu_{2-x}Se$ thin film for sample-1: as-deposited films were annealed at different temperature in the range 30-250°C.

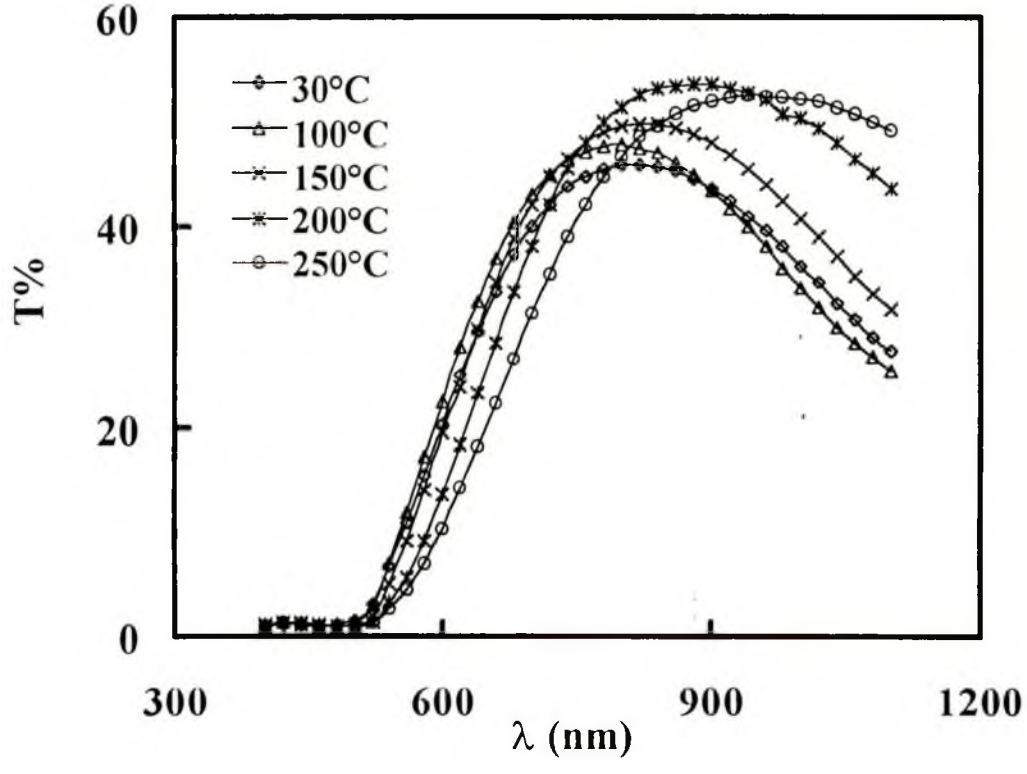

Fig. 5.24. The optical transmittance spectra of $Cu_{2-x}Se$ thin film for sample-2: as-deposited films were annealed at different temperature in the range 30-250°C.

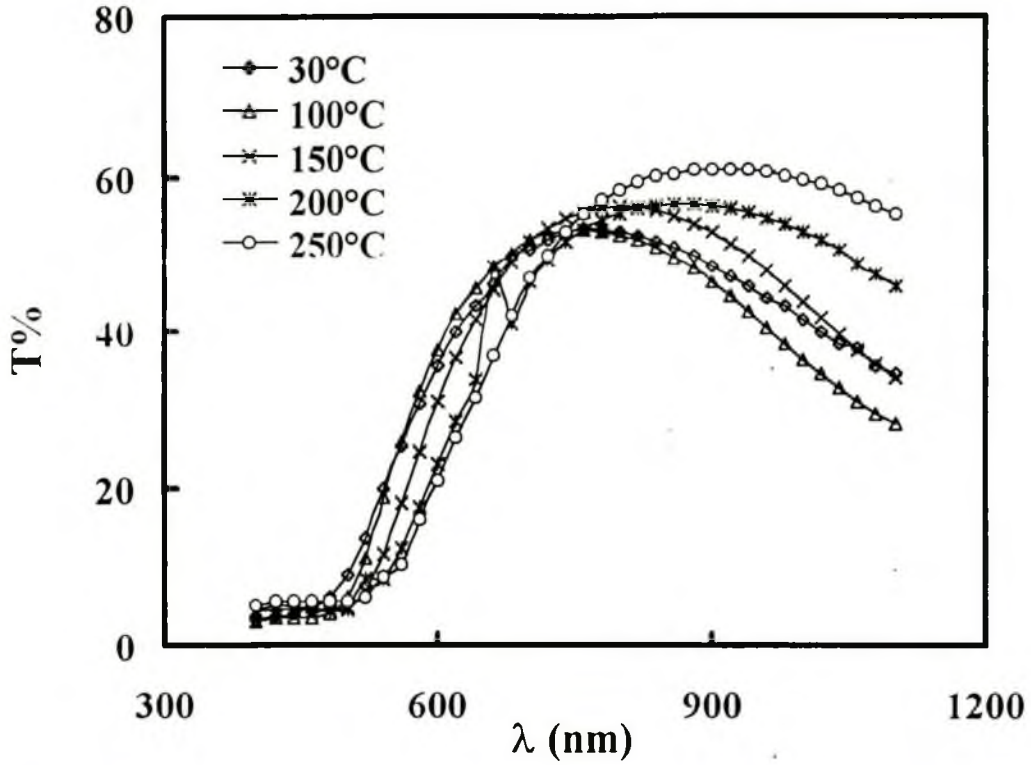

Fig. 5.25. The optical transmittance spectra of $Cu_{2-x}Se$ thin film for sample-3: as-deposited films were annealed at different temperature in the range 30-250°C.

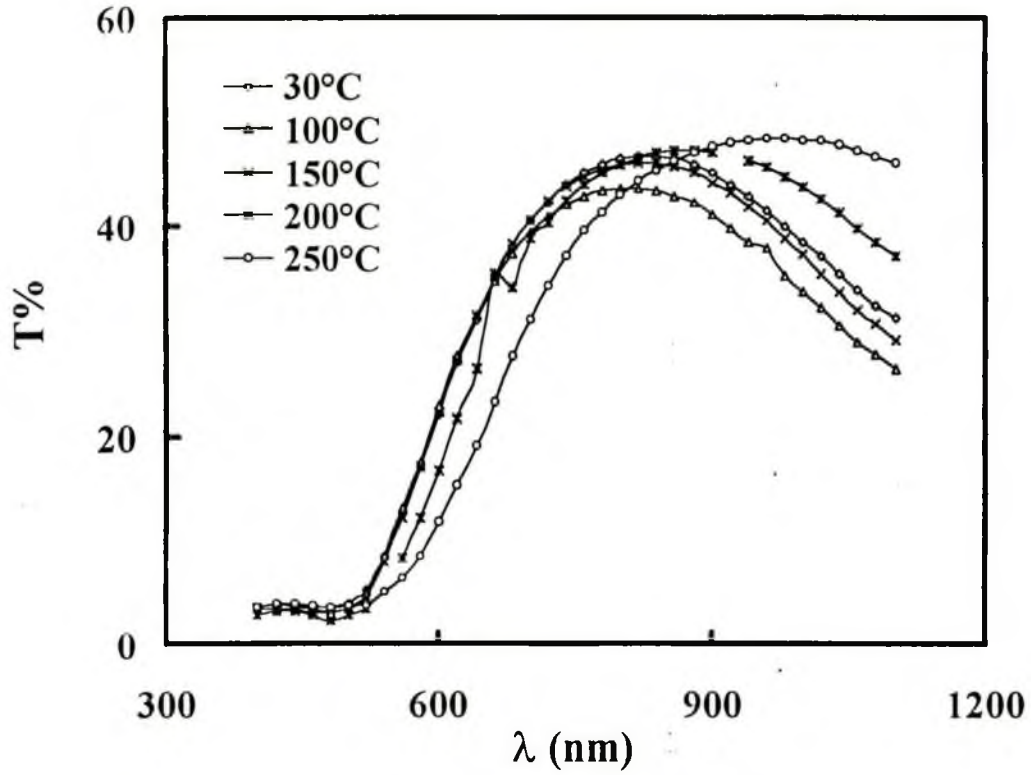

Fig. 5.26. The optical transmittance spectra of $Cu_{2-x}Se$ thin film for sample-4: as-deposited films were annealed at different temperature in the range 30-250°C.

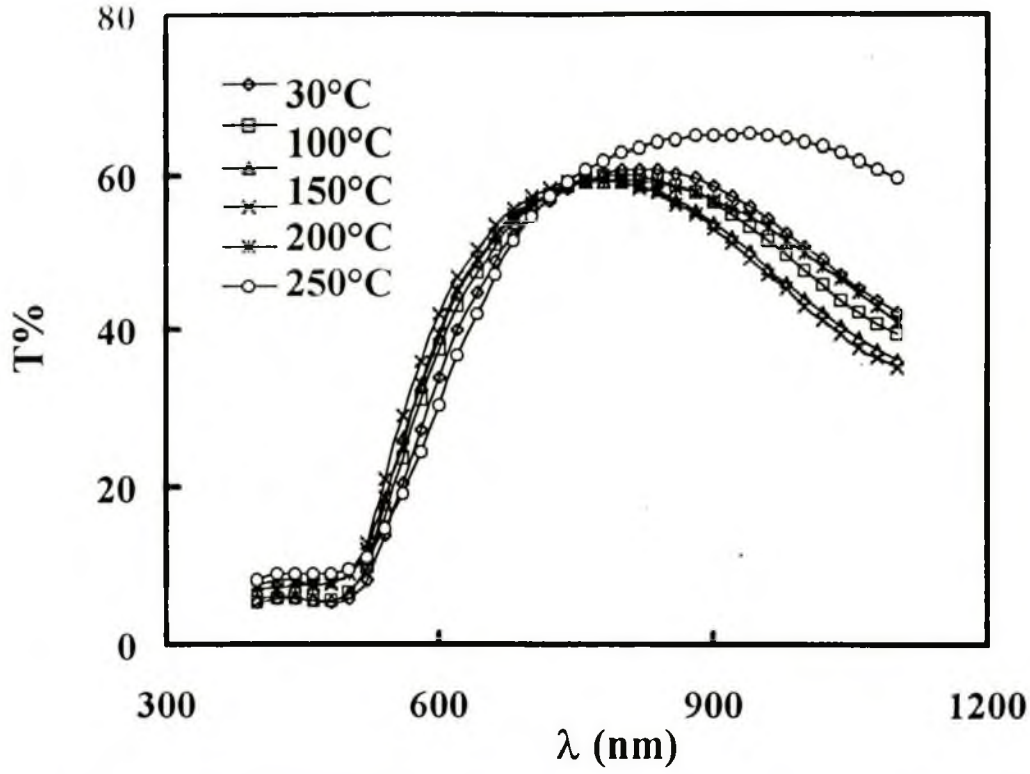

Fig. 5.27. The optical transmittance spectra of $Cu_{2-x}Se$ thin film for sample-5: as-deposited films were annealed at different temperature in the range 30-250°C.

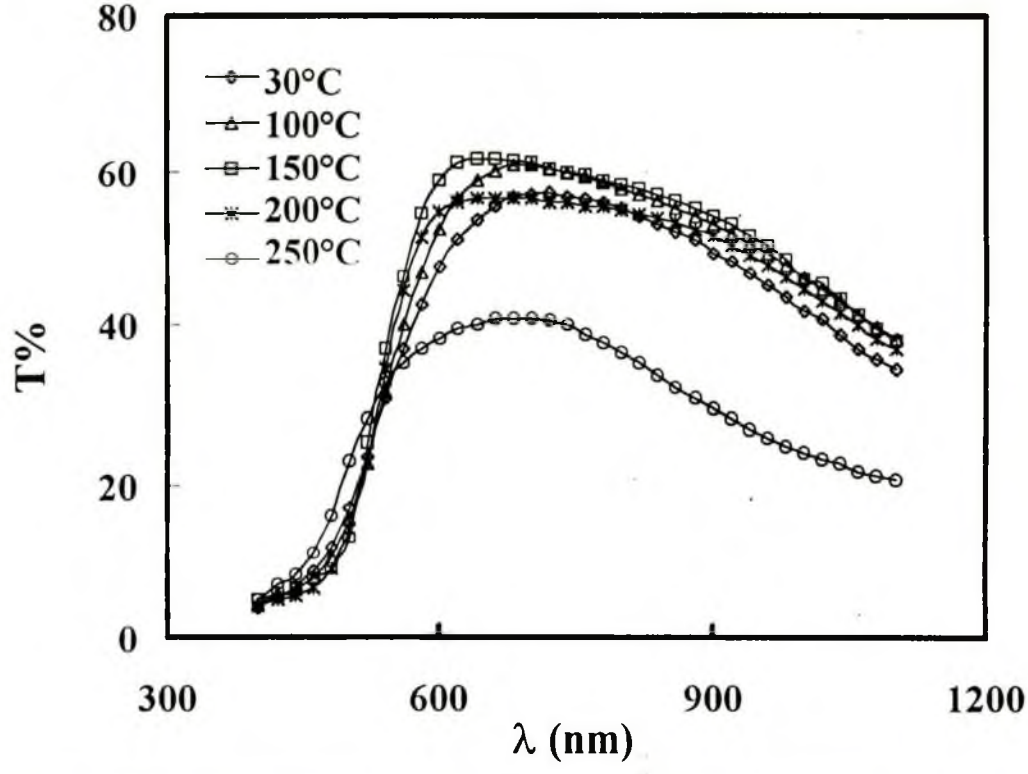

Fig. 5.28. The optical transmittance spectra of $Cu_{2-x}Se$ thin film for sample-6: as-deposited films were annealed at different temperature in the range 30-250°C.

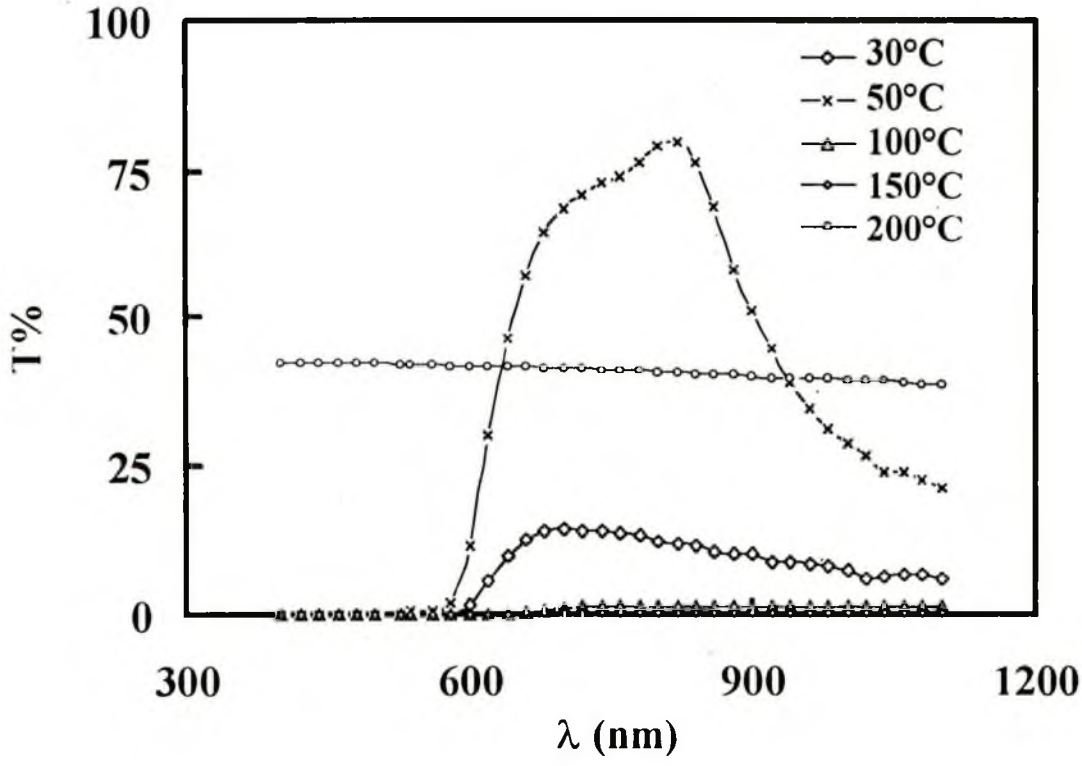

Fig. 5.29. The optical transmittance spectra of $Cu_{2-x}Se$ thin film for sample-7: as-deposited films were annealed at different temperature in the range 30-200°C.

range 400–1100nm. The spectra show that the transmittance increases from wavelength of 1100nm. A gradual decrease in transmittance is observed in the lower wavelength region and this may due to absorption by free carrier in the degenerate films. The peak values of transmission spectra are seen at around 650–900 nm means that the absorption started around the same wavelength and the transmittance becomes very low at $\lambda < 500$ nm. In the near infrared, the transmittance decreases with the increase of wavelength. This can be summarized by mentioning that the copper selenide thin films (as-deposited by CBD and annealed at different temperature from 30–250°C) have very low transmittance, ~1–5%, in the visible-UV region; low to moderate transmittance, 5–50% in the visible range and moderate to lower moderate transmittance, 50–20% in the visible-infrared region. Again the as-deposited vacuum evaporated film show low transmittance ~ 2–15% at the visible wavelength, that increases upto ~80% by annealing at 50°C for one hour. The absorption started at wavelength of 820nm. After annealing above 50°C the transmittance become very low (~1–3%). Further annealed above 200°C there is no significant change in transmittance spectra (Fig. 5.33).

Figures 5.30–5.36 represents the variation of reflectance (R %) of samples 1–7 with λ. Reflectance is found to be about 6–45% at the wavelength range 400–1100 nm. It is observed in the R (%) vs λ curves that there are two peaks around 500–600nm and 800nm. Both the peaks shift to higher wavelength with annealing temperature. The second R (%) peak appears at the same wavelength region where the transmittance peak appears in Figs. 5.23-5.29. These behaviors are in well agreement with the published results of $Cu_{2-x}Se$ thin film prepared by CBD techniques with $CuSO_4.5H_2O$ at 25°C for 8 hrs [11]. Noticeable change of reflectance is observed due to annealing at different temperatures. In Figs. 5.30–5.34, it can be seen that the intensity of the first peak decreases and that of the second peak increases with the decreases of Cu concentration. A close inspection of the spectra shows that the intensity of both the peak are about to be same for samples-2 and 3. For vacuum deposited sample 20–32% reflectance is found for sample annealed at 50°C, that reduces to 2–10% after annealed above 50°C. The behavior of lower reflectance and higher transmittance obtained in our experiment makes the materials suitable as an electro-conductive window coating.

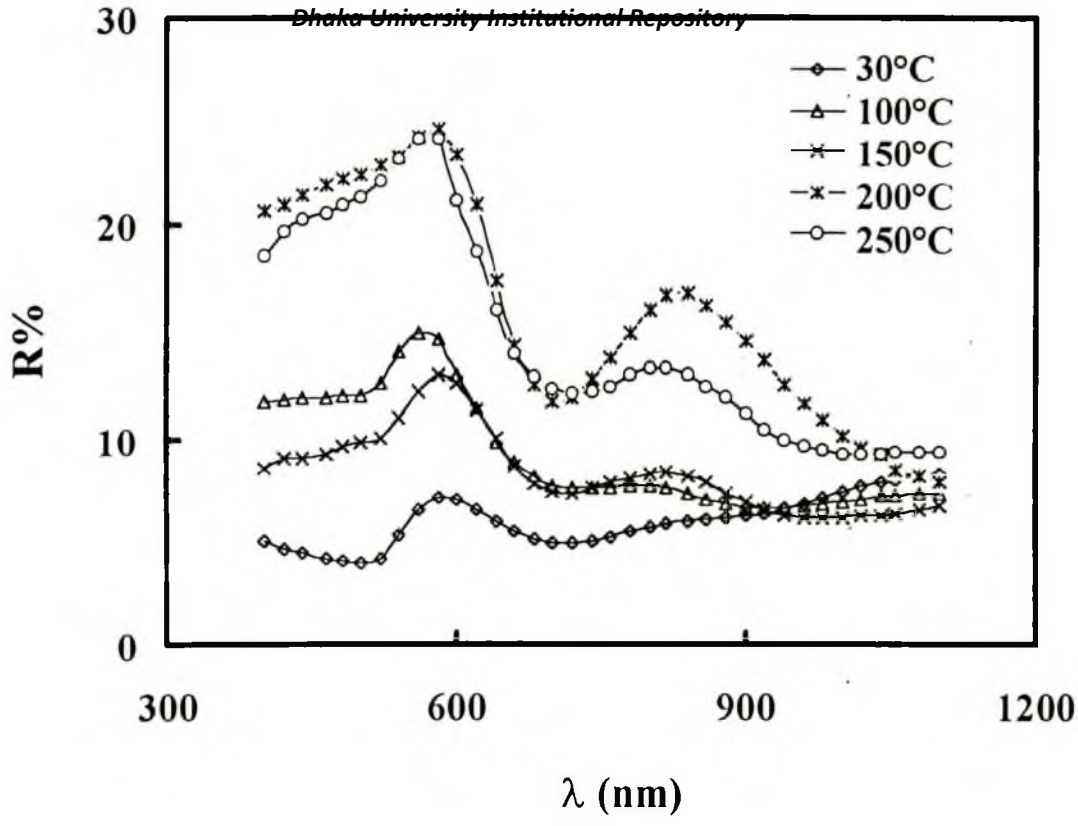

Fig. 5.30. The optical reflectance spectra of $Cu_{2-x}Se$ thin film for sample-1: as-deposited films were annealed at different temperature in the range 30-250°C.

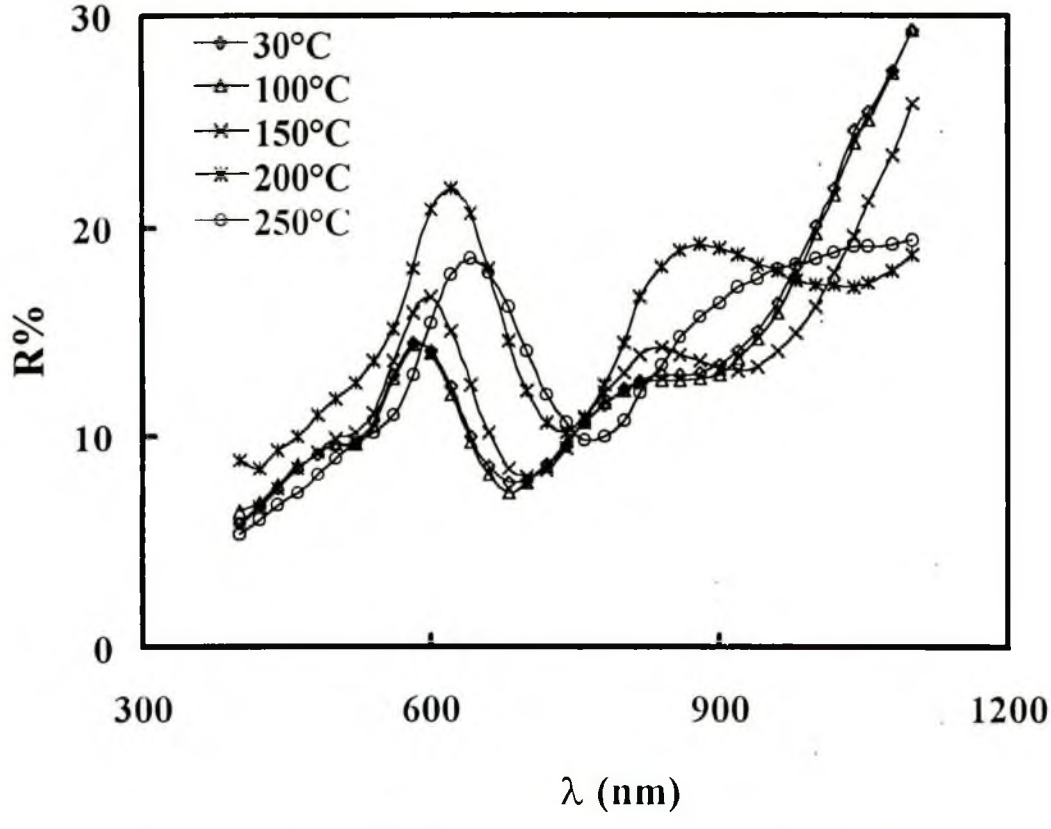

Fig. 5.31. The optical reflectance spectra of $Cu_{2-x}Se$ thin film for sample-2: as-deposited films were annealed at different temperature in the range 30-250°C.

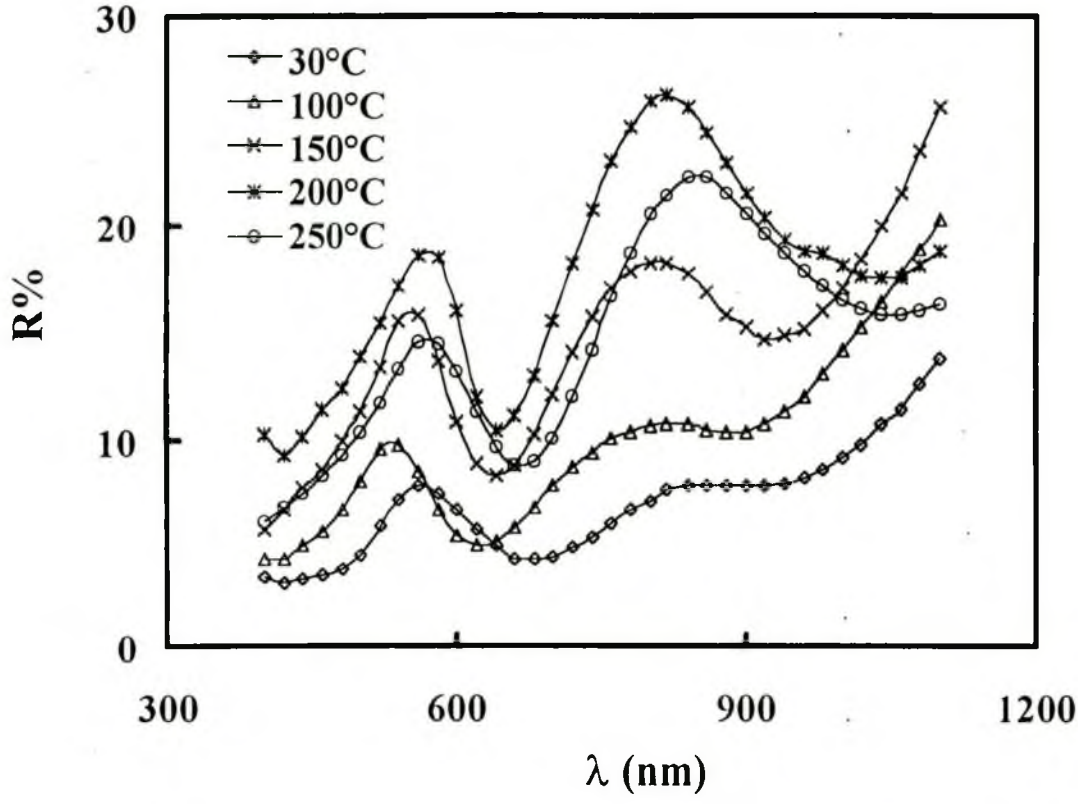

Fig. 5.32. The optical reflectance spectra of $Cu_{2-x}Se$ thin film for sample-3: as-deposited films were annealed at different temperature in the range 30-250°C.

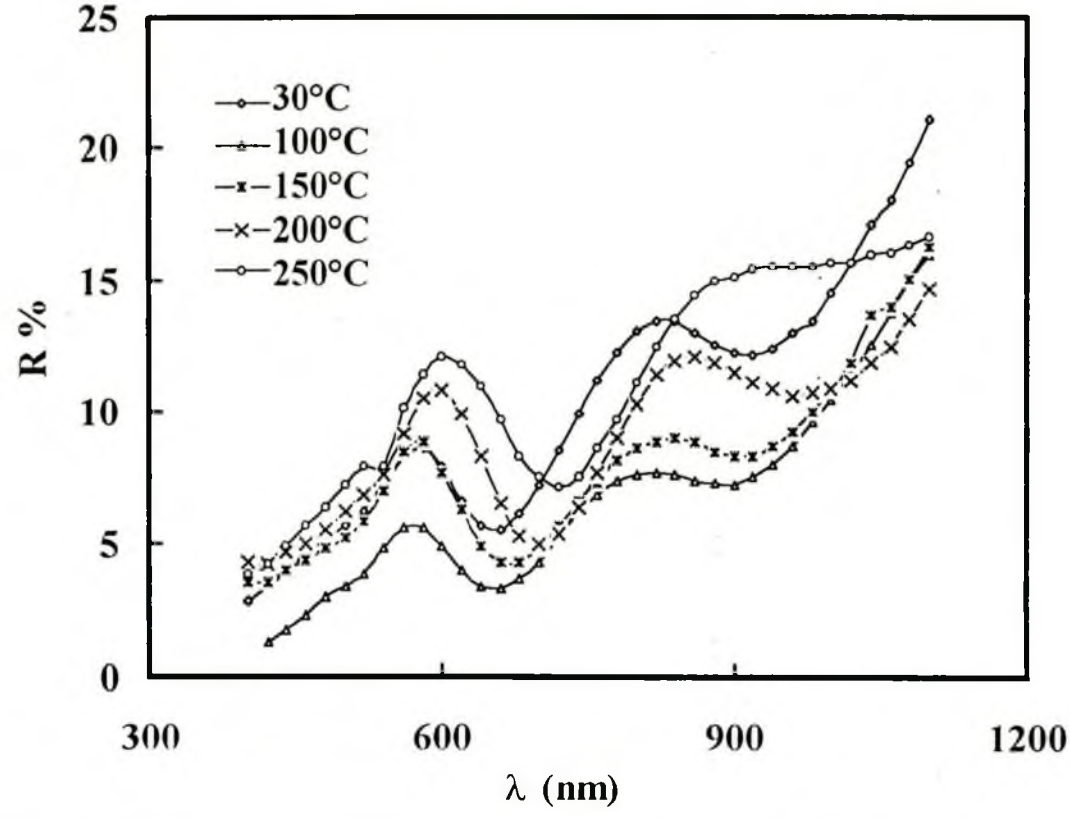

Fig. 5.33. The optical reflectance spectra of $Cu_{2-x}Se$ thin film for sample-4: as-deposited films were annealed at different temperature in the range 30-250°C.

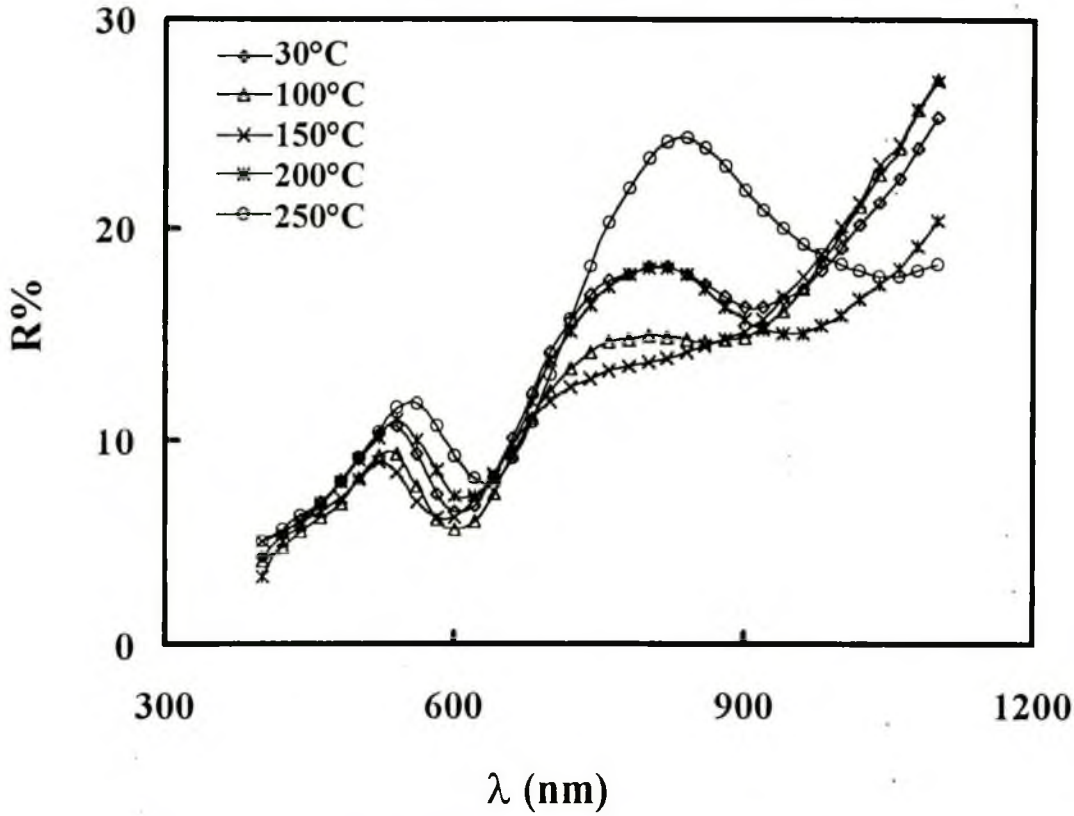

Fig. 5.34. The optical reflectance spectra of $Cu_{2-x}Se$ thin film for sample-5: as-deposited films were annealed at different temperature in the range 30-250°C.

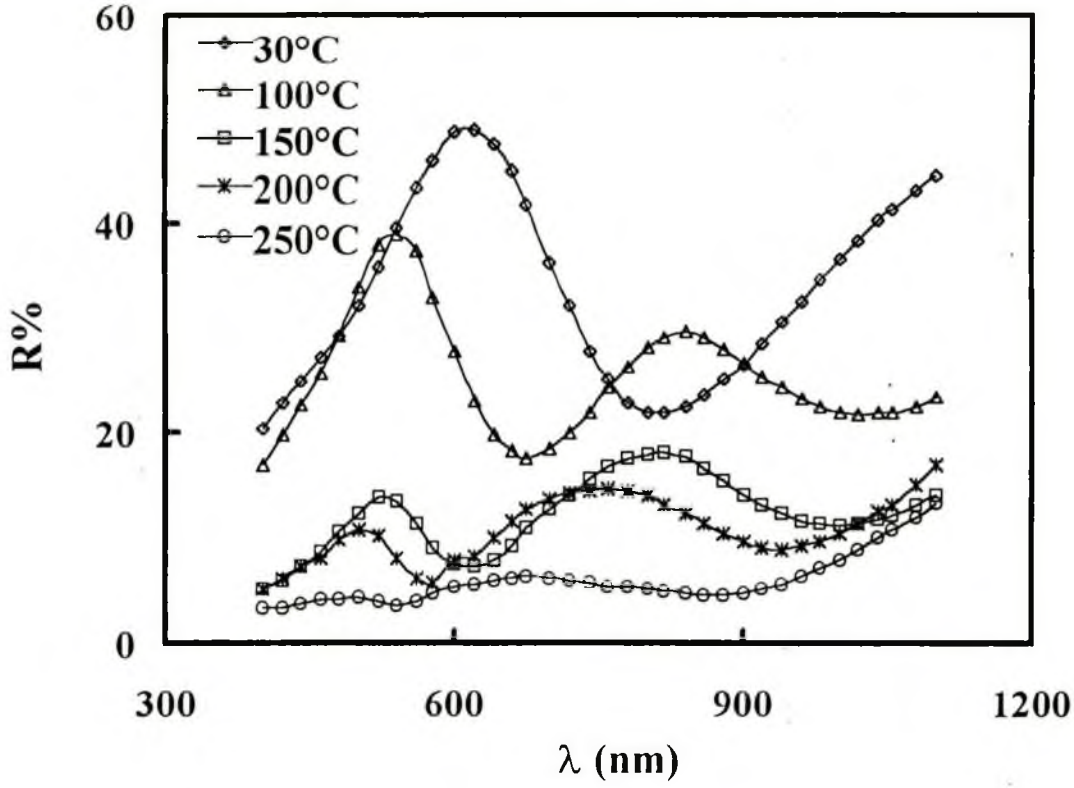

Fig. 5.35. The optical reflectance spectra of $Cu_{2-x}Se$ thin film for sample-6: as-deposited films were annealed at different temperature in the range 30-250°C.

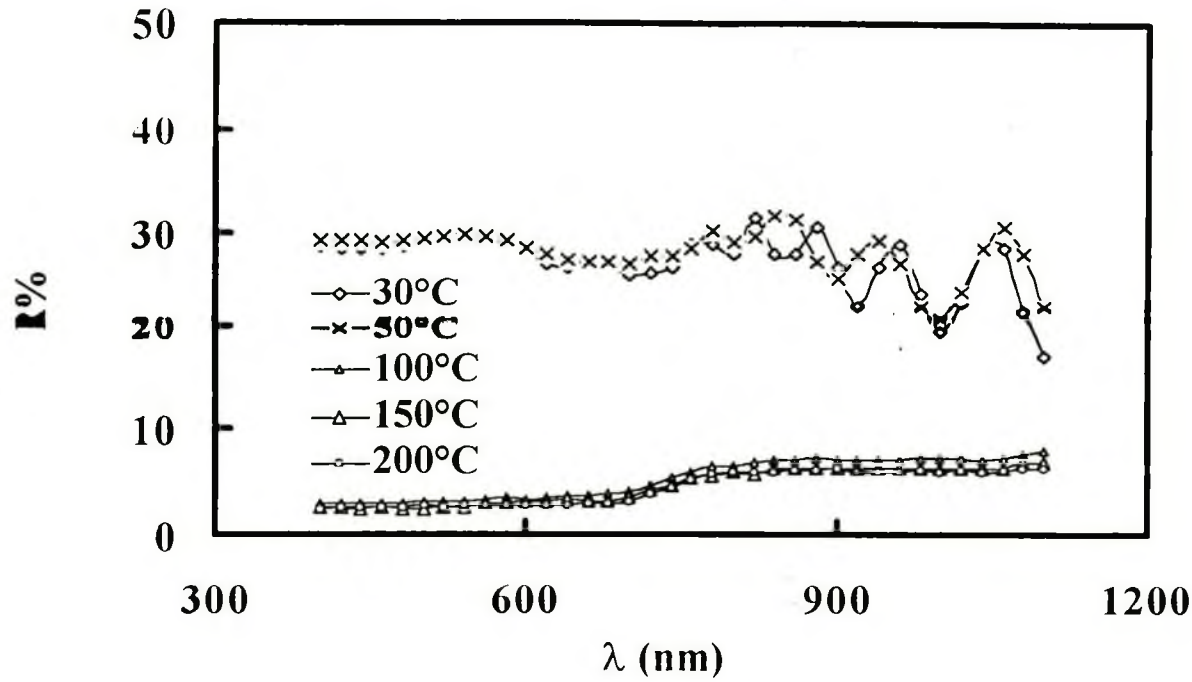

Fig. 5.36. The optical reflectance spectra of $Cu_{2-x}Se$ thin film for sample-7: as-deposited films were annealed at different temperature in the range 30-200°C.

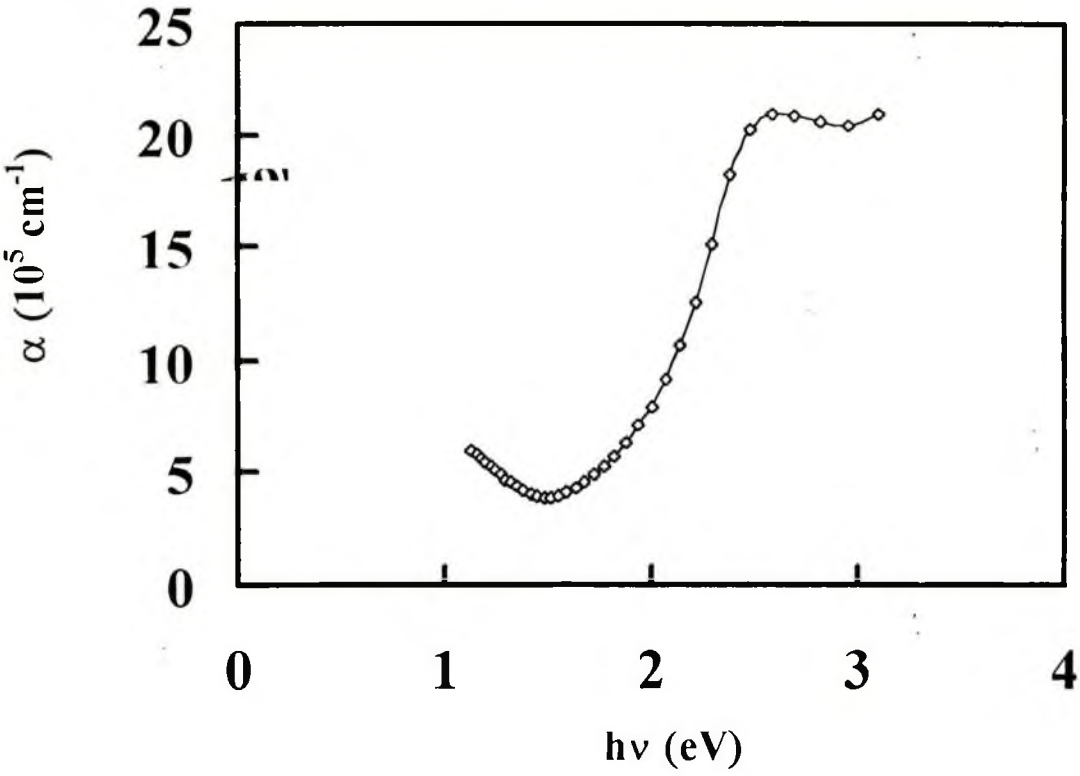

Fig. 5.37. α versus hν curve for as-deposited $Cu_{2-x}Se$ thin film.

For low transmittance and low reflectance, vacuum deposited thin film can be used (except annealing about 50°C) as a selective absorber for the conversion of solar radiation into heat. Peak wavelength values of transmittance and reflectance are listed in Table 5.4–5.9 for samples 1-6.

5.8 BAND GAP MEASUREMENT

The band gap values for the films have been estimated using the optical spectra. For this, the transmittance spectra have been corrected for the loss due to reflections using the relation $T_{corr.} = \{T(\%)/(100 - R(\%))\} \times 100$. We assume that the predominant component in the reflected intensity is due to the air-film interface. The absorption coefficients (α) for band-to-band transition across the gap at different wavelengths are calculated using the corrected transmittance values from $\alpha = (1/t)\ln(100/T_{corr})$, where t is the film thickness [3, 12].

The α vs hν curve is presented in Fig. 5.37 for sample-1. It is seen that α is non-linear with hν. A maximum of 1.43×10^3 cm^{-1} absorption coefficients is observed around 3.1 eV (400 nm).

The direct and indirect band gap values are obtained from plots of α^2 and $\alpha^{1/2}$, against the corresponding value of the photon energy hν (eV), respectively. Such plots for the films (as-deposited and annealed) are shown in Figs. 5.38-5.43 for samples 1-6 respectively for the determination of direct and indirect band gaps. In all the figures, (a) for the estimation of direct band gap of as-deposited sample, (a′) is that for direct band gap for the sample annealed at 250°C, (b) for the estimation of indirect band gap of as-deposited sample, (b′) is that for indirect band gap for the sample annealed at 250°C. Extrapolating the straight-line part of the curve in these figures to the energy axis, where $\alpha^2=0$, gives the values of band gap for direct transitions ($E_{g.dir}$) and to where $\alpha^{1/2}=0$ gives the values of band gap for indirect transitions ($E_{g.indir}$). The $E_{g.dir}$ varies in the range of 1.9-2.7 eV and the $E_{g.indir}$ is in the range of 1.3-1.95 eV for all samples from as-deposited to all annealed samples upto 250°C. This behavior would not be a correct conclusion because the optical absorption coefficients in the range of photon energy used are $>10^4$ cm^{-1}-typical realm of direct gap absorption [3]. In both cases the optical absorption coefficient does not drop to zero because of the setting in

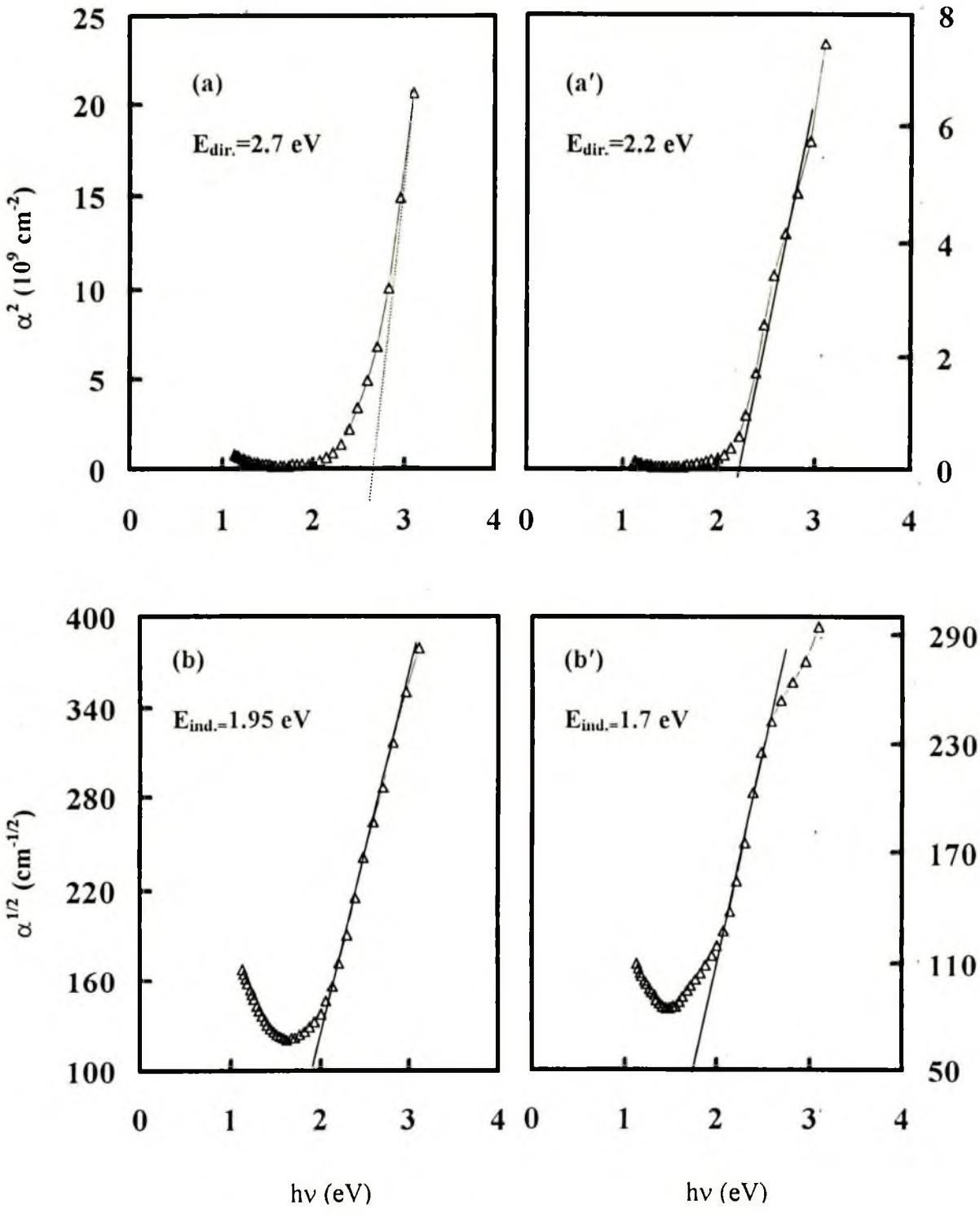

Fig. 5.38. Estimation of band gap for sample-1, (a) direct band of as-deposited film, (a′) is that of annealed at 250°C, and (b) for indirect band gap of as-deposited film, (b′) is that for annealed at 250°C.

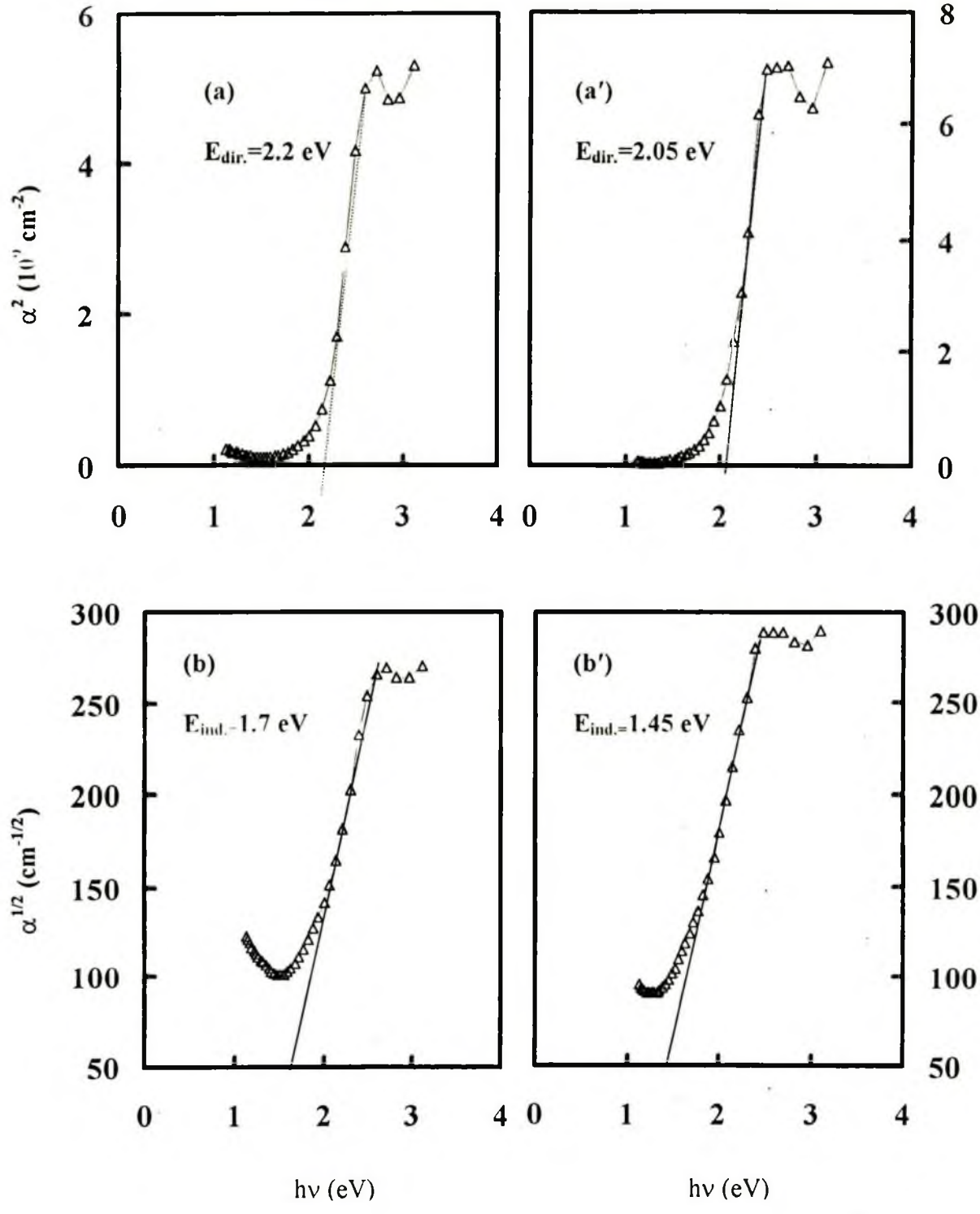

Fig. 5.39. Estimation of band gap for sample-2, (a) direct band of as-deposited film, (a′) is that of annealed at 250°C, and (b) for indirect band gap of as-deposited film, (b′) is that for annealed at 250°C.

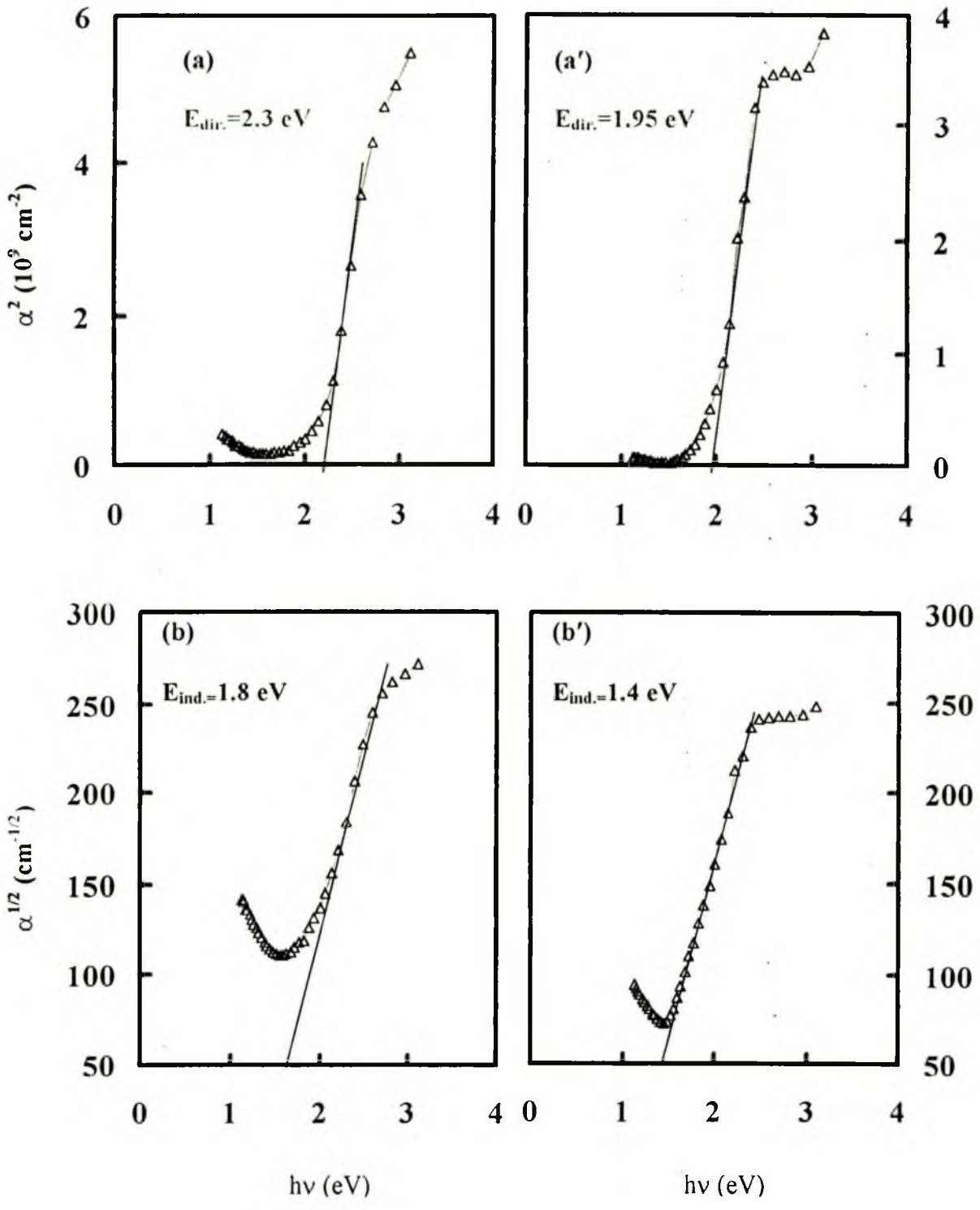

Fig. 5.40. Estimation of band gap for sample-3, (a) direct band of as-deposited film, (a′) is that of annealed at 250°C, and (b) for indirect band gap of as-deposited film, (b′) is that for annealed at 250°C.

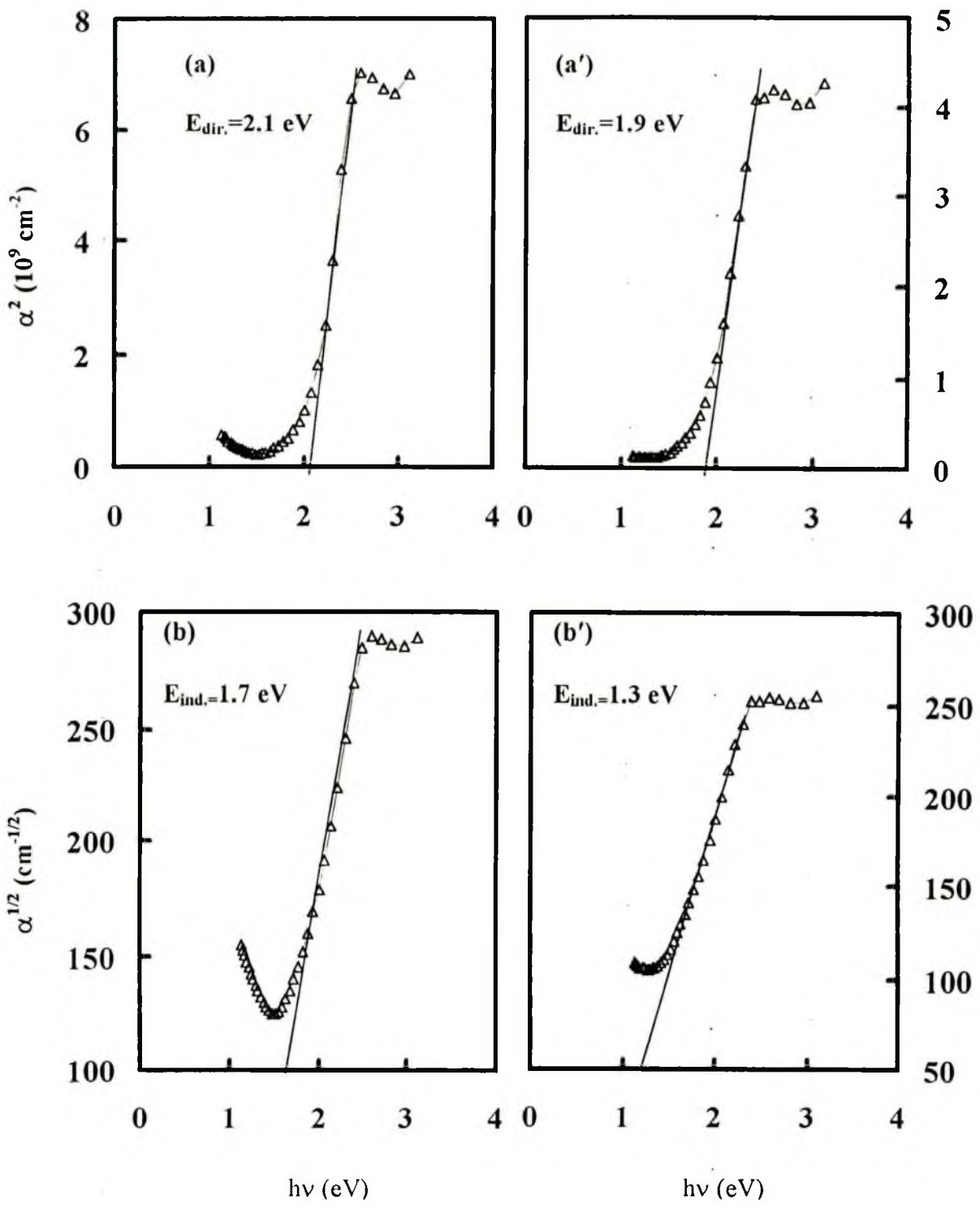

Fig. 5.41. Estimation of band gap for sample-4, (a) direct band of as-deposited film, (a′) is that of annealed at 250°C, and (b) for indirect band gap of as-deposited film, (b′) is that for annealed at 250°C.

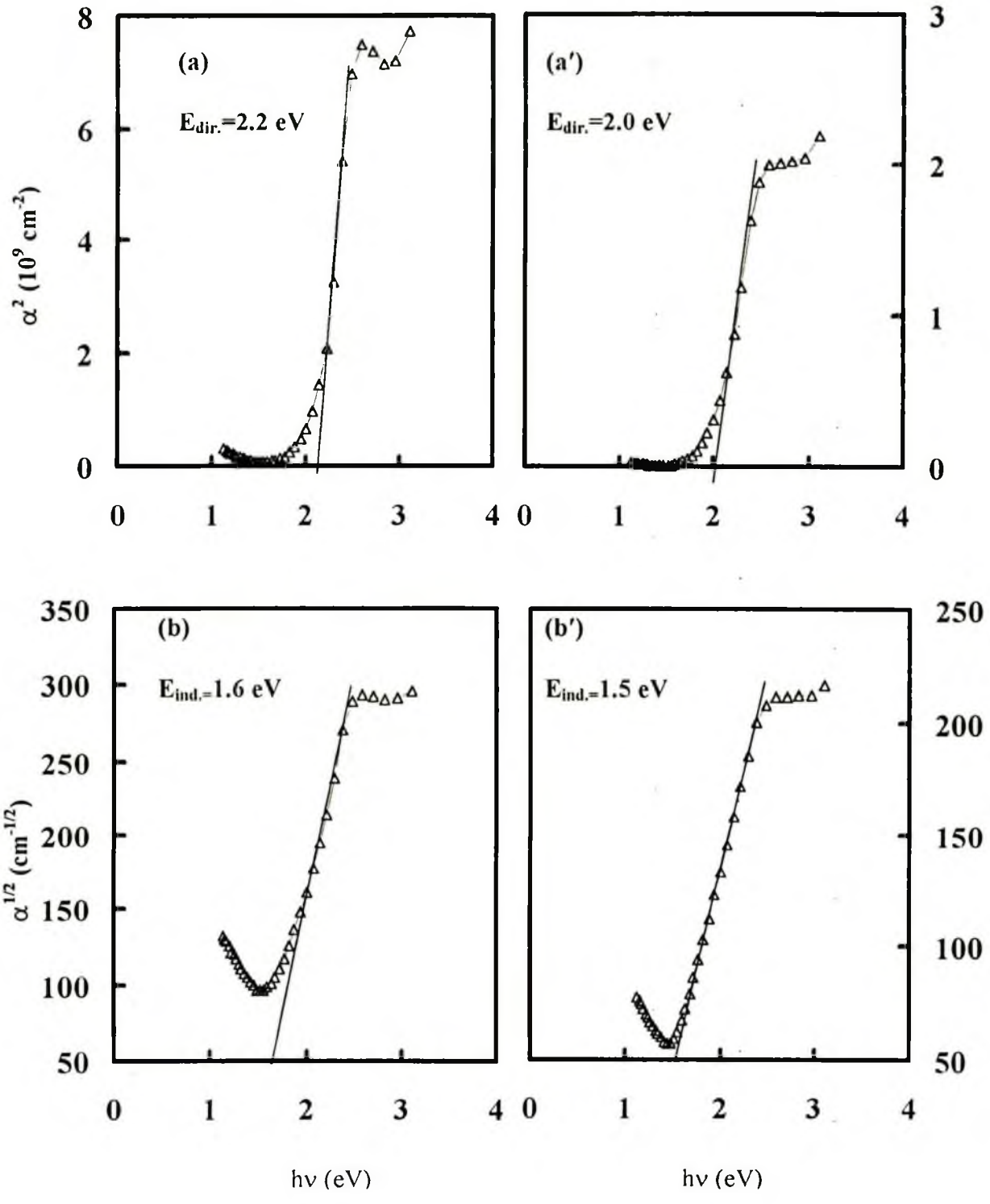

Fig. 5.42. Estimation of band gap for sample-5, (a) direct band of as-deposited film, (a′) is that of annealed at 250°C, and (b) for indirect band gap of as-deposited film, (b′) is that for annealed at 250°C.

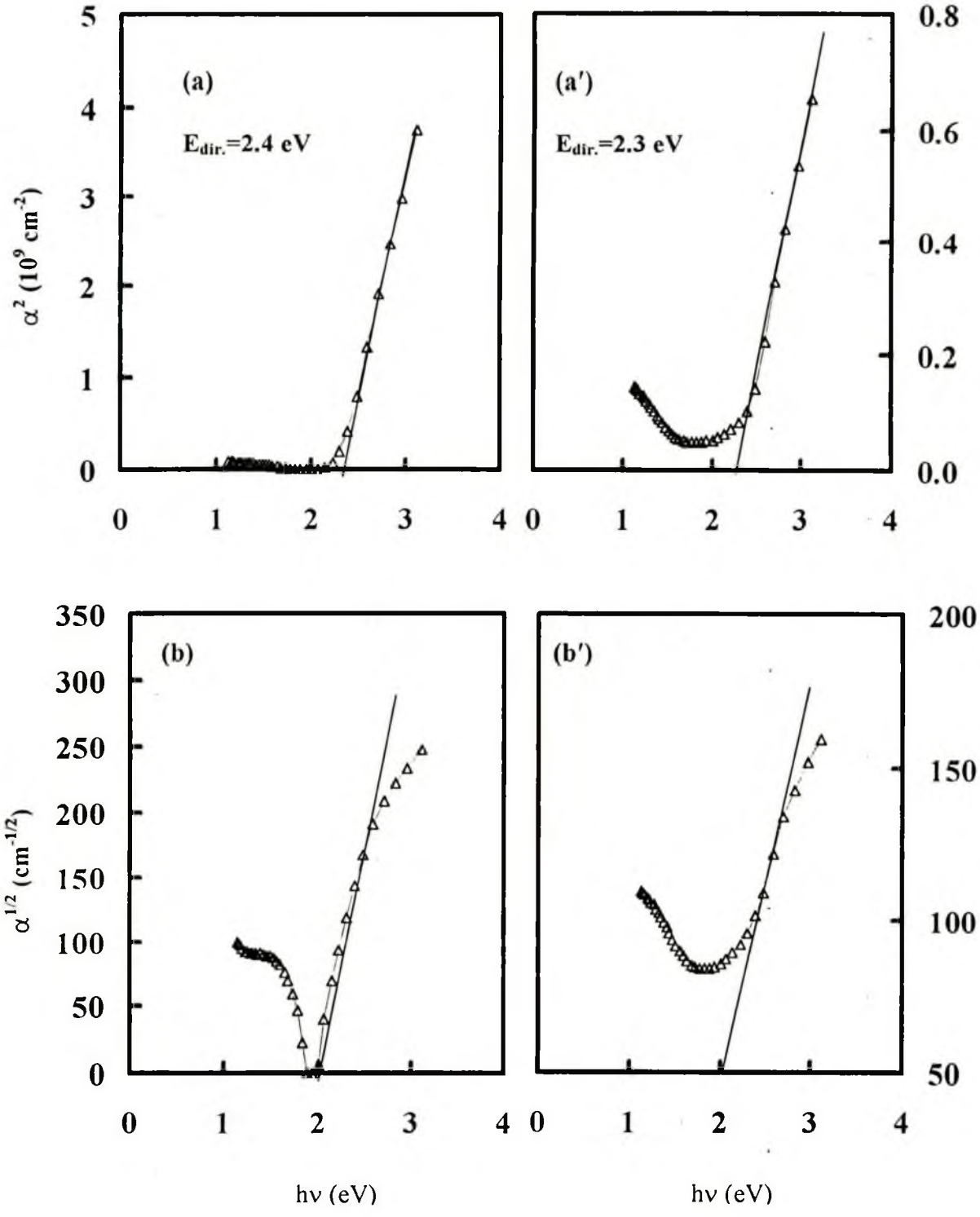

Fig. 5.43. Estimation of band gap for sample-6, (a) direct band of as-deposited film, (a′) is that of annealed at 250°C, and (b) for indirect band gap of as-deposited film, (b′) is that for annealed at 250°C.

of free carrier absorption before the band-to-band transitions disappear. Hence it is not possible to analyze the low energy region in the band-to-band absorption corresponding to indirect gaps. The values indicated above for the indirect band gap, are considered to be the upper limit. The larger band gap values in the as prepared samples compared with that of the annealed samples are due to the quantum confinement effect [13,14] arising from smaller grain size in the former. All these optical band gap values are close to that $Cu_{2-x}Se$ thin film prepared by CBD technique using N, N-dimethylselenourea reported earlier [3,12,15] for the materials used for solar cells, which means that these materials have good chance to be used for this purpose. It is observed that both direct and indirect band gap values of as-deposited samples are higher compared with those of the annealed samples. The decrease of band gap due to annealing may be understood by the improvement of crystallinity of the as-deposited film on annealing as observed in XRD. Direct and indirect band gap values for corresponding samples are listed in Table 5.4-5.9.

Table 5.4. Direct and indirect band gap values, peak wavelength values of T% and R% and their corresponding maximum T% and R% values of sample-1 for different annealing temperatures.

Temperature (°C)	Direct band gap (eV)	Indirect band gap (eV)	Peak value for T%		Peak value for R%			
					1st peak		2nd peak	
			λ(nm)	T%	λ(nm)	R%	λ(nm)	R%
30	2.6	1.95	762	50.6	580	7.2	---	---
100	2.4	2	732	51.8	566	15.1	---	---
150	2.3	1.7	801	59.1	582	13.2	---	---
200	2.2	1.6	961	63.1	572	24.8	833	16.9
250	2.2	1.7	860	64.5	556	24.4	---	---

Table 5.5. Direct and indirect band gap values, peak wavelength values of T% and R% and their corresponding maximum T% and R% values of sample-2 for different annealing temperatures.

Temperature (°C)	Direct band gap (eV)	Indirect band gap (eV)	Peak value for T%		Peak value for R%			
					1st peak		2nd peak	
			λ(nm)	T%	λ(nm)	R%	λ(nm)	R%
30	2.2	1.7	811	46.1	587	14.7	---	---
100	2.2	1.9	795	48	586	14.5	----	---
150	2.2	1.8	831	50	591	61.8	840	14.3
200	2.1	1.7	889	53.8	622	21.9	----	---
250	2.05	1.4	946	52.7	640	18.8	----	----

Table 5.6. Direct and indirect band gap values, peak wavelength values of T% and R% and their corresponding maximum T% and R% values of sample-3 for different annealing temperatures.

Temperature (°C)	Direct band gap (eV)	Indirect band gap (eV)	Peak value for T%		Peak value for R%			
					1st peak		2nd peak	
			λ(nm)	T%	λ(nm)	R%	λ(nm)	R%
30	2.3	1.8	776	53.4	564	7.9	798	18.3
100	2.3	1.9	755	53.2	532	10.1	------	-----
150	2.1	1.6	799	56.2	551	16.1	-----	-----
200	2	1.5	877	56.6	566	18.8	836	26.4
250	1.95	1.4	904	61.1	570	14.7	844	22.6

Table 5.7. Direct and indirect band gap values, peak wavelength values of T% and R% and their corresponding maximum T% and R% values of sample-4 for different annealing temperatures.

Temperature (°C)	Direct band gap (eV)	Indirect band gap (eV)	Peak value for T%		Peak value for R%			
					1st peak		2nd peak	
			λ(nm)	T%	λ(nm)	R%	λ(nm)	R%
30	2.1	1.7	820	46.9	580	8.6	820	13.5
100	2.05	1.7	820	43.8	560	5.6	820	7.7
150	2.1	1.6	840	46.2	580	8.8	840	9
200	2	1.5	880	47.5	600	10.8	860	12.1
250	1.9	1.3	980	48.6	600	12.1	940	15.6

Table 5.8. Direct and indirect band gap values, peak wavelength values of T% and R% and their corresponding maximum T% and R% values of sample-5 for different annealing temperatures.

Temperature (°C)	Direct band gap (eV)	Indirect band gap (eV)	Peak value for T%		Peak value for R%			
					1st peak		2nd peak	
			λ(nm)	T%	λ(nm)	R%	λ(nm)	R%
30	2.2	1.6	818	60.8	538	10.7	---	---
100	2.1	1.6	783	59.3	527	9.5	---	----
150	2.1	1.7	776	59.6	526	8.9	---	----
200	2.1	1.5	790	59.4	537	10.9	809	18.3
250	2.0	1.5	928	57.1	555	11.8	835	24.5

Table 5.9. Direct and indirect band gap values, peak wavelength values of T% and R% and their corresponding maximum T% and R% values of sample-6 for different annealing temperatures.

Temperature (°C)	Direct band gap (eV)	Indirect band gap (eV)	Peak value for T%		Peak value for R%			
					1st peak		2nd peak	
			λ(nm)	T%	λ(nm)	R%	λ(nm)	R%
30	2.4	2	709	57.3	616	49	---	---
100	2.4	2	691	56.9	535	39.9	847	29.8
150	2.4	2	654	62	527	13.9	804	18
200	2.4	2	654	56.8	502	10.8	----	---
250	2.4	2	682	41	---	---	818	4.9

5.9 BAND GAP VARIATION WITH TEMPERATURE

Figure 5.44 and 5.45 shows the variation of direct and indirect band gap for all samples with different annealed temperatures for 1 hour of copper selenide thin film. From these graphs, it is found that both the direct and indirect band gaps slowly decrease upto 250°C and the band gap can not be estimated for the samples annealed above 250°C.

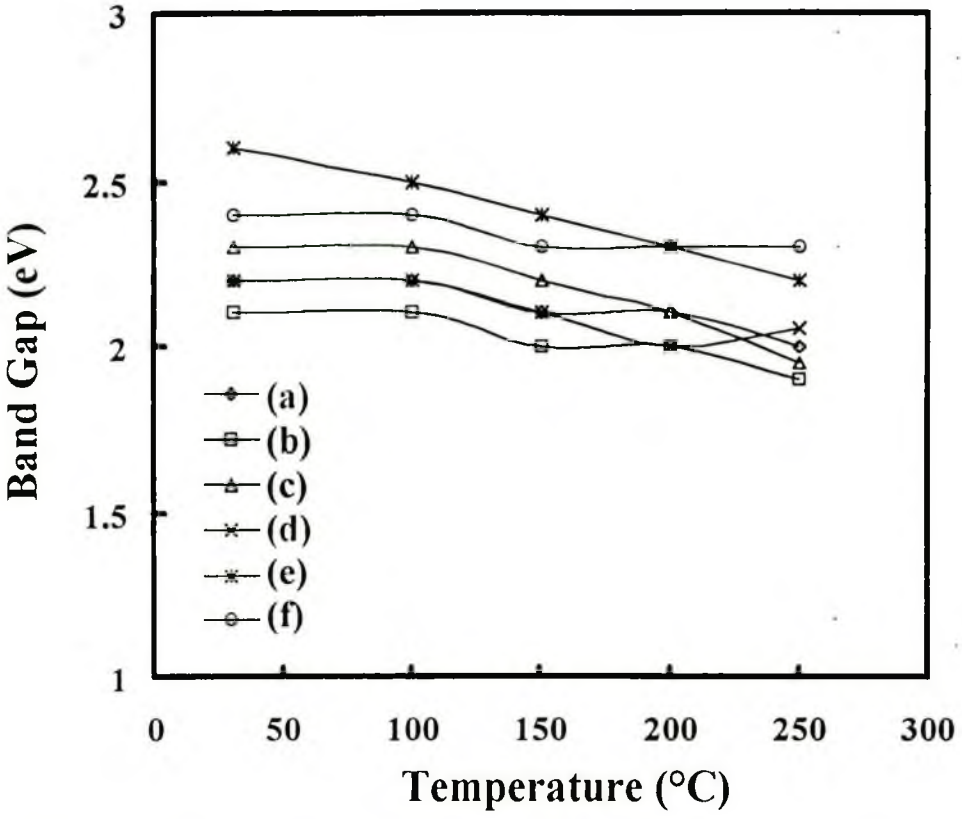

Fig. 5.44. Variation of Direct band gap with different annealed temperatures for 1 hour of $Cu_{2-x}Se$ thin film: curve (a-f) for sample (1-6).

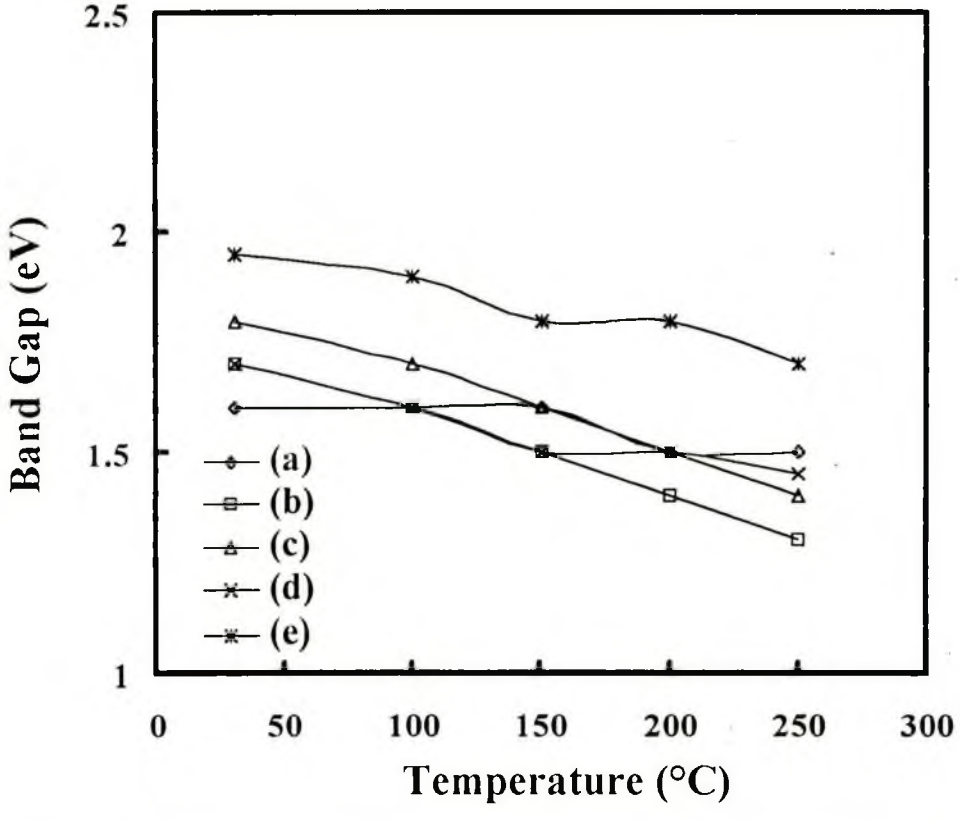

Fig. 5.45. Variation of Indirect band gap with different annealed temperatures for 1 hour of $Cu_{2-x}Se$ thin film: curve (a-e) for sample (1-5).

REFERENCES

1. K. L. Chopra, R. C. Kainthla, D. K. Pandya, and A. P. Thakoor, *Physics of Thin Films*, **12** (1982) 201
2. R. C. Kainthla, Ph. D. Thesis, Indian Institute of Technology, Delhi (1980).
3. V. M. Garcia, P. K. Nair and M. S. T. Nair, *J. Cryst Growth*, **203** (1999) 113.
4. R. Heyding and R. M. Murray, *Can. J. Chem.*, **54** (1976) 841.
5. M. Lakshmi, K. Bindu, S. Bini, K.P.Vijaykumar, C. Sudha Kartha, T. Abe and Y. Kashiwaba, *Thin Solid Films*, **386** (2001) 127.
6. E. Andrade, V. M. García, P. K. Nair, M. T. S. Nair, E. P. Zavala, L. Huerta. and M. F. Rocha. *Instruments and Methods in Physics Research* B **161-163** (2000) 635.
7. S. H. Johan, *Bull. Soc. Fr. Mineral Crystallogr.* **94** (1971) 162.
8. C. S. Barret and T.B. Massalski, *Structure of Metals*, McGraw-Hill, New York, (1966).
9. Z. Ogirelec and D. Selinger, *J. Mat. Sci.*, **6** (1971) 136.
10. A. Mondal and P. Pramanik, *J. Solid State Chemistry*, **47** (1983) 81.
11. P. K. Nair, V. M. Garcia, O Gomez-Daza and M. T. S. Nair, *Semicond. Sci. Technol.* **16** (2001) 855.
12. G. Hodes, A. A. Yayor, F. Decker and P. Motisuke, *Physical Review B*, **36** (1987) 4215.
13. V. M. Garcia, M . T. S. Nair, P. K. Nair and R. A. Zingaro, *Semicond. Sci. Technol.*, **12** (1997) 645.
14. A. M. Hermann and L. Fabick, *J. Crystal Growth*, **61** (1983) 658.
15. K. L. Chopra and S. R. Das, *Thin Film Solar Cells*, Plenum Press, New York (1983).

CHAPTER 6

CONCLUSIONS

A low cost Chemical Bath Deposition (CBD) system has been developed in our laboratory. Good quality thin films of smooth surface of copper selenide thin films of compositions $Cu_{2-x}Se$ (x=0.1–0.5) and Cu_3Se_2 were deposited using sodium selenosulfate as a source of selenide ions. Structural, electrical and optical properties of the films have been investigated. When the film annealed at 250°C in air, the phase $Cu_{1.8}Se$ and Cu_3Se_2 becomes crystalline, with structures of berzelianite (cubic) and tetragonal, respectively, whereas, the as deposited film was found dis-order. The crystallinity is very low in as-deposited samples, but that improves on annealing in air at 250°C. The grain size of the as-deposited samples was very small which can be increased about 30% owing to annealing in air at 250°C.

It is found that as-deposited samples and films annealed upto 250°C have low resistivity between $(2–25)\times10^{-3}$ Ω-cm. Hall effect measurements performed on as-deposited thin films and found Hall coefficients in the range $(1.2–1.3)\times10^{-5}$ $cm^3A^{-1}S^{-1}$, carrier concentrations in the range $(5–6)\times10^{23}$ cm^{-3} and Hall mobility in the range $(1–2)\times10^{-3}$ $cm^2/(V\text{-}S)$. Optical absorption in the films are found from free carrier absorption in the near infrared region with a maximum absorption coefficient of $\sim10^5$ cm^{-1}. The films showed very low transmittance, ~1–5%, in the visible-UV region; low to higher transmittance, 5–75% in the visible range and moderate to lower moderate transmittance, 50–20% in the visible-infrared region and very low reflectance, 0–1%, in the visible-UV region, low reflectance, 10–25% in the visible range and low to lower moderate reflectance (above 25%) in the visible-infrared region. These properties of lower reflectance and higher transmittance are close to those desired for an ideal solar control coating. The peak values of transmission spectra are seen at around 650-900 nm means that the absorption started around the same wavelength and the transmittance becomes very low at $\lambda < 500$ nm that can be used as radiation filters. The band gap for direct

transitions, $E_{g.dir}$ varies in the range 1.9–2.6 eV and that for indirect transition $E_{g.indir}$ is in the range 1.3–2.0 eV from as-deposited to annealed sample. The indirect band gap being near the optimum value for solar cell application. In conclusion, this work reveals that CBD technique can be used to prepare thin films of $Cu_{2-x}Se$ and Cu_3Se_2 and these films can be used in various purposes of thin film technology especially for solar cell application.

The as-deposited vacuum evaporated film that have low transmittance and reflectance and both these parameter increase by annealing upto 50°C and can back to very low by annealing above 50°C. For low transmittance and low reflectance, vacuum deposited thin film can be used (after annealing above 50°C) as a selective absorber for the conversion of solar radiation into heat.

SUGGESTION FOR FURTHER WORK

The application of copper selenide thin films as absorber materials in solar cells would requires further work, first to modify the deposition process to attain higher thickness and to develop post deposition processing to reduce the conductivity of the films by two to three order of magnitude. This is required because, to create the depletion region in the copper selenide absorber in the heterojunction configuration, so that the band-to-band optical absorption results in charge carrier separation. High *p*-type electrical conductivity has been observed for the copper selenide films, which may be used as radiation filters. It should be improved the theoretical analysis of the optical absorption related to the electrical properties of the films; the effects of thin films should be considered.

For the application in solar cell, as photovoltaic devices, photoconductivity measurement is necessary because the carriers generated by photoexcitation will move under the influence of an applied field. If they survive recombination, they will reach the ohmic contacts at the ends of the semiconductor bar giving an increase of current known as photocurrent.

The grain size would also be required to improve to result in high mobility life-time product. Further work from our laboratory would address these issues in the thin film deposition, post deposition processing, and development of applications of the films. The possibility of creating new ternary compounds $CuInSe_2$ using the chemically deposited $Cu_{2-x}Se$ film as a precursor may be by far the most prospective application of this deposition technique.

Although, the above explained work is very important to do for understanding the material and applications, I could not finish the work due to the constraint of time. I hope I would be able to continue this work for my future Ph.D. programme in this laboratory.

ACADEMIC ACHIEVEMENTS

Publications

1. Al – Mamun and A. B. M. Obaidul Islam, "Structural, Electrical and Optical Properties of Copper Selenide Thin Films Deposited by Chemical Bath Deposition Technique" (submitted to *Thin Solid Films*).

International Conference

1. Al – Mamun and A. B. M. Obaidul Islam, "Charecterisation of Electrical and Optical Properties of Chemically-Deposited Copper Selenide thin films ", has been accepted for oral presentation in the *International Conference on Advancement in Science and Technology* (*iCAST*), to be held in Kuala Lampur, Malaysia, August 5-7, 2003.
2. Al – Mamun and A. B. M. Obaidul Islam, "Characterization of Copper Selenide Thin Films Deposited by Chemical Bath Deposition Technique"; has been accepted for presentation at the forthcoming *International Meeting on Applied Physics (APHYS-2003)*, in Badajoz, Spain, October 14-18, 2003.

National Conference

1. Al – Mamun and A. B. M. Obaidul Islam, "Structural and Optical Characterization of Chemically-Deposited Copper Selenide Thin Films"; Extended abstract of *First Symposium of STRC on Role of Semiconductors for the Technological Development*, Dhaka, Bangladesh, (Feb. 01, 2003).
2. Al – Mamun and A. B. M. Obaidul Islam, "A Study of Copper Selenide Thin Films by Vacuum Evaporation Technique"; Extended abstract of *First Symposium of STRC on Role of Semiconductors for the Technological Development*, Dhaka, Bangladesh, (Feb. 01, 2003).
3. Al – Mamun and A. B. M. Obaidul Islam, "Chemical Bath Deposition of Copper Selenide Thin Film"; Extended abstract of *Electronic Society Conference*, Dhaka, Bangladesh, (April 17-19, 2003).
4. Al – Mamun and A. B. M. Obaidul Islam, "A Study of Copper Selenide Thin Films by Chemical Bath Deposition Technique"; Submitted for Extended abstract of *Bangladesh Solar Energy Society*, Dhaka, Bangladesh, (July 20, 2003).